

Air-Sea Interactions on Titan: Lake Evaporation, Atmospheric Circulation, and Cloud Formation

Scot C. R. Rafkin* and Alejandro Soto

Department of Space Studies, Southwest Research Institute, 1050 Walnut Street, Suite 300, Boulder, CO, USA, rafkin.swri@gmail.com.

*Corresponding Author

Keywords: Titan, Titan Seas, Titan Lakes, Air-Sea Interaction, Sea breeze, Titan Clouds

Tables: 2

Figures: 30

Supplemental Files: 67

Abstract

Titan's abundant lakes and seas exchange methane vapor and energy with the atmosphere via a process generally known as air-sea interaction. This turbulent exchange process is investigated with an atmospheric mesoscale model coupled to a slab model representation of an underlying lake. The impact of lake size, effective lake mixed layer depth, background wind speed, air-lake temperature differential, atmospheric humidity, and diabatic heating of the atmosphere on air-sea interaction processes is studied through 67 two-dimensional simulations. The general, quasi-steady solution is a non-linear superposition of a plume circulation driven by the buoyancy of evaporated methane and an opposing thermally direct (sea breeze) circulation driven by the thermal contrast between the cold marine layer over the lake and the warmer inland air. The specific solution depends on the value of selected atmosphere and lake property parameters and ranges from a persistent and strong methane-rich plume circulation over the lake with little to no sea breeze, or a rapidly developing sea breeze with a highly suppressed plume

circulation. The magnitude of sensible and latent heat fluxes varies by up two orders of magnitude depending on the specific solution. The solutions that appear most consistent with limited observational constraints are those where a sea breeze circulation is able to offset the opposing plume circulation. This scenario results in a cool, moist, and statically stable shallow marine layer with nearly calm winds and small turbulent flux exchanges with an underlying lake that is at least 2 K colder than the atmosphere. In contrast, some configurations produced extreme scenarios with strong surface winds that could trigger waves, supersaturated layers at the top of the plume circulation that would be conducive to cloud formation, and lakes cold enough to freeze. These extreme scenarios are unlikely to be realistic based on limited observational constraints.

1. Introduction

The global cycling of methane on Titan must be dominated on short climatological timescales by the exchange between the atmosphere, where the bulk of free methane is thought to reside, and the surface, which includes lakes, seas, and possibly a damp regolith [e.g., Atreya et al., 2006; Lunine and Atreya, 2008; Aharonson et al., 2009; Schneider et al., 2012]. While the amount of methane in the near-surface is uncertain [e.g., Zarnecki et al., 2005; Hayes et al., 2008; Mitchell et al., 2008; Atkinson et al., 2010; Turtle et al., 2011; Hamelin et al., 2012; Turtle et al., 2018] there is no doubt that Titan's surface, particularly the northern high latitudes at present, is covered with lakes that are likely to contain substantial amounts of liquid methane [Cordier et al., 2009; Cordier et al., 2012; Lorenz et al., 2014]. These lakes serve as the only contemporary, persistent, and known source of methane to the atmosphere.

The exchange of sensible heat and latent heat (i.e., evaporation) between the lakes and the atmosphere is accomplished through turbulent fluxes. The study of the turbulent exchange process falls under the research umbrella of air-sea interaction, which has a deep and rich history in the terrestrial literature [e.g.,

Bjerkenes, 1964; Pond, 1971; Hsu, 2005; Bishop et al., 2017]. On Earth, air-sea interaction plays a significant if not dominant role in phenomena that include sea and lake breezes [Pielke et al., 1974; Smith, 1988; Crosman and Horel, 2010], cloud formation [Oliver et al., 1978; Kingsmill et al., 1995; Miller et al., 2003], lake effect snowstorms [Lavoie, 1972; Chou and Atlas, 1982], the El Niño/Southern Oscillation [Emanuel, 1987; Zebiak, 1993; Alexander et al., 2002], and tropical cyclone development [Emanuel, 1986; Wu et al., 2005; Black et al., 2007]. Although sea breezes and ENSO-like climate oscillations have yet to be detected or observed on Titan, the presence of cloud features have been hypothesized to form as a result of sea breeze and local lake evaporation [Brown et al., 2009a; Brown et al., 2009b]. General circulation modeling studies of Titan have shown lakes have an impact on polar meteorology [Tokano, 2009] and the overall global distribution of methane [Lora and Ádámkóvics, 2017]. Variations in the methane distribution are manifested as clouds far from the methane source [Rodríguez et al., 2009; Rannou et al., 2006] and drive deep convection [Mitchell et al., 2009], which provides a mechanism by which evaporated methane is returned to the surface [Tokano, 2011; Hueso and Sanchez-Lavega, 2006; Rafkin and Barth, 2015]. Even tropical cyclones, driven by air-sea interaction, cannot be ruled out on Titan [Tokano et al., 2013].

The importance of air-sea interaction on Titan may extend beyond meteorological features. Sea breezes locally modify the large-scale background wind. Over lakes, the wind perturbations can disturb the lake surface, which is manifested as waves, and winds can drive internal circulations and convection that chemically and thermally mix the lake [Tokano and Lorenz, 2015; Tokano and Lorenz, 2016]. Climatological mean wind speeds at the surface are generally thought to be very weak and unlikely to force waves on a regular basis [Lorenz et al., 2005; Lorenz et al., 2010; Lorenz and Hayes, 2012; Hayes et al., 2013]. Radar observations of Titan lakes generally revealed them to be smooth if not glassy [Wye et

al., 2009; Grima et al., 2017], and the Cassini Visible and Infrared Mapping Spectrometer (VIMS) observed specular reflections that imply little to no lake roughness [Stephan et al., 2010; Barnes et al., 2011; Zebker et al., 2014]. On the other hand, evidence for some wave activity was found [Barnes et al., 2014], and waves are one possible explanation for “magic islands” (ephemeral and localized radar-derived roughness) in Ligeia Mare [Hofgartner et al., 2016]. Sea breezes may be the key to understanding lake roughness observations and may be important for understanding chemical and energy cycling.

There are also future operational and mission applications to better constraining air-sea interactions on Titan. The Titan Mare Explorer (TiME) previously proposed under NASA Discovery would have placed a floating spacecraft in Ligeia Mare [Stofan et al., 2013]. Refined expectations of the meteorology and the air-sea interactions that this spacecraft would have directly experienced and measured would likely have benefited that mission design [Lorenz et al., 2012; Lorenz and Mann, 2015; Lorenz, 2015], as it will for any future Titan lake explorers. While the New Frontiers Titan Dragonfly mission [Lorenz et al., 2018] currently under consideration by NASA will reconnoiter the tropics far from any seas, the physics of air-sea interaction provides useful guidance for interpreting meteorological conditions over damp ground should the dunes turn out to be so.

Air-sea interaction has not been widely investigated on Titan. Mitri et al. [2007], hereafter M07, is presently the most comprehensive attempt to model the process. Using a 1-D analytical model of the lake-atmosphere system, M07 found relatively large lake evaporation rates—sufficient to reduce lake levels by ~0.3 to 10 m over a season in the absence of any precipitation or subsurface resupply. As a consequence of the large evaporation rates ($\sim 0.3 \times 10^3$ to 5×10^3 kg m⁻² yr⁻¹), M07 also determined that evaporation from lakes alone was sufficient, by orders of magnitude, to resupply atmospheric methane

against photochemical destruction. The fundamental principle behind the M07 model is that subsaturated air blowing over a lake will induce evaporation until a balance condition of sensible and latent heat flux is established. Evaporation will cool the lake and moisten the atmosphere. As the lake (but not the atmosphere) cools, sensible heat flux increases. At the same time, the moistening atmosphere and cooling lake drives down the latent heat flux. When the two fluxes are equal and opposite, air-sea interaction is assumed to reach an equilibrium state by which the lake temperature and fluxes may be diagnosed given a constant initial air temperature.

The goal of this paper is to advance the understanding of air-sea interaction on Titan through the use of an atmospheric model that explicitly captures many of the complex, non-linear feedbacks between the atmosphere and underlying liquid reservoir. We seek to establish the nature and dynamics of atmospheric circulations driven by air-sea interaction, the thermodynamic structure of the atmosphere and its potential for cloud formation, and the potential for generating waves that would have been observable by Cassini or future orbiters. We further seek to evaluate and test assumptions of prior models of Titan air-sea interaction, to provide an update on global lake evaporation rates, and to introduce a useful and developing model tool for characterizing the marine environment in support of future Titan concepts and missions.

2. Model Description

We have developed a Titan mesoscale model based on the National Center for Atmospheric Research's (NCAR) Weather Research and Forecasting model (WRF), which we call mtWRF (mesoscale Titan WRF)¹. WRF is an atmospheric model that is regularly used for terrestrial meteorological research and numerical weather prediction. We use the Advanced Research WRF (ARW) dynamical core as the basis for mtWRF. This dynamical core solves the fully compressible, Eulerian, non-hydrostatic fluid equations on an Arakawa C horizontal grid and a modified sigma pressure vertical coordinate [Skamarock, et al., 2008].

The radiative time constant in Titan's lower troposphere is much longer than a Titan year, therefore there is only a very weak diurnal signal in the atmosphere [Tomasko et al. 2008]. Although there is a diurnal signal in the ground temperatures, this signal is primarily in the tropics and over the Titan year the polar regions, where the lakes are located, have almost no diurnal signal in the ground temperature [Tokano 2005]. For these reasons, most of the mtWRF simulations shown here do not use a radiative transfer scheme, although implementation of such a scheme is planned for the future. In a small number of simulations we do explore the effects of atmospheric radiation through the use of a Newtonian relaxation scheme.

We set the atmospheric and surface constants to match those of Titan, as shown in Table 1. Specifically, the atmospheric composition and related thermodynamic properties were changed to match those of a

¹ mtWRF is not related to the TitanWRF model, except that both models are derived from the same terrestrial NCAR WRF model. Otherwise, the development of mtWRF and TitanWRF are independent.

nitrogen atmosphere with methane. The gravity and planetary radius were also changed to Titan values.

Table 1 shows the various model parameters used in the mtWRF model.

Symbol	Unit	Value	Parameter	Ref.
m_{N_2}	amu	28.0134	Atomic weight of N_2	2
m_{CH_4}	amu	16.042646	Atomic weight of CH_4	2
m_{dry}	g/molecule	28.67	Mean molecular weight of air	1
R	$J\ mol^{-1}\ K^{-1}$	8.3145	Molar gas constant for Titan	2
R_d	$J\ kg^{-1}\ K^{-1}$	290.0	Dry air gas constant for Titan	1
R_v	$J\ kg^{-1}\ K^{-1}$	518.275	Methane vapor air gas constant (R/m_{CH_4})	2
$c_{p,air}$	$J\ kg^{-1}\ K^{-1}$	1044.0	Specific heat of Titan's air	1
$c_{p,v}$	$J\ kg^{-1}\ K^{-1}$	1950	Methane vapor specific heat, constant pressure	3
$c_{v,v}$	$J\ kg^{-1}\ K^{-1}$	1431.71	Methane vapor specific heat, constant volume ($c_{p,v} - R_v$)	2,3
$c_{p,l}$	$J\ kg^{-1}\ K^{-1}$	3379	Methane liquid specific heat, constant pressure @ 94 K	5
L_v	$J\ kg^{-1}$	5.1×10^5	Enthalpy of vaporization of methane at 112 K	6,7
ρ_a	$kg\ m^{-3}$	447	Density of the atmosphere at 94 K	5
ρ_{l,CH_4}	$kg\ m^{-3}$	447	Density of liquid methane at 94 K	4
ν_a	$m^2\ s^{-1}$	1.18×10^{-6}	Viscosity (momentum diffusivity) of Titan's atmosphere	11
α_a	$m^2\ s^{-1}$	1.5×10^{-6}	Thermal diffusivity of the atmosphere	5
α_{land}	$m^2\ s^{-1}$	8.93×10^{-8}	Thermal diffusivity of the regolith	9
D_{CH_4}	$m^2\ s^{-1}$	2.05×10^{-6}	Methane vapor diffusivity	5
k_{l,CH_4}	$W\ m^{-1}\ K^{-1}$	0.2	Thermal conductivity of methane liquid	5
k_a	$W\ m^{-1}\ K^{-1}$	0.01	Thermal conductivity of the atmosphere	5,10,11
I_{land}	$J\ m^{-2}\ K^{-1}\ s^{-0.5}$	33gvm4.7	Thermal inertia of a porous icy regolith, i.e. the land	9
I_{lake}	$J\ m^{-2}\ K^{-1}\ s^{-0.5}$	812.4	Thermal inertia of hydrocarbon lakes	9

References:

- [1] PDS Planetary Atmospheres Node, http://atmos.nmsu.edu/education_and_outreach/encyclopedia/gas_constant.htm
- [2] Lodders and Fegley, *The Planetary Scientist's Companion*, Oxford University Press, New York, 1998.
- [3] http://www.engineeringtoolbox.com/methane-d_980.html, with an extrapolation from 200 K to 100 K.
- [4] http://www.engineeringtoolbox.com/methane-d_1420.html
- [5] P.J. Linstrom and W.G. Mallard, Eds., *NIST Chemistry WebBook, NIST Standard Reference Database Number 69*, National Institute of Standards and Technology, Gaithersburg MD, 20899, <http://webbook.nist.gov>, (retrieved January 29, 2016)
- [6] Majer, Vladimír, and Henry V. Kehiaian. *Enthalpies of vaporization of organic compounds: a critical review and data compilation*. Ed. Václav Svoboda. Vol. 32. Oxford: Blackwell Scientific, 1985.

- [7] W.E. Acree, Jr., J.S. Chickos, "Phase Transition Enthalpy Measurements of Organic and Organometallic Compounds" in *NIST Chemistry WebBook, NIST Standard Reference Database Number 69*, Eds. P.J. Linstrom and W.G. Mallard, National Institute of Standards and Technology, Gaithersburg MD, 20899, <http://webbook.nist.gov>, (retrieved February 16, 2015).
- [8] Hayes, A., Lorenz, R., Donelan, M., Manga, M., Lunine, J., Schneider, T., Lamb, M., Mitchell, J., Fischer, W., Graves, S., Tolman, H., Aharonson, O., Encrenaz, P., Ventura, B., Casarano, D., and Notarnicola, C. (2013). Wind driven capillary-gravity waves on Titan's lakes: Hard to detect or non-existent? *Icarus*, 225(1):403 – 412.
- [9] Tokano, T. (2005). Meteorological assessment of the surface temperatures on Titan: constraints on the surface type. *Icarus*, 173(1):222 – 242. Hapke Symposium.
- [10] Hathi, B., Ball, A., Banaszkiwicz, M., Daniell, P., Garry, J., Hagermann, A., Leese, M., Lorenz, R., Rosenberg, P., Towner, M., and Zarnecki, J. (2008). In situ thermal conductivity measurements of Titan's lower atmosphere. *Icarus*, 197(2):579 – 584, doi:<http://dx.doi.org/10.1016/j.icarus.2008.05.006>.
- [11] Stephan, K., Krauss, R., and Laesecke, A. (1987). Viscosity and Thermal Conductivity of Nitrogen for a Wide Range of Fluid States. *Journal of Physical and Chemical Reference Data*, 16(4):993– 1023, doi:<http://dx.doi.org/10.1063/1.555798>.

The atmospheric surface layer is the layer where there are turbulent exchanges between the surface and atmosphere. mtWRF uses Monin-Obukhov (MO) similarity theory as described by Janjić [1990, 1994] to calculate surface fluxes; this is the Mellor-Yamada-Janić (MYJ) physics option in WRF [Skamarock et al., 2008]. The MO parameterization solves for the bulk aerodynamic coefficient, C_D , in the bulk aerodynamic flux formulation:

$$\rho_a \overline{w'\chi'} = C_D \|\vec{V}\| (\chi_a - \chi_{sfc}) \quad (1)$$

where ρ_a is atmospheric density, $\overline{w'\chi'}$ is the Reynolds averaged correlation of subgrid vertical velocity (w) and the quantity of interest (χ), \vec{V} is the horizontal wind vector at the roughness height, and $\chi_a - \chi_{sfc}$ is the difference between the value of the quantity in the atmosphere and surface. C_D is a function of subgrid scale turbulence, as diagnosed through the Bulk Richardson Number, which itself is a function of atmospheric stability and wind shear. Fluxes will tend to be large if turbulence is large (e.g., an unstable atmosphere or large wind shear), if wind speed is large, or if there is a large difference between the

atmosphere and surface property. In contrast, a stable atmosphere, low wind speeds, or similar atmospheric and surface properties will result in a reduced flux.

Because of the lower Titan gravity, the relationship between the roughness length, z_0 , and the friction velocity, u_* , are modified from the base WRF code. In Janjic [1994], the roughness length is calculated as:

$$z_0 = \frac{0.11\nu_a}{u_*} + \frac{0.018u_*^2}{g}$$

where ν_a is the viscosity (momentum diffusivity) of the atmosphere and g is the gravity. Fig. 1 shows the difference between the friction velocity generated roughness length on Titan versus Earth. On Titan, the roughness length is larger for nearly all values of friction velocity.

Traditionally, the atmospheric surface layer over a liquid body has been partitioned into three regimes: (1) a smooth and transitional regime, (2) a rough regime, and (3) a rough regime with spray [Janjic, 1994]. The transitions between these regimes, determined by a roughness Reynolds number ($Rr = z_0u_*/\nu$), represent an increase in the roughness and wave activity of lake and ocean surfaces. Since Cassini observations have only seen smooth to possibly slightly perturbed lake surfaces (Grima et al. 2017), we have applied only the smooth and transitional portion of the atmospheric surface layer calculations. This configuration is appropriate for the available data and the type of initial mesoscale investigation that we are conducting.

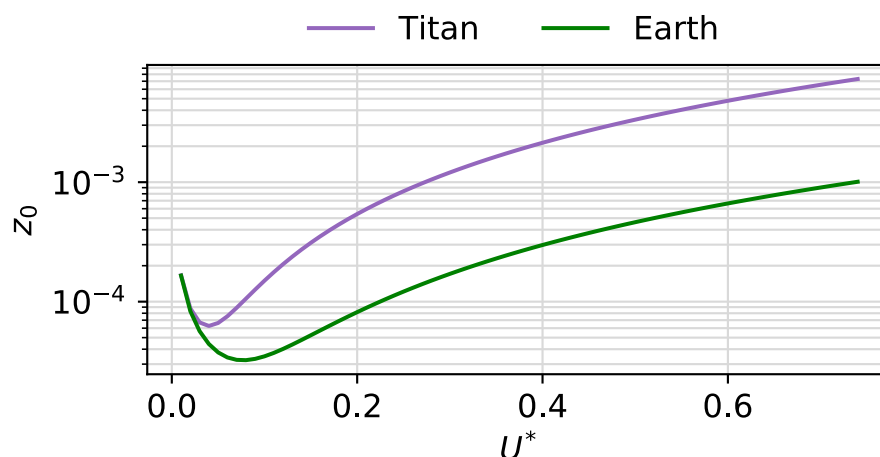


Figure 1. The relationship between z_0 and u_* for Titan and Earth, based on the formulation from Janjic [1994].

Calculating the exchange of fluxes between the subsurface and the surface for both lakes and land requires values for the molecular diffusivities of momentum, heat, and methane vapor. The MYJ scheme uses diffusivities that are constant with respect to temperature and pressure. The NIST Chemistry Webbook provides the atmospheric viscosity of a pure nitrogen atmosphere for a range of temperatures and pressures [Lemmon et al. 2017]. Fig. 2 shows the momentum diffusivity (i.e., kinematic viscosity), the thermal diffusivity, and the methane vapor diffusivity as a function of temperature from 90 K to 100 K. Similarly, the thermal diffusivity was derived from the thermal conductivity provided by the NIST Chemistry Webbook. Finally, the vapor diffusivity for methane in Titan’s atmosphere was derived using an equation from Graves et al. [2008] and Lorenz [1993]. The surface layer physics in mtWRF use a constant value for each of the diffusivities, and the values at 94 K are chosen for mtWRF, as shown in Table 1 and Fig. 2.

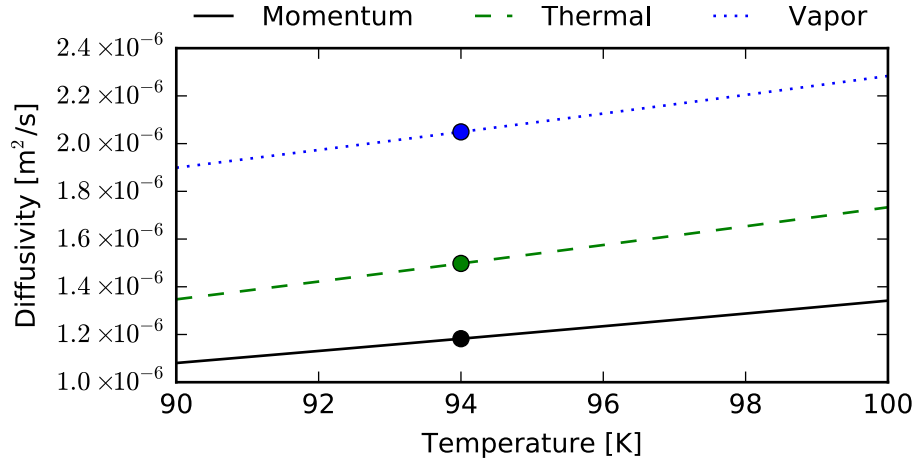


Figure 2. The momentum, thermal, and vapor diffusivities of Titan's atmosphere as a function of temperature. The circle represent the values used in mtWRF. The value of the fixed diffusivities are within 10% the range of values expected for typical Titan surface temperatures.

The surface fluxes of heat and moisture generated by the atmospheric surface layer scheme are the lower boundary conditions for the planetary boundary layer (PBL) scheme that parameterizes subgrid scale atmospheric eddy diffusion. The model uses the Mellor-Yamada-Janjic (MYJ) implementation to calculate turbulent kinetic energy vertical mixing the in the PBL [Skamarock et al., 2008].

We included a slab lake model in mtWRF to account for a cooling lake on Titan. This slab model assumes that thermodynamic and energetic balance occurs instantaneously over a single layer in the lake with a thickness defined as the mixed layer depth. Since radiative transfer is assumed unimportant over the mesoscale simulation timescale, the slab lake model has only three variables: lake depth, sensible heat flux, and latent heat flux, which form a prognostic lake temperature equation:

$$\frac{dT_L}{dt} = -\frac{1}{c_L \rho_L D} (c_A \rho_A \overline{w' T'} + L \rho_A \overline{w' q'}) \quad (2)$$

where T_L is the lake temperature, t is time, c_L is the lake specific heat, ρ_L is the lake density, D is the depth of the lake, c_A is the atmospheric specific heat, ρ_A is the atmospheric density, w is the upward velocity, T

is the atmospheric temperature, L is the enthalpy of vaporization, and q is the specific humidity. Fig. 3 shows the lake cooling rates achieved for a range of lake depths and heat fluxes ($c_A \rho_A \overline{w' T'} + L \rho_A \overline{w' q'}$). As expected, the shallow mixed layers can quickly cool. A 10 meter deep lake with a 100 W/m^2 of upward heat flux will freeze (lake temperature somewhere below $\sim 90 \text{ K}$) in a handful of tsols while a 500 meter deep lake with 100 W/m^2 of upward heat flux requires a good part of a Titan season to do the same.

The saturation vapor pressure for methane over liquid methane is calculated from the vapor pressure relation provided by Moses et al. [1992]. Binary (N_2 and CH_4) or more complicated solutions of liquids (e.g., addition of C_2H_6) is not directly accounted for, but could be approximated through a simple scaling constant that adjusts the saturation vapor pressure based on the assumed mixture of compounds. With respect to the moisture flux (Eq. 1), such a constant is effectively the same as altering the atmospheric humidity so that the difference between the atmospheric vapor content and saturation vapor content is appropriately changed.

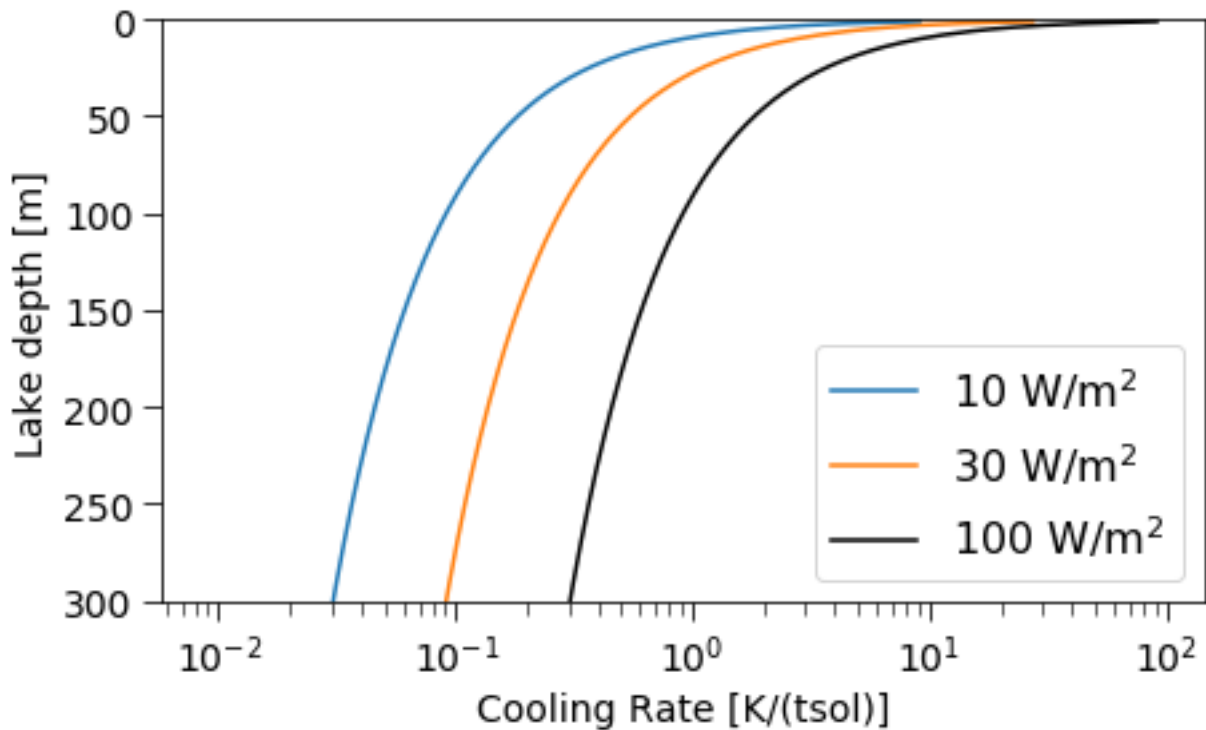


Figure 3. Lake mixed layer cooling rates for a range of mixed layer depths and upward surface energy fluxes in the single slab lake model. The cooling rates are shown for a Titan day (tsol), which is ~ 15.95 Earth days.

Over land, the surface is assumed to be dry and the surface temperature is fixed at the value specified at initialization. Latent heat fluxes are not calculated over land, but sensible heat fluxes are, and the constant land surface temperature implies that the ground serves as an infinite heat reservoir.

To initialize the mesoscale simulations, we started with vertical temperature and methane mixing ratio data obtained from the Huygens Atmospheric Structure Instrument (HASI) and the Gas Chromatograph Mass Spectrometer (GCMS) on the Huygens lander probe [Fulchignoni et al., 2005; Niemann et al., 2005]. This baseline sounding was then modified to meet the specific goals of the numerical modeling experiments. The resulting sounding was used to uniformly initialize the model. Because Titan's atmosphere exhibits only a small variation of temperature as a function latitude and longitude, the HASI

temperature profile is very similar to temperature profiles measured by the Cassini Radio Occultation experiment and the Voyager mission [Schinder et al., 2011], particularly in the lower portion of the atmosphere. Thus, using the HASI temperature profile in our soundings was reasonable for our idealized experiments.

For the initialization of methane humidity in the atmosphere, the majority of simulations are started with a sounding that has zero atmospheric methane. To understand the effects of an initial atmospheric methane profile, two types of initial methane profiles were created (Fig. 5). The first profile type has a constant relative humidity from the surface up to 30 km, after which the profile follows a constant mixing ratio. Generally speaking, because temperature decreases with height, a constant relative humidity profile translates to a decrease in mixing ratio as a function of height. We classify this first type of profile as “unstable”, because the initial virtual temperature profiles have vertical buoyancy due to the gradient in methane mixing ratio (Fig. 6). The second profile type has a constant mixing ratio from the surface up to the height where the relative humidity reaches 100%. At this point, the mixing ratio follows the methane saturation curve up to 30 km, after which the profile follows a constant mixing ratio. Since mixing ratio is constant in the lower atmosphere, and because temperature is decreasing with height, these profiles are stable; there is no initial buoyancy at the surface. The constant methane mixing ratio from 30 km to the top of the model matches the constant mixing ratio observed by the Huygens GCMS [Niemann et al., 2005, Niemann et al., 2010].

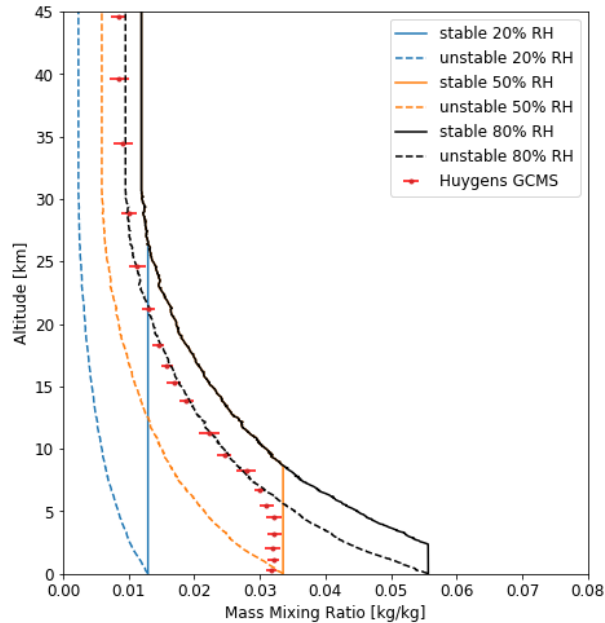


Figure 5. The mixing ratio as a function of altitude for various methane soundings (lines), compared to the Huygens GCMS data (red points with error bars) taken from Niemann et al., [2010].

For each type of methane profile, we generated profiles with an initial surface relative humidity of 20%, 50%, and 80%. Fig. 5 displays all six methane profiles compared to the methane profile measured by the Huygens GCMS [Niemann et al., 2010]. All three of the stable profiles eventually follow a 100% relative humidity curve at altitude. Fig. 6 shows the virtual potential temperature profiles calculated using the methane soundings in Fig. 5 and the temperature profile provide by the HASI data. Any profile where the virtual potential temperature decreases with height is statically unstable. The stable profile that starts with 50% relative humidity at the surface most closely resembles the Huygens GCMS data. By running simulations of both the unstable and stable methane profiles, we have explored a wide range of possible methane soundings that may occur on Titan.

Most of the simulations were initialized with a sounding that had no initial horizontal or vertical wind. In the few simulations that had an initial wind, a vertically uniform wind was applied to the sounding (see Table 2 for a list of simulations and their initializations).

The model domain is 1600 km wide and approximately 20 km deep. The width and depth were chosen so that lateral and top boundaries were significantly distant from the lake, which is centered in the horizontal domain. The maximum lake dimension varies from 32 km to 300 km depending on the simulation. Horizontal grid spacing is 2 km, which is adequate for resolving the structure of a sea breeze. The lowest level vertical spacing is approximately 3 m and is gradually stretched with height to approximately 500 m spacing at the top of the model. There are 60 vertical levels.

The horizontal boundary conditions of a mesoscale model (or any model) have the potential to generate non-physical signals that propagate through the rest of the model domain. This propagation of boundary-generated noise is particularly challenging for idealized simulations that require numerical conditions rather than physically-generated values. We have experimented with both open and periodic boundary conditions as well as a number of domain sizes in order to find an initial model configuration that generates numerically stable simulations over the longest duration possible. We desire to run these mesoscale simulations as long as reasonably possible to insure that our experiments are reaching a dynamic and thermodynamic steady-state. To do so, we needed to minimize numerical noise generated by the boundary conditions. Based on numerous experiments, the mtWRF simulations are run with open or periodic boundary conditions that are set many 100s of km away from the edge of a simulated lake, which typically provides stable simulations that run for at least 10 tsols. The numerical considerations of

a very weakly forced system like Titan are of great enough concern that a section of this paper is dedicated specifically to this topic.

The model integration produces tendencies in SI units of seconds (s); however, units of hours or days in this paper are with respect to Titan. A Titan day is known as a Titan sol or tsol for short, and there are 24 hours in a tsol. Seconds retain their SI definition.

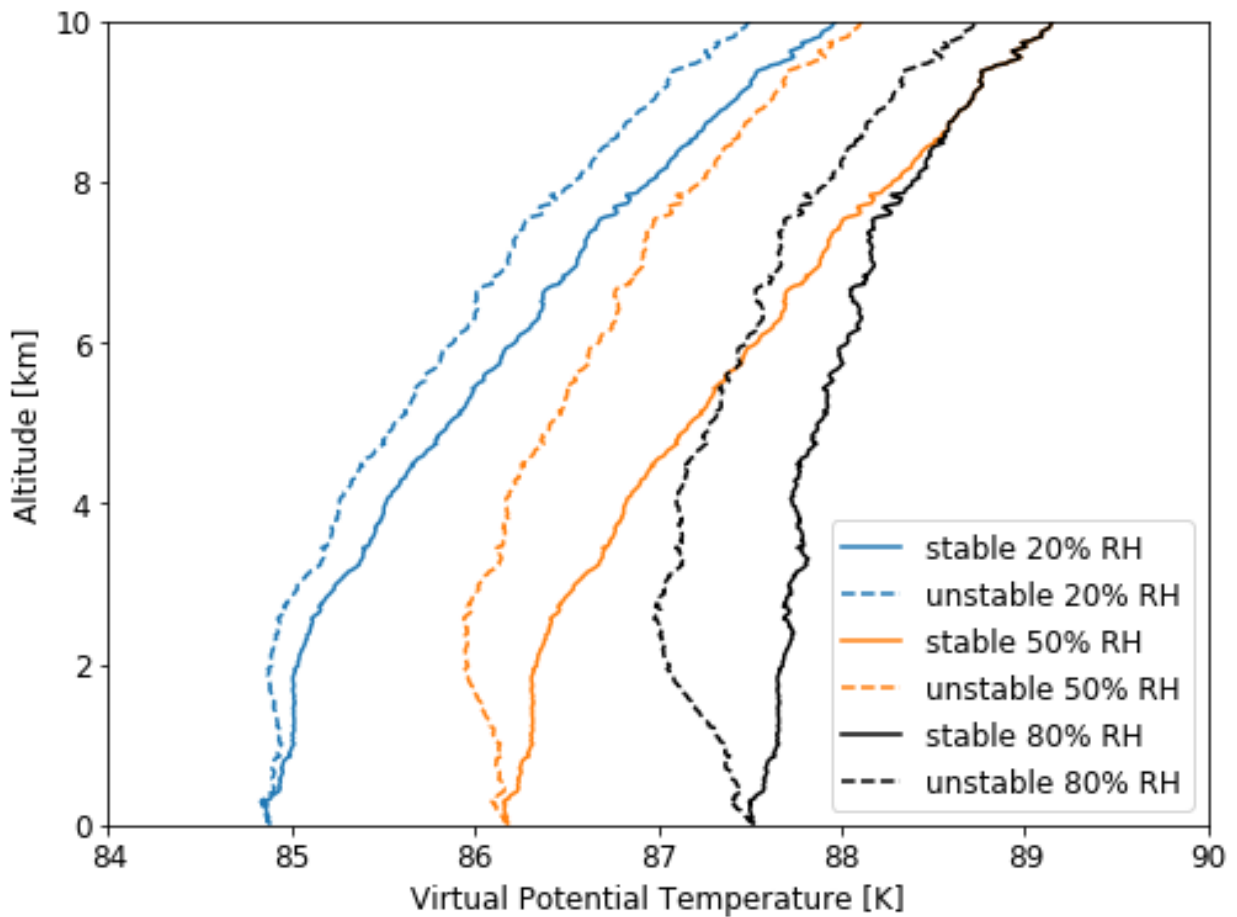


Figure 6. The virtual potential temperature profiles of the six methane soundings, calculated by using the temperature profile from the HASI instrument.

3. The Canonical Circulation

All the simulations performed in this study show the same general solution; the different, specific solutions are variations on a theme that is illustrated schematically in Fig. 7. Since the atmosphere is initially set to a subsaturated condition, there is an initial burst of evaporation. The increase in methane vapor produces a virtual temperature effect—an increase in positive buoyancy due to the lower molecular weight methane compared to the moist nitrogen atmosphere. Compared to water vapor on Earth, methane is $18 \text{ g mol}^{-1}/16 \text{ g mol}^{-1} = 112.5\%$ more buoyant on a molecule per molecule basis. That buoyancy effect can be further magnified on Titan, because the saturation mixing ratio of methane is usually much higher than water. The result of the positive buoyancy is a rising plume of moist air and the accompanying

circulation demanded by mass conservation: A land breeze converging over the center of the lake and a divergent circulation aloft. The circulation is generally fully mature in ~6 hours, although there is some variability depending on the specifics of the modeling scenario.

The evaporating lake cools as the land breeze intensifies, which initiates a sensible heat transfer from the atmosphere to the lake and the cooling of the near-surface atmosphere. Over time, the growing pool of cold air over the lake initiates a direct thermal simulation—a sea breeze—circulating in the opposite sense of the land breeze. Generally, the sea breeze circulation tends to be shallower than the plume land breeze, and destructive interference is most pronounced in the lowest layers of the atmosphere. The result is a decrease of surface winds above the lake. The decrease in wind speed in conjunction with the increasingly stable atmosphere leads to a diminishment of all fluxes (Eq. 1). The final quasi-steady state is a very shallow, cold, stable, and moist (but not saturated) marine boundary layer over the lake. Fluxes over the lake are small due to low wind speeds and increased stability. The latent heat flux is also reduced, because the cooling lake lowers the saturation vapor pressure, and when combined with the moistening atmosphere, the vertical moisture gradient is reduced (Eq. 1). The final, quasi-steady solution is a classic cool and stable marine boundary layer.

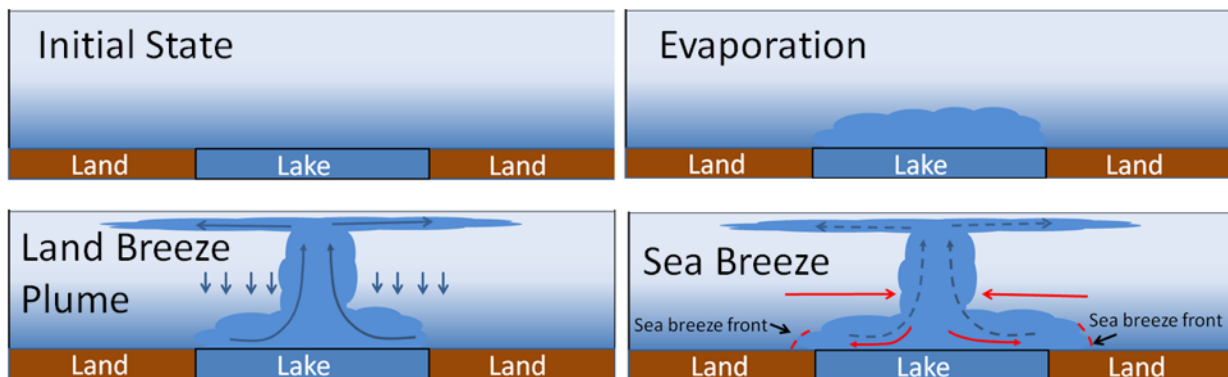


Figure 7. Idealized evolutionary states of an atmospheric circulation associated with a Titan lake. Note that blue shading in the atmosphere represents vapor structures not cloud. Starting from an initial static state with a subsaturated atmosphere and identical lake and atmosphere temperatures (top left), evaporation results in the moistening of the atmosphere directly above the lake (top right). The moist air is buoyant and a plume of methane-rich air rises, which establishes a land breeze circulation (dark arrows, bottom left). The lake cools due to evaporation, which increases as the land breeze intensifies. The atmosphere above the lake begins to cool through sensible heat fluxes. As the air cools, density increases and begins to drive a sea breeze circulation (red arrows, bottom right) acting in opposition to the land breeze (dashed arrows, bottom right). Destructive interference between the two circulations results in a decrease of near-surface winds. The atmospheric stability also increases, which tends to decrease latent and sensible heat fluxes. A sea breeze front demarcates a narrow transition between the land air mass and the marine layer.

Of course, on real Titan the atmosphere doesn't "spin-up" from some arbitrary initial condition. The model spin-up period might be regarded as an unrealistic state to be neglected until a more steady-state solution is obtained. Complete neglect of the spin up solution, however, would overlook the tendency for a real buoyancy circulation to operate behind whatever net, steady-state circulation may be present. The forcing behind a buoyant land breeze circulation is a real physical process. The strength of the initial plume circulation, the strength of the sea breeze, and the overall evolution and balance between these two opposing circulations depends on a variety of factors including the temperature differential between the lake and that atmosphere, the initial atmospheric humidity, and the depth of the lake mixed layer.

Results from a simulation with a 300 km lake illustrate well the canonical solution (Fig. 8). For reference, Ligeia Mare, the second largest lake on Titan has dimensions of approximately 350 x 420 km. The largest lake, Kraken Mare is closer to 1000 km x 400 km. Thus, a 300 km lake (in 2-D) is representative of the larger lakes on Titan. The fields are averaged over a period of 6 Titan hours (24 hours per tsol) in order to mute transient (but physically real) circulations that would otherwise obfuscate the bulk circulation. The vertical domain is truncated in the plots so that greater detail can be seen in the lower atmosphere where the bulk of the circulation is found. Recall that the top of the model domain is approximately 20 km.

The initial plume circulation is evident within the first 6-hour averaging period (Fig. 8a). A bubble of methane-rich air has broken away from the surface source and has nearly reached its buoyant equilibrium level near 4 km. The width of the plume is approximately the same as that of the lake, although the zero mixing ratio contour line indicates that a limited amount of moisture has made its way inland. The circulation accompanying the buoyant plume is clearly defined by low level inflow and upper level outflow. Over time, this circulation would be expected to keep the low level moisture horizontally confined close to the lake while advecting methane to greater distances in the outflow aloft. Since the low level flow is from the dry land toward the moist lake, the moistening over land must be due to some amount of downward mixing from the moist air aloft. The high methane mixing ratios in the shallow atmospheric layer just above the lake will eventually evolve into the stable marine boundary layer. The peak average wind speeds are approximately 1 m/s, although the surface winds are smaller in magnitude due primarily to the effect of surface friction.

After one tsol (Fig. 8b), a sea breeze circulation has been established. It is confined roughly to the dimensions of the lake and is, initially, approximately the same depth (~3.5 km) as the plume circulation. Meanwhile, the remnants of the initial plume circulation have propagated out towards the edge of the domain. Separating the two circulations is a region of overturning winds. Examination of intermediate times (e.g., via an animation using supplementary data) shows that the intervening region of disorganized winds propagates outward as what can best be described as a long wavelength solitary gravity wave [e.g., Christie et al., 1978]. Presumably, this transient wave is triggered by the modestly rapid development of the sea breeze which runs counter to the plume circulation.

By two tsols (Fig. 8c), the transition region has begun to move out of the domain. It leaves in its wake the background plume circulation, which is to say that the transition region appears to move through the steadier plume circulation. There is some disruption of the coherence of the background plume circulation, but it is still clearly evident in the wake of the transient wave. This is what might be expected of a gravity wave moving through a steadier background state. The enhanced export of vapor at altitude is now clearly evident, while the low level vapor remains largely confined within the lake boundaries.

At three tsols (Fig. 8d) the quasi-steady solution has been obtained. Over the lake, a mature sea breeze circulation is present, and the marine boundary layer remains confined to the immediate vicinity of the lake. Any vapor found at a distance from the lake is due almost entirely to the transport from the initial plume circulation. Above the main sea breeze circulation cell is the remnant plume circulation outflow, and above that are vertically damped gravity waves. The overall vertical scale of the combined sea breeze and larger buoyancy circulation remains at ~ 3 km. The sea breeze circulation is confined to the lowest ~ 2 km and the marine layer is only 200 m to 300 m deep.

Fig. 9 focuses on the rightmost half of the sea breeze. The structure of the leftmost sea breeze is nearly identical. Three distinct regions can be identified based on wind, vapor, and temperature structure. The first region is the marine layer directly over the lake. The second region is a transition region extending from the lakeshore to the sea breeze front located at approximately $x=1005$ km. The third region is the nearly unmodified atmosphere further inland. The sea breeze does continue to move slowly inland with time even though the structure is quasi-steady state. By five tsols, the sea breeze front is at $\sim x=1100$ km (not shown). The frontal displacement of ~ 100 km over two tsols gives a propagation speed of ~ 3 cm/s.

Simulation 4

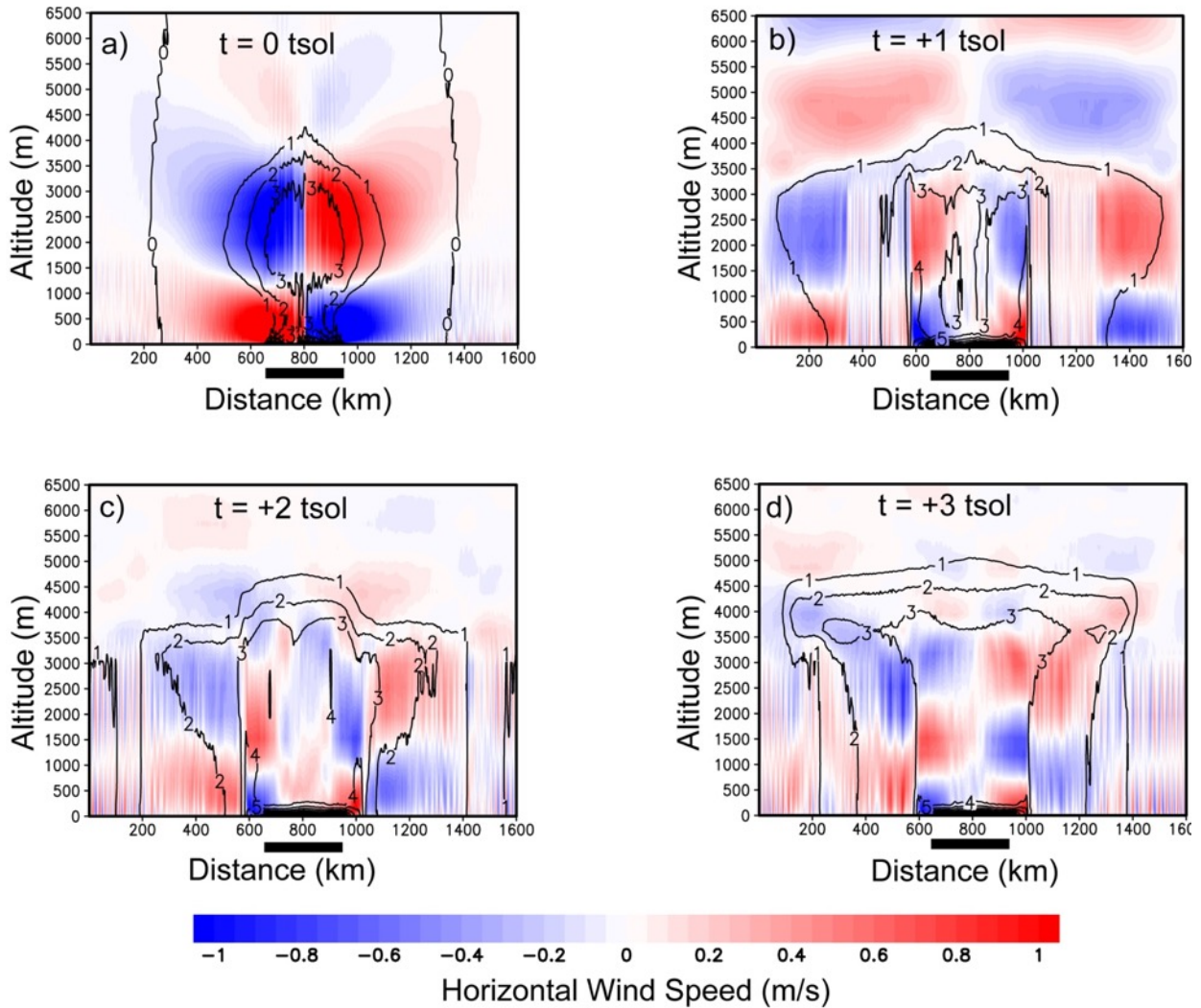


Figure 8. Bulk sea breeze evolution for a 300 km lake. Horizontal velocity is shaded with red (positive) values indicating flow from left to right and blue (negative) values indicating flow from right to left. Contours are methane mixing ratio (g/kg). The 300 km lake domain is shown by the black bar below the horizontal axis. The initial buoyant vapor plume (a) is gradually replaced by a quasi-steady sea breeze circulation with fronts that remain just beyond the coast in (c) and (d). All fields are averaged over a 6 hour period with the referenced time indicating the starting time of the 6 hour average.

The marine region is characterized by an extremely stable and shallow (< 300 m) boundary layer with a relative humidity that peaks at only ~30%. This is moist compared to the initial dry atmosphere. The

temperature in the lowest atmospheric layer is 92.7 K compared to almost 94 K farther inland. It is not well mixed, and vertical motion is suppressed in the highly stable layer. The onshore flow in the marine layer increases as a function of height up to the top of the inversion. The onshore flow persists up to ~800 m where it reverses to form the sea breeze return flow. Vertical motion is more evident in the return circulation where the atmospheric stability is lower. Although the marine layer is very shallow, the atmosphere over the lake is colder than the atmosphere over land up to an altitude of ~1 km. The marine layer is moist, but it is not near saturation, and no clouds would be expected to form. A more detailed analysis of the possibility of clouds is given in Section 8.

The transition region is marked by an increase in horizontal and vertical wind variability indicative of convective overturning. The intensity of the convection is small at the lakefront, but grows rapidly more intense over land up to the sea breeze front. Due to the convection, the horizontal wind is not steady-state, and the direction changes as convection cells evolve. The vapor field shows an increase in height from the nominal ~200 m at the shoreline up to ~1 km at the front, although the highest values of moisture remain over the lake. At least part of the decrease in peak vapor values in the transition region can be attributed to the increased mixing associated with the convection that more evenly distributes the vapor over the depth of the boundary layer. Temperatures are notably warmer at the lakefront and increase moving inland towards the front. The capping inversion gradually erodes until it is completely gone at the front.

The sea breeze front is marked by a sharp transition from the moist marine layer into the very dry air mass over land. What vapor there is over land was dominantly transported there by the upper portion of the initial plume circulation. There is also a well-defined increase in temperature horizontally across the front

up to a height of ~ 1 km. Convection intensity is notable in both the horizontal wind and vertical wind on land side of the front. Vertical velocity over is > 50 cm/s at ~ 1.5 km altitude on the land side of the sea breeze with the highest values tending to occur at or nearby the front; however, there are turbulent circulations and vertical velocity updrafts/downdrafts of ~ 5 cm/s over land extending to the edge of the modeling domain (not shown). The juxtaposition of the cold marine air over the warm land produces a shallow unstable convective layer that drives the turbulence. By Earth standards, both the horizontal and vertical wind speeds are small, but on Titan, these perturbations are modest and may very well be typical.

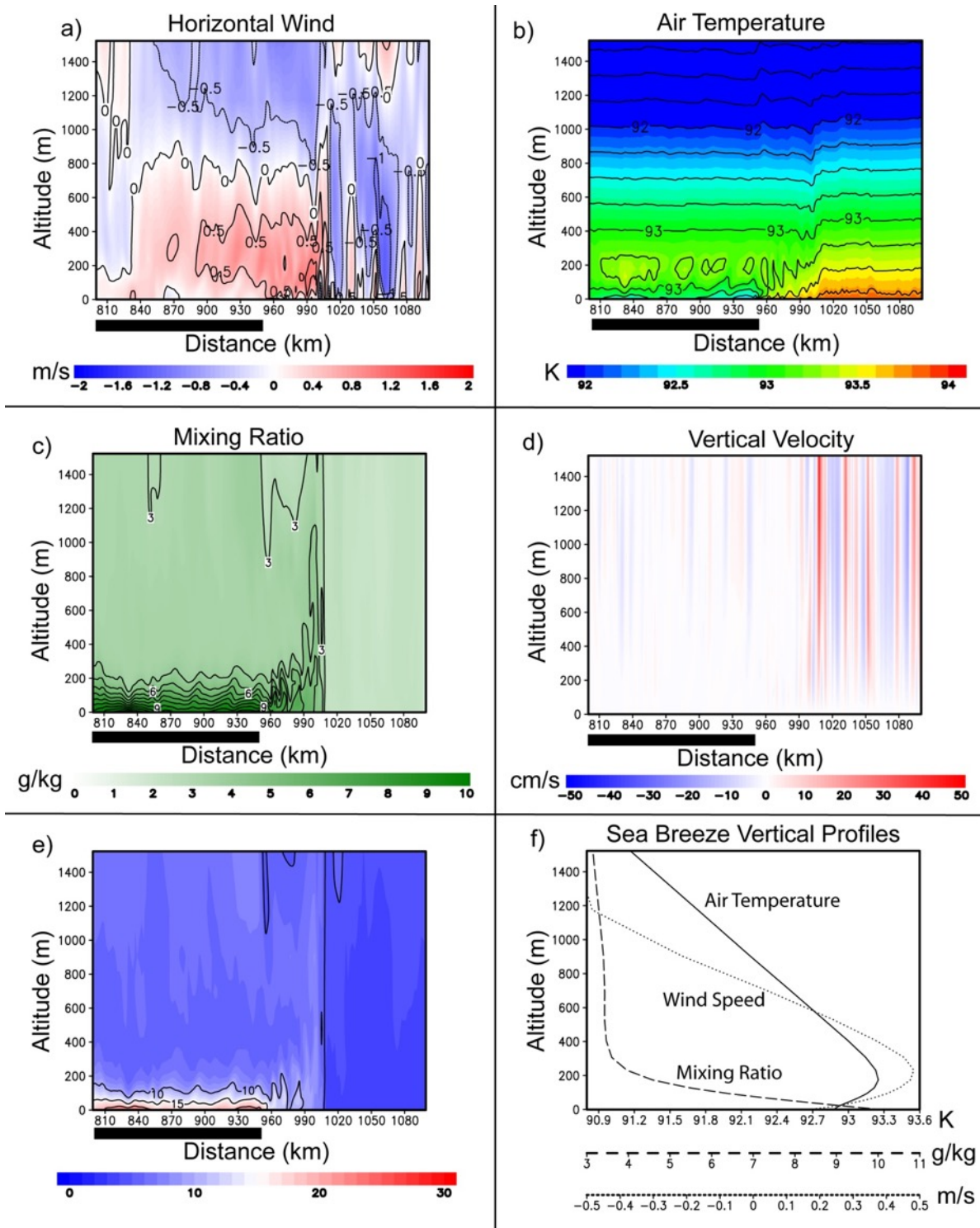


Figure 9. The instantaneous (not averaged) sea breeze and marine boundary layer structure (a-e) for Simulation 4 at 3 tols. The domain occupied by the lake is shown as a black bar on the horizontal axis. Panel (f) is also instantaneous in time, but horizontally averaged from 800 km to 1000 km.

Analysis of the lake temperature, near-surface wind and air temperature, and surface fluxes explains the behavior and structure of the atmosphere over the three regions. Hovmöller diagrams (Fig. 10) provide a good overview of the variations and their relationship to one another. The sign of the fluxes are defined with respect to the atmosphere, so that a positive sensible or latent heat flux represents an energy gain by the atmosphere. Additional insight is gained by averaging the properties over the lake to a single value and exploring the variations over time (Fig. 11). The time series of properties at a single near-surface point (Fig. 12) is also instructive, because it brings out details that are lost in the averaging and which are difficult to visually extract from the Hovmöller presentations.

The effect of the initial plume circulation is clear in Fig. 10. A burst of latent heat flux occurs at the start of the simulation, and once the lake begins to cool the heat flux begins to ramp up in response to the plume circulation. In less than one τ_{sol} , the fluxes over the lake drop back down to smaller values due to the establishment of the stable marine boundary layer. In contrast, the sensible heat flux at the shoreline and just inland are at a maximum once the marine layer develops. As discussed above, this is the result of the cold marine air flowing over the warm land.

Regardless of the magnitude of latent and sensible heat flux over the lake, the Bowen ratio is remarkably without any fine-scale spatiotemporal structure. The ratio slowly increases in magnitude in time (becoming increasingly negative), and the most negative values are found near the shore. The lake surface temperature shows a similar pattern suggesting that it is the dominant controlling factor in the Bowen

ratio. Even though the turbulent fluxes are bursty and transient in nature, the Bowen ratio remains steady. The constancy of the Bowen ratio is remarkable in the average (Fig. 11) and even instantaneously (Figs. 10 and 12). There is a very strong coupling between the sensible and latent heat flux such that their ratio is nearly invariant no matter the magnitude of turbulent flux activity.

The Hovmöller diagrams (Fig. 10) show coherent spatial structures except in the Bowen ratio and lake surface temperature. Some of these structures move from the center of the lake outward toward the coast while others emanate from the coastline and move toward the center of the lake. Since these patterns occur simultaneously, at least some of the features propagate counter to the prevailing wind and cannot be advective. Gravity waves launched at the sea breeze front and those associated with the plume circulation are likely mechanistic candidates. As the coherent structures move across the lake, the fluxes respond to the small changes in wind speed, temperature and vapor. Where the winds are strongest, the fluxes are largest, and changes in air temperature and vapor follow from that.

The instantaneous values (Fig. 12) have a signature of the coherent structures as they pass over a point on the lake. There are periods of several hours where the sensible and latent heat fluxes increase in magnitude by a factor of two to four. These periods are well correlated with an increase in wind speed, mixing ratio and relative humidity. The bulk of the change in humidity appears to be due to changes in vapor content rather than air temperature. The air temperature also has variability, but the magnitude of the changes is muted compared to the other parameters. Turbulent mixing is likely damping the air temperature variations that should be directly connected to the sensible heat flux.

The lake cools most rapidly during the strong methane plume phase of the simulation. Once the plume circulation settles down and the sea breeze is established, it is generally coldest near the lake shore where the winds tend to be strongest and warmest at the center of the lake where there is a wind stagnation point. Fetch distance appears to play a role in this, as the sensible heat flux continually cools the air as it traverses over the lake. Importantly though, the magnitude of the fluxes are also largest at the shoreline, primarily due to the strong winds, and this contributes to a strong local cooling. Fetch may allow for an increase in wind speed close to shore, but as noted above, that is also the nature of a sea breeze with a stagnation point over the center of the lake. Due to the initial plume circulation, the lake temperature drops below what is likely to be the freezing point. Since the model does not have lake phase change physics, the lake continues to cool to perhaps a nonphysical state. The possibility and implications of a frozen lake are considered in Section 6.

Since the Bowen ratio never reaches -1.0 , flux equilibrium between the sensible and latent heat fluxes is not achieved [Mitri et al., 2009]. This means that the lake will continue to cool, which little by little should continue to strengthen the marine inversion, continue to stabilize the air, and feedback to suppress and limit the fluxes. If a flux equilibrium condition were to be achieved it would likely take many tens of tsols, and at the point the value of the fluxes may very well be effectively zero. The rate of cooling (Fig. 11 and Fig. 12) decreases with time, and this is tied directly to the decrease in flux magnitude with time.

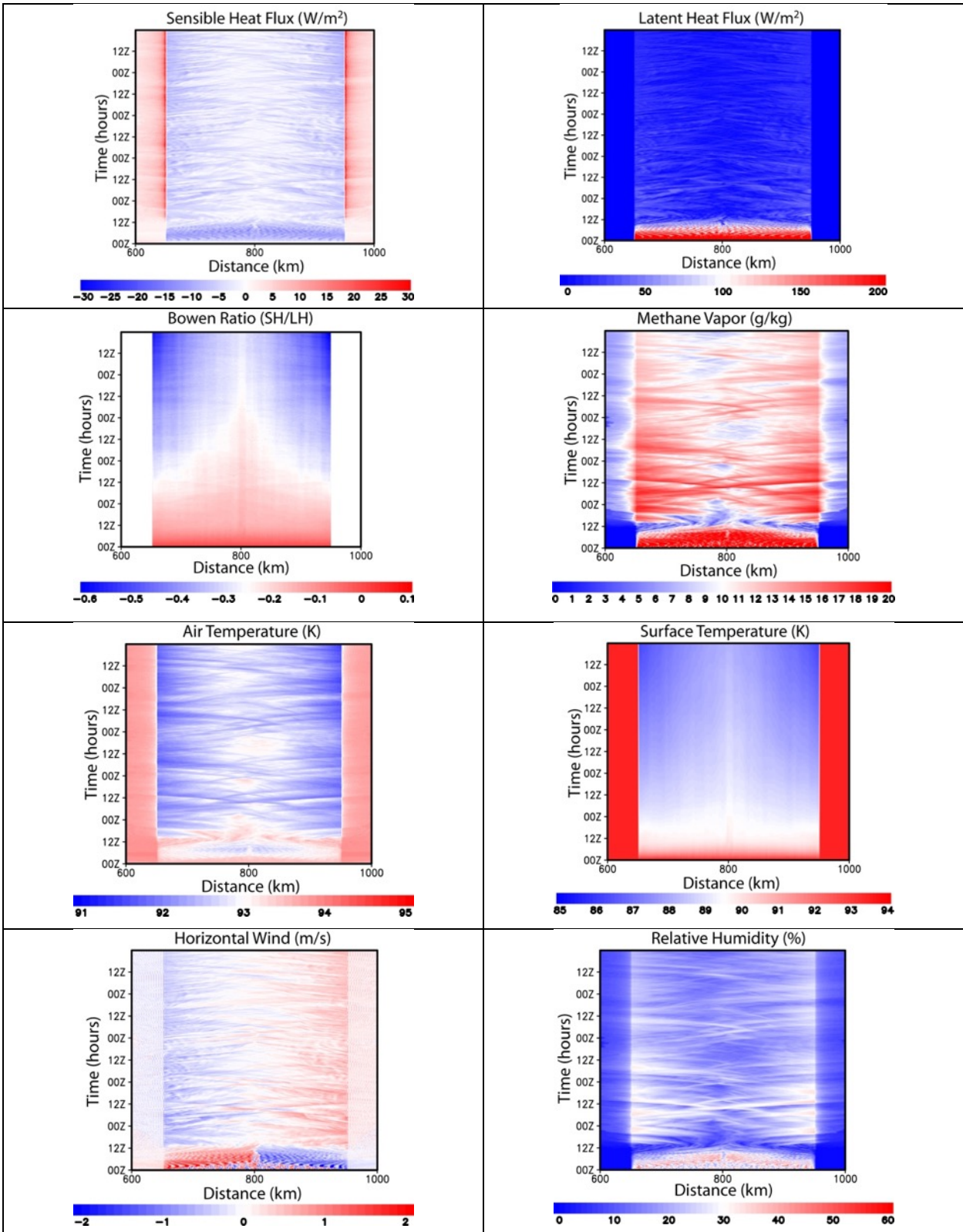


Figure 10. Hovmöller diagrams of canonical lake and atmospheric properties from Sim4. The spin-up period dominated by a vapor plume circulation is less than 1 tsol. After spin-up, a sea breeze circulation develops superimposed on the plume circulation. The lake extends from 650 to 950 km.

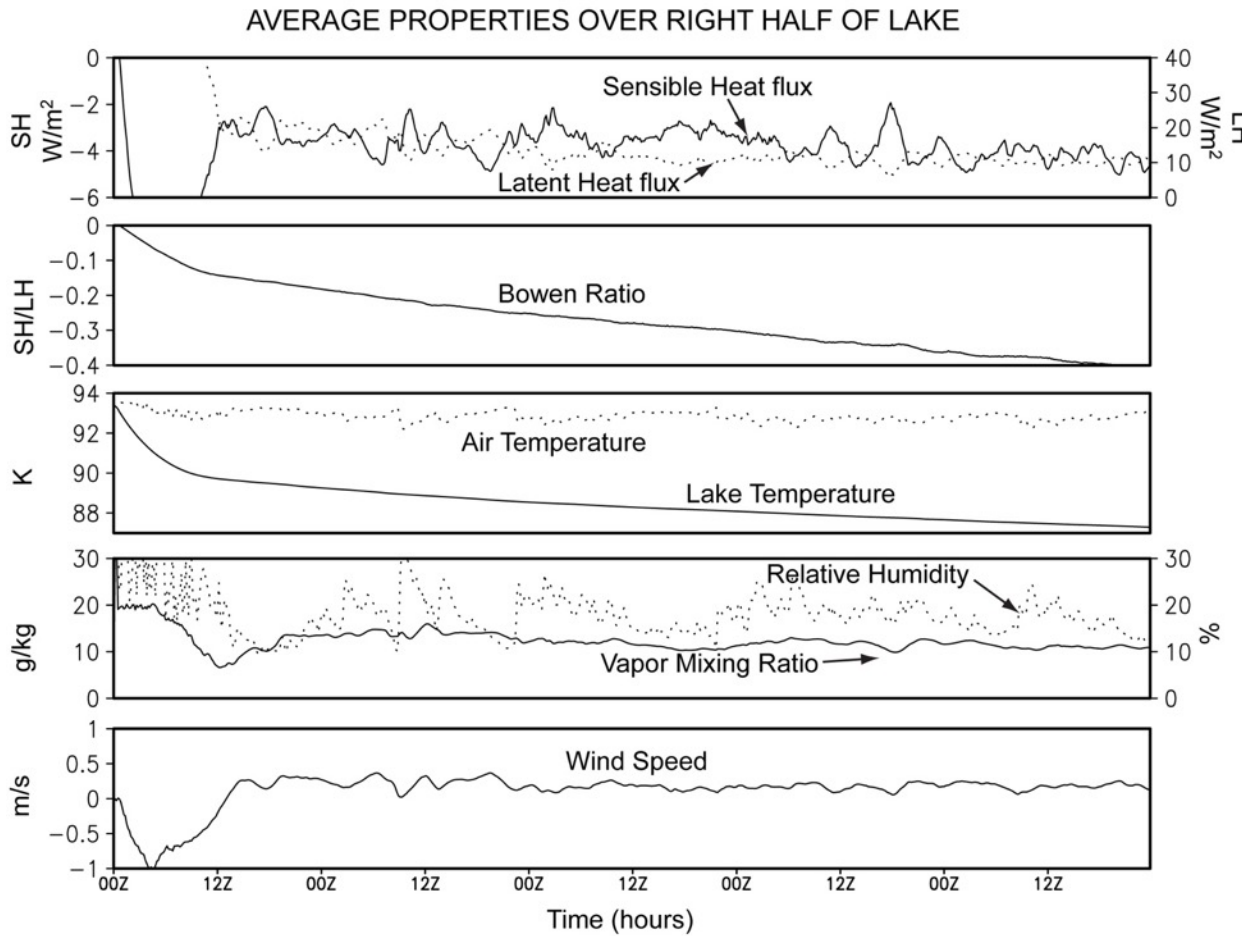


Figure 11. Average properties over right half of the lake for Sim4 (300 km lake). Top to bottom: Sensible heat flux (solid W/m^2) and Latent heat flux (dotted W/m^2); Bowen ratio; SST (solid K) and air temperature (dotted K); methane mixing ratio (solid g/kg) and relative humidity (dashed %); wind speed (m/s).

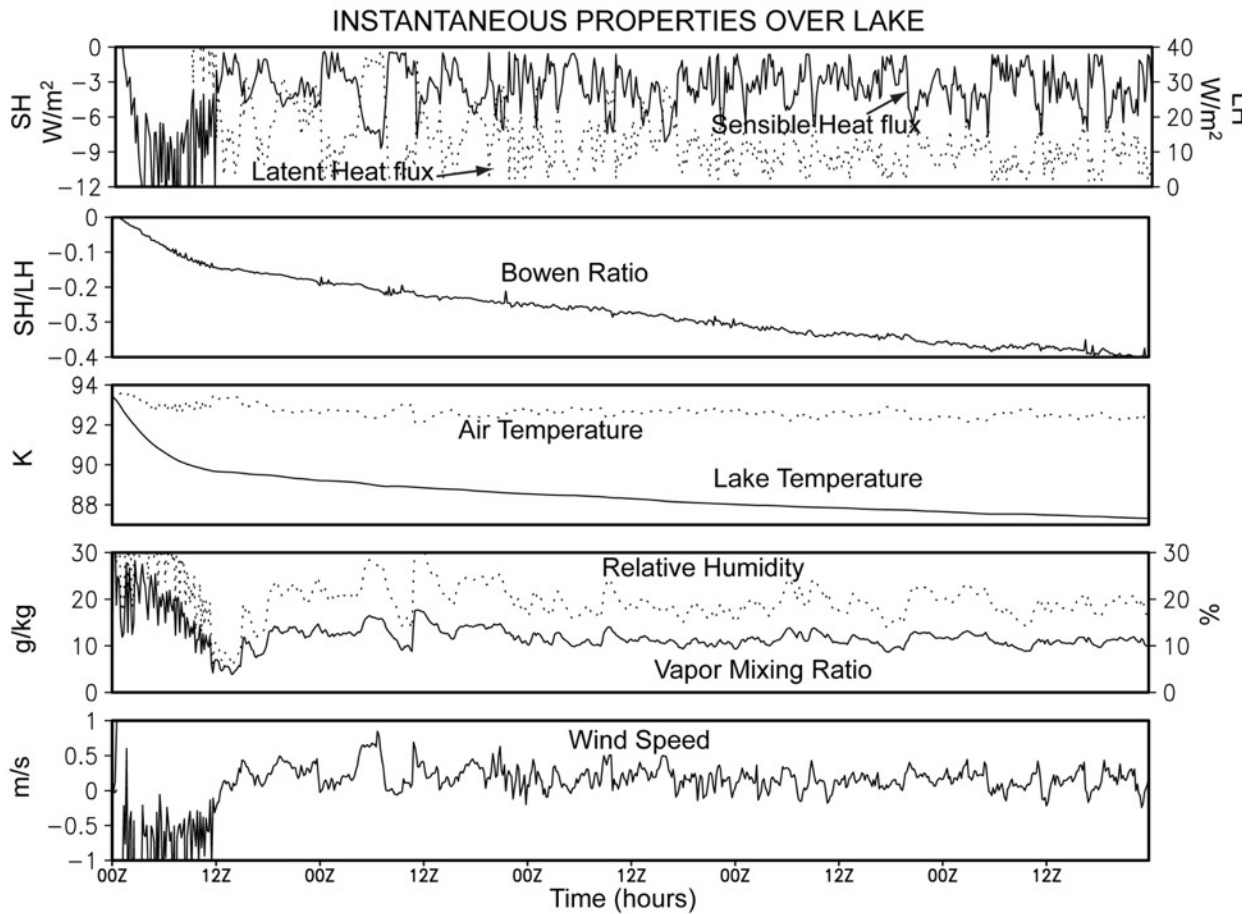


Figure 12. Instantaneous values from one quarter of the way across the right side of the lake for Sim4 (300 km lake). Top to bottom: Sensible heat flux (solid W/m^2) and Latent heat flux (dotted W/m^2); Bowen ratio; SST (solid K) and air temperature (dotted K); methane mixing ratio (solid g/kg) and relative humidity (dashed %); wind speed (m/s).

4. Parametric Studies

Variations from the canonical solution are closely tied to a specific set of initial parameters. Changing these parameters produces variations in the evolution of the system, which we investigated. The variable parameters include lake size, lake mixing depth, initial lake and atmosphere temperatures, atmospheric relative humidity, mean background wind, and diabatic forcing to mimic atmospheric radiative processes (Table 2). We also experimented with different subgrid scale diffusion settings. While changes to diffusion

slightly altered the solution, it did not change any important details. The canonical solution in previous figures was taken from Simulation #4.

Table 2. Key parameter settings for the mtWRF simulations

Simulation	Lake Size (km)	Mixed Layer Depth (m)	Lake Temp (K)	Land Temp (K)	Initial Wind (m/s)	Relative Humidity (%)	Boundary Condition	Duration (tsols)	Newtonian Constant (hours)	Notes
1	32	1	93.47	93.47	0	0	open	10	N/A	
2	32	1	93.47	93.47	0	0	periodic	10	N/A	
3	100	1	93.47	93.47	0	0	periodic	5	N/A	
4	300	1	93.47	93.47	0	0	periodic	5	N/A	Canonical solution.
5	100	10	93.47	93.47	0	0	periodic	5	N/A	
6	100	100	93.47	93.47	0	0	periodic	5	N/A	
7	100	30	93.47	93.47	0	0	periodic	5	N/A	
8	100	100	93.47	93.47	1	0	periodic	5	N/A	
9	100	100	93.47	93.47	3	0	periodic	5	N/A	
10	100	100	94.47	93.47	0	0	periodic	5	N/A	
11	100	100	92.47	93.47	0	0	periodic	5	N/A	
12	100	100	93.47	94.47	0	0	periodic	5	N/A	
13	100	100	93.47	92.47	0	0	periodic	5	N/A	
14	100	1	93.47	93.47	0	0	periodic	5	1	
15	100	1	93.47	93.47	0	0	periodic	5	12	
16	100	1	93.47	93.47	0	0	periodic	5	24	
17	100	1	93.47	93.47	0	0	periodic	5	36	
18	100	1	93.47	93.47	0	0	periodic	5	48	
19	100	1	93.47	93.47	0	0	periodic	5	48	diffusion 6th_opt = 2; factor = 0.12
20	100	1	93.47	93.47	0	0	periodic	5	48	diffusion 6th_opt = 2; factor = 0.25
21	100	1	93.47	93.47	0	0	periodic	5	48	diffusion 6th_opt = 2; factor = 0.50
22	100	1	93.47	93.47	0	0	symmetric	5	N/A	
23	300	10	93.47	93.47	0	0	periodic	5	N/A	
24	300	100	93.47	93.47	0	0	periodic	5	N/A	
25	300	30	93.47	93.47	0	0	periodic	5	N/A	
26	300	100	93.47	93.47	1	0	periodic	5	N/A	
27	300	100	93.47	93.47	3	0	periodic	5	N/A	
28	100	100	87.47	93.47	0	0	periodic	5	N/A	
29	100	100	89.47	93.47	0	0	periodic	5	N/A	
30	100	100	91.47	93.47	0	0	periodic	5	N/A	
31	300	100	87.47	93.47	0	0	periodic	5	N/A	
32	300	100	89.47	93.47	0	0	periodic	5	N/A	
33	300	100	91.47	93.47	0	0	periodic	5	N/A	
34	300	1	93.47	93.47	0	20%	periodic	5	N/A	"unstable", constant RH to 30 km
35	300	1	93.47	93.47	0	50%	periodic	5	N/A	"unstable", constant RH to 30 km
36	300	1	93.47	93.47	0	80%	periodic	5	N/A	"unstable", constant RH to 30 km
37	300	1	93.47	93.47	0	0	periodic	5	1	
38	300	1	93.47	93.47	0	0	periodic	5	12	
39	300	1	93.47	93.47	0	0	periodic	5	24	
40	300	1	93.47	93.47	0	0	periodic	5	36	
41	300	1	93.47	93.47	0	0	periodic	5	48	
42	300	1	93.47	93.47	0	0	periodic	5	72	
43	300	1	93.47	93.47	0	0	periodic	5	96	
44	300	100	93.47	93.47	0	0	periodic	5	1	
45	300	100	93.47	93.47	0	0	periodic	5	12	
46	300	100	93.47	93.47	0	0	periodic	5	24	
47	300	100	93.47	93.47	0	0	periodic	5	36	
48	300	100	93.47	93.47	0	0	periodic	5	48	
49	300	100	93.47	93.47	0	0	periodic	5	72	
50	300	100	93.47	93.47	0	0	periodic	5	96	
51	100	100	91.47	93.47	3	0	periodic	5	N/A	
52	300	100	87.47	93.47	0	80%	periodic	5	N/A	"unstable", constant RH to 30 km
53	300	1	87.47	93.47	0	80%	periodic	5	N/A	"unstable", constant RH to 30 km
54	300	1	87.47	93.47	0	0	periodic	5	N/A	

55	300	1	89.47	93.47	0	0	periodic	5	N/A	
56	300	100	93.47	93.47	1	0	open	5	N/A	open boundary conditions.
57	300	100	93.47	93.47	3	0	open	5	N/A	open boundary conditions.
58	100	100	91.47	93.47	3	0	open	5	N/A	open boundary conditions.
59	300	1	91.47	93.47	0	0	periodic	5	N/A	
60	300	1	93.47	93.47	0	20%	periodic	5	N/A	"stable" methane profile.
61	300	1	93.47	93.47	0	50%	periodic	5	N/A	"stable" methane profile.
62	300	1	93.47	93.47	0	80%	periodic	5	N/A	"stable" methane profile.
63	300	100	87.47	93.47	0	80%	periodic	5	N/A	"stable" methane profile.
64	300	1	87.47	93.47	0	80%	periodic	5	N/A	
65	300	1	93.47	93.47	1	0	open	5	N/A	
66	300	1	93.47	93.47	3	0	open	5	N/A	
67	100	1	91.47	93.47	3	0	open	5	N/A	

4.1. Variations in Lake Dimension

A 300 km lake is comparable in dimension to the largest lakes on Titan—Kraken Mare and Ligea Mare. There are numerous smaller lakes that collectively could provide sources and sinks of heat and moisture similar to that of the largest reservoirs. It is worthwhile to test in the model whether smaller lakes drive similar circulations to the canonical solution.

Simulations #2 and #3 are identical to the baseline canonical case (Simulation #4) except for the lake size. The evolution of the atmospheric circulation for these two simulations are shown in Fig. 13 and Fig. 14, respectively, and may be compared directly with Fig. 8. Both simulations show an initial buoyant moisture plume in the first six hours. The width of the moisture plume scales with the size of the lake; the smaller the lake the narrower the plume. The depth of the plume also shows a dependence on the lake size. The 32 km lake plume rises to ~3 km, the 100 km to ~3.5 km and the 300 km to ~4 km. The increasing depth can most readily be explained by a greater entrainment of dry air by the more narrow plumes. This is not dissimilar to entrainment effects on terrestrial clouds [e.g. Gregory, 2001; Redelsperger et al., 2002]. The depth of the inflow layer is comparable in all simulations (~1 km). The depth of the outflow layer is slightly larger for the larger lakes. The magnitude of the inflow and outflow are all comparable, but there is a

trend for the larger lakes to have slightly higher mean winds. This trend is consistent with lower entrainment and slightly greater buoyancy.

By one t_{sol} , all the simulations show the development of a sea breeze superimposed on the preexisting and larger buoyancy circulation. Like the 300 km simulation, the sea breeze is confined very close to the coastline, but it does propagate slowly inland over time. A similar, very shallow marine layer forms in all the simulations. Figs. 15 and 16 show the time series of average lake properties, which can be compared directly to Fig. 11. The trends in all simulations are very similar. The initial large spike in fluxes associated with the buoyant plume is present, followed by the relaxation to quasi-steady circulation with a superimposed sea breeze. The cooling of the lake to ~ 88 K, the cooling of the atmosphere, the slow march of the Bowen ratio toward ~ -0.4 over the five t_{sol} period, the very low wind speeds, and general decrease in sensible heat flux to increasingly small values is consistent between all the runs. One interesting difference is that the average relative humidity over the lake decreases with lake size. The 300 km, 100 km, and 32 km lakes have marine layer relative humidity of $\sim 20\%$, $\sim 15\%$, and $\sim 10\%$, respectively. The likely explanation for this difference is fetch distance and the ability for the circulation to more easily mix drier from land into the air over the lake. Regardless, the atmosphere does not continue to moisten despite continuous evaporation.

An unexpected but important result is that the smaller lake simulations tend to become increasingly asymmetric with time. The asymmetry is a non-physical solution, because the simulation is constructed to be symmetric about the lake with symmetric forcing; whatever occurs on the left side of the domain should be exactly mirrored on the right side. Not all the simulations exhibit such a strong break from symmetry—most do not and for discernable reasons. Once asymmetries are established, they can be

exacerbated by the lateral boundary conditions. The reason and implications of the breakdown of symmetry is discussed later (See §9). Even in the 100 km simulation (Sim #3, Fig. 14) with the most grievous asymmetry, the overall lake properties and evolution of fluxes are in family with the overwhelming trends and tendencies from the entire ensemble of parametric studies with stable and symmetric solutions. So, while the exact atmospheric circulation may not be fully representative of reality in a minority of the simulations, the general steady-state thermodynamic solution appears to be robust. Regardless of the scale of the lake, the overall behavior of the atmosphere-lake system is similar, and this generally means that any size lake may be used to investigate the impact of other parameters on the system. The 300 km lake is used as the control scenario, because it provides a greater number of domain points over the lake and also exhibits a high degree of symmetry. Table 2 shows that many parameteric studies were conducted for a 100 km lake and a handful for the 32 km lake. It is not feasible to display the results of all these simulations, but the data for all the simulations are provided as supplementary material in NetCDF format. Analyses of all these data demonstrate that the 300 km lake is indeed sufficiently representative of the results for the smaller lakes.

Simulation 2

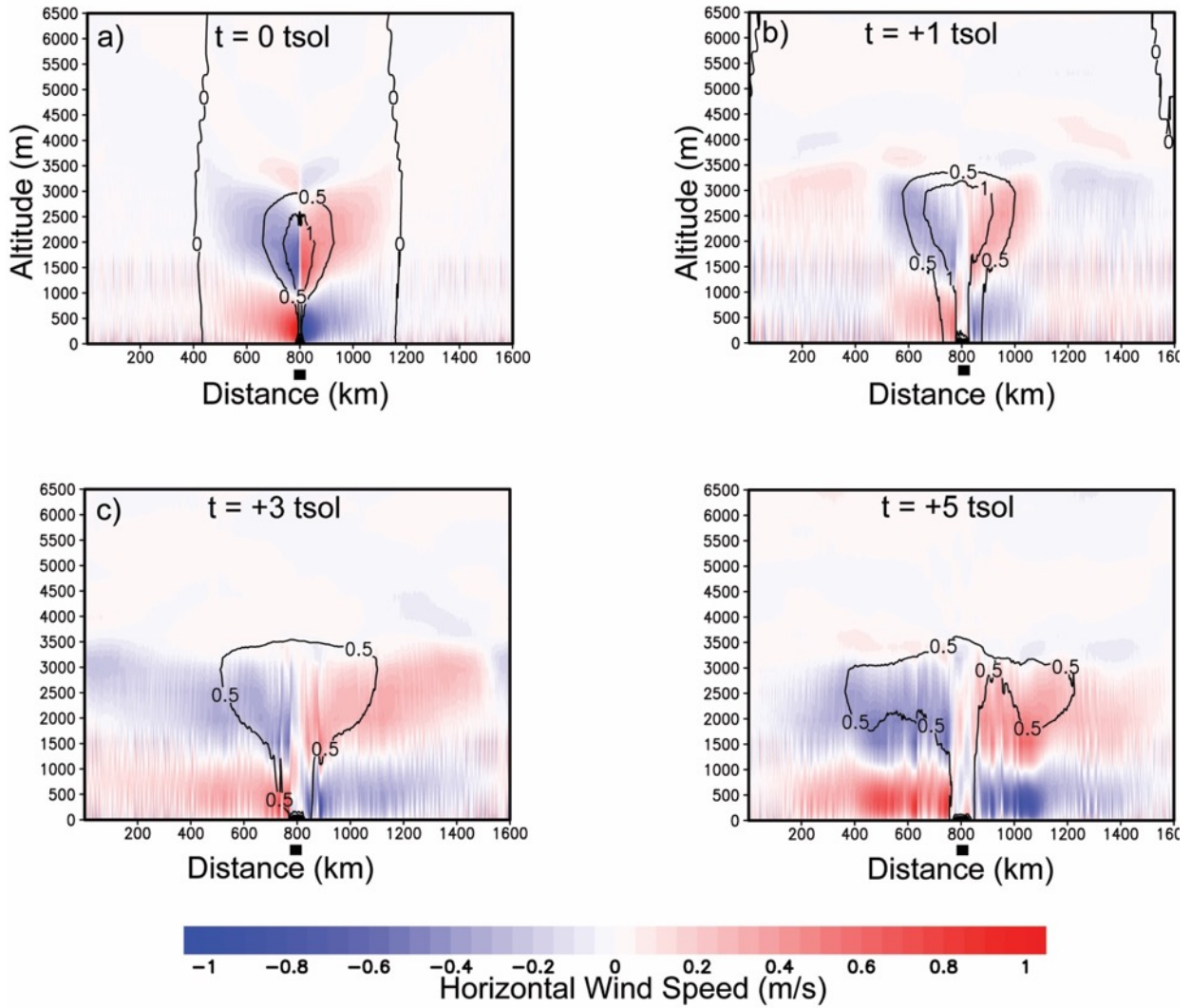


Figure 13. Sea breeze evolution for a 32 km lake. Note the different analysis times compared to the canonical simulation shown in Fig. 8. Horizontal velocity is shaded with red (positive) values indicating flow from left to right and blue (negative) values indicating flow from right to left. Contours are methane mixing ratio (g/kg). The lake domain is shown by the black bar below the horizontal axis.

Simulation 3

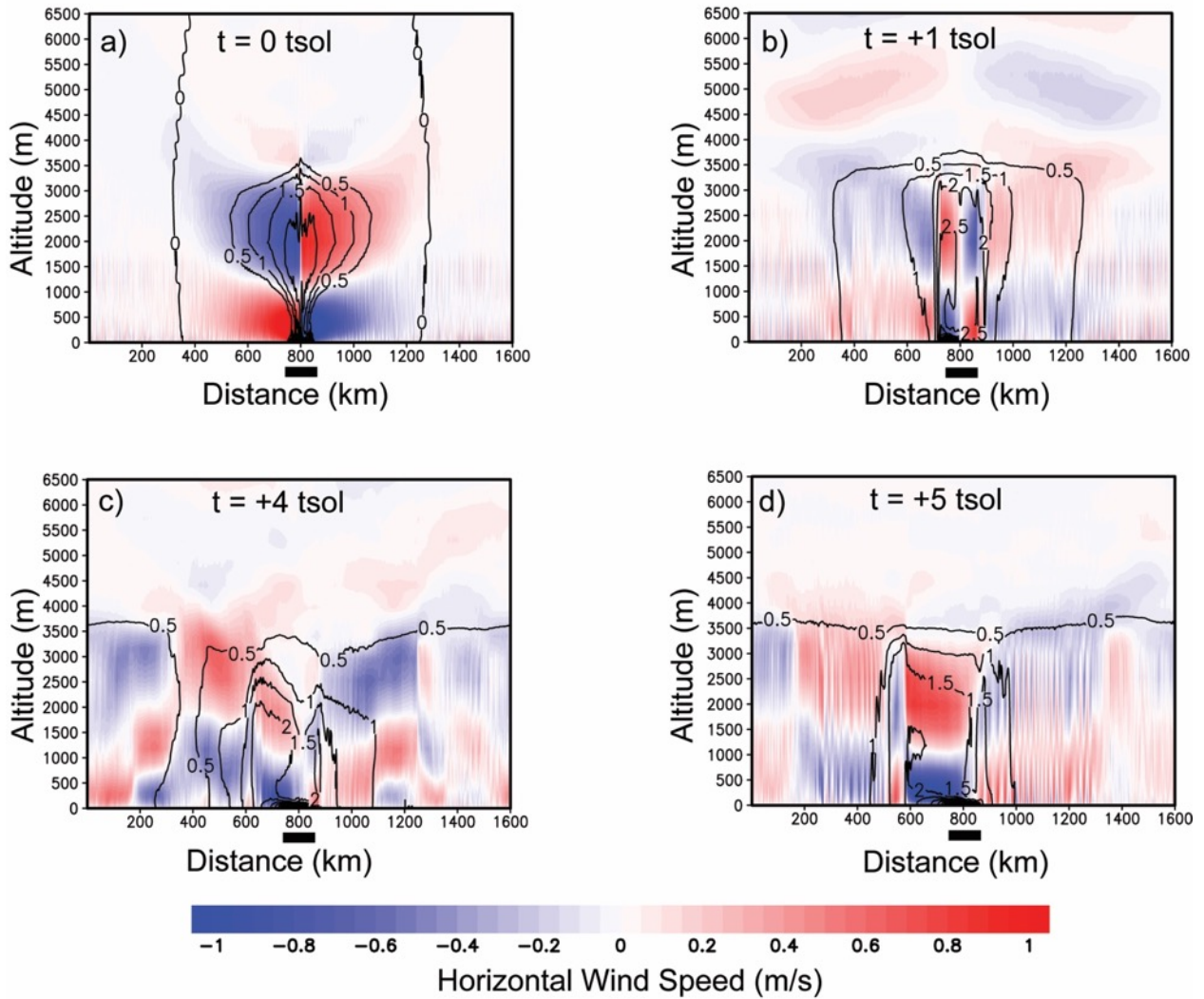


Figure 14. Evolution of sea breeze for a 100 km lake. Note the asymmetry that develops by tsol 4. Horizontal velocity is shaded with red (positive) values indicating flow from left to right and blue (negative) values indicating flow from right to left. Contours are methane mixing ratio (g/kg). The lake domain is shown by the black bar below the horizontal axis.

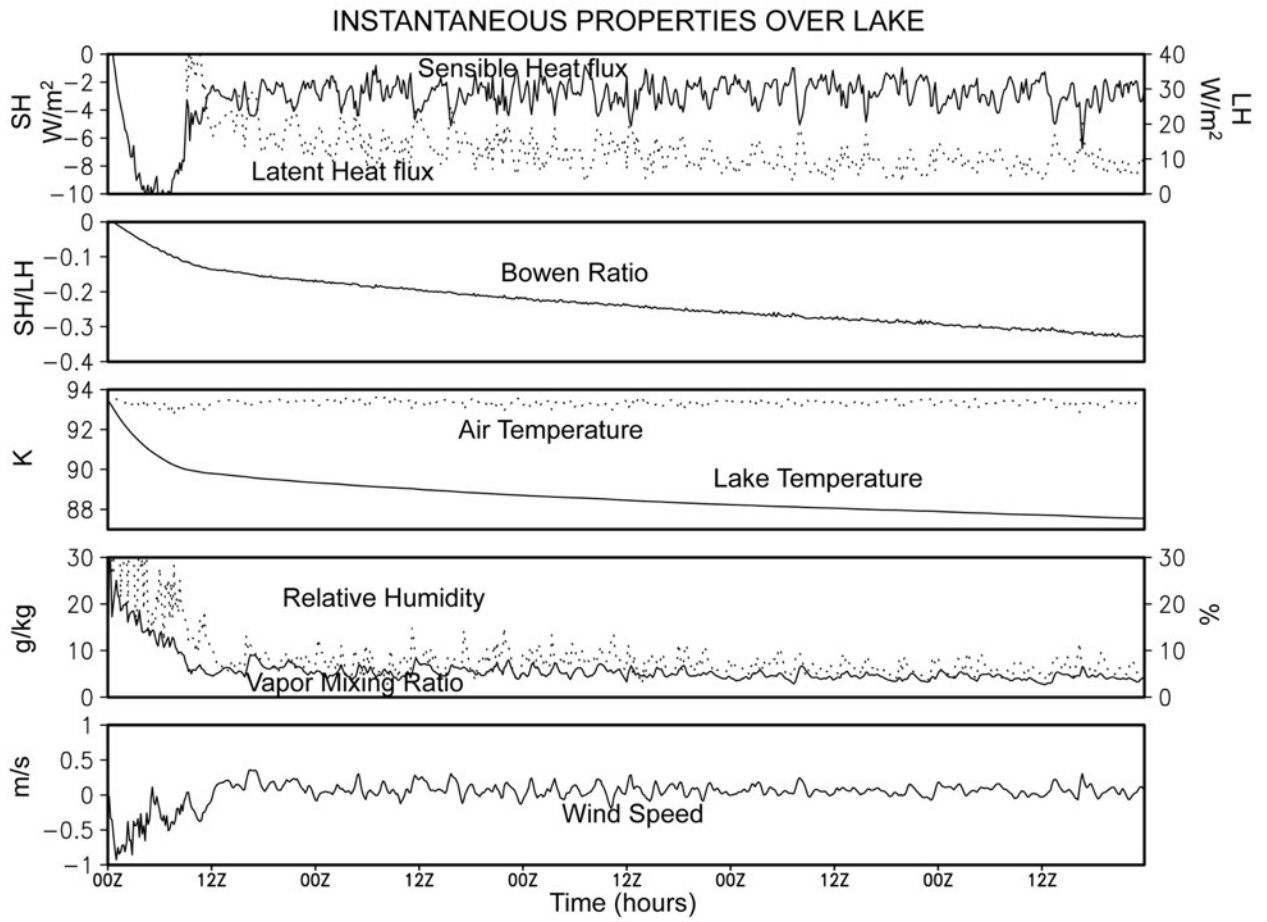


Figure 15. Time series for a 32 km lake (Simulation 2).

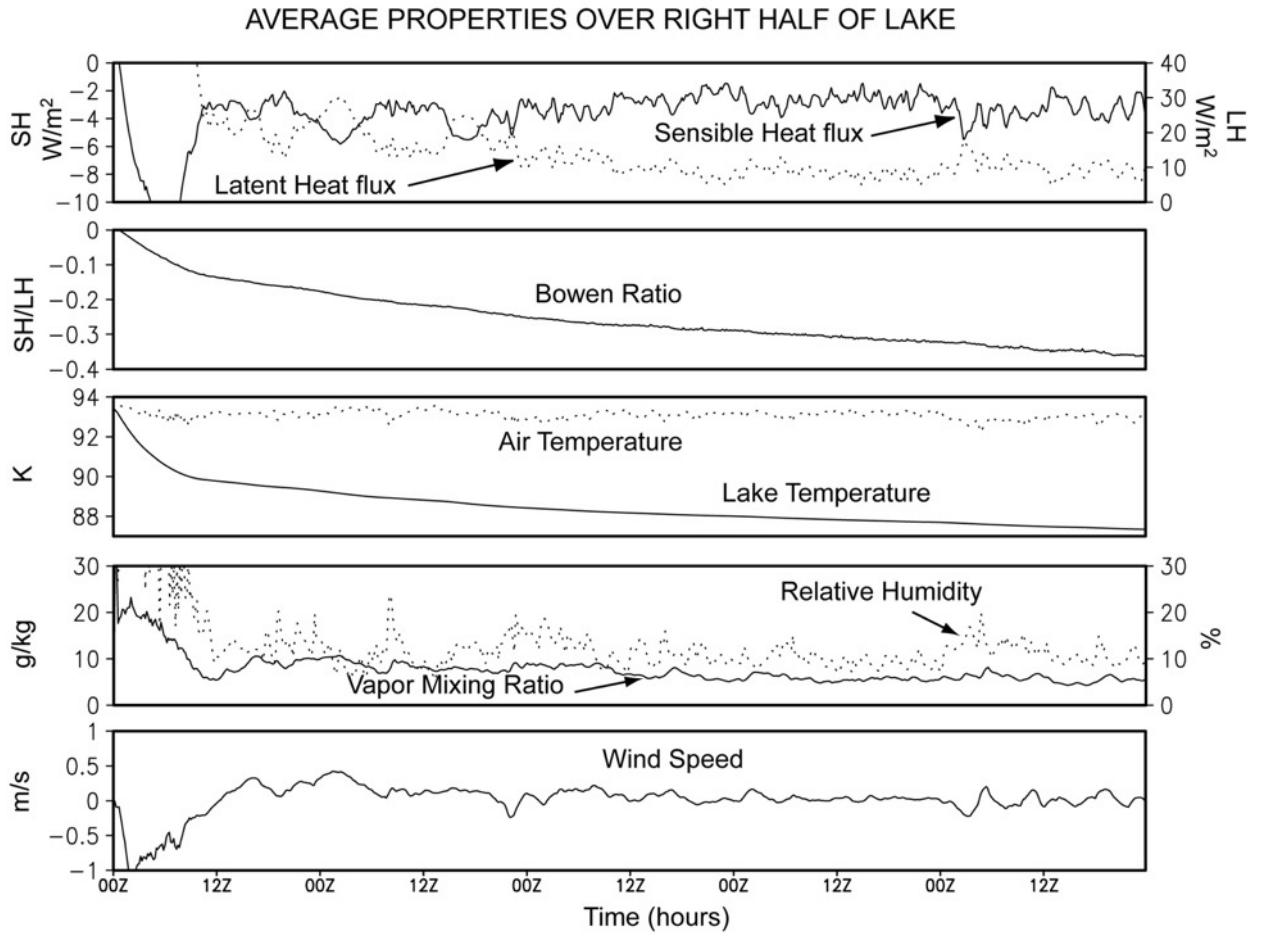


Figure 16. Time series for a 100 km lake (Simulation 3).

4.2. Effect of Lake Mixed Layer Depth

Per Fig. 3, the cooling of the lake depends on the depth of the assumed mixed layer, all other things being equal. Simulations 2, 3, and 4 exchange energy over a very shallow 1 m lake depth and this drives a large response in lake temperature that in turn feeds back to the fluxes. The cold lake should produce a relatively large heat flux due to the large sea-atmosphere temperature gradient while having a relatively small latent heat flux due to the temperature-dependent decrease in saturation vapor pressure. A modification of the evolution of the circulation might also be expected as the lake mixed layer depth is changed. The initial plume circulation should remain mostly unaltered. However, the large evaporation driving that plume will have a diminishing effect on lake cooling as the mixed layer depth increases. With less lake cooling and a corresponding lower sensible heat flux, the atmospheric cooling should also be reduced, and this should slow the development of the opposing sea breeze circulation.

Simulations 23, 24 and 25 test the effect of mixed layer depth for the 300 km lake scenario, and the time series of key physical variables are shown in Fig. 17 (compare to Fig. 11). The results are consistent with expectations. For the largest mixed layer depth (100 m), the cooling of the lake is very small and an effectively perpetual plume circulation is present. No discernable sea breeze circulation develops, because in the absence of an impactful cooling sensible heat flux, the cold, dense air that drives a sea breeze does not develop. The latent heat flux is large compared to the sensible heat flux; the Bowen ratio is near zero, consistent with the fluxes. Near-surface wind is persistently at ~ 1 m/s, which indicates a nearly persistent plume circulation. Somewhat surprising is the very slight *increase* in near-surface atmospheric temperature. Given the very small cooling heat flux and near constant lake temperature, the increase must be a dynamical effect; weak mean downwelling or mixing of higher potential temperature air from aloft would produce the warming. Since the mean motion associated with the

plume over the lake is upward and is by definition near zero very close to the surface, it may be concluded that it is mixing, not mean adiabatic motion that forces the very weak temperature increase. The vapor mixing ratio is two to three times higher than in the canonical case with a commensurate higher relative humidity (up to 70% in Simulation 24). The saturation mixing ratio at the temperature of the air is closer to 70 g/kg, so despite the relatively large values, the air is still well below saturation. The moist air may be considered a marine layer of sorts, but it is not cool marine in the traditional sense.

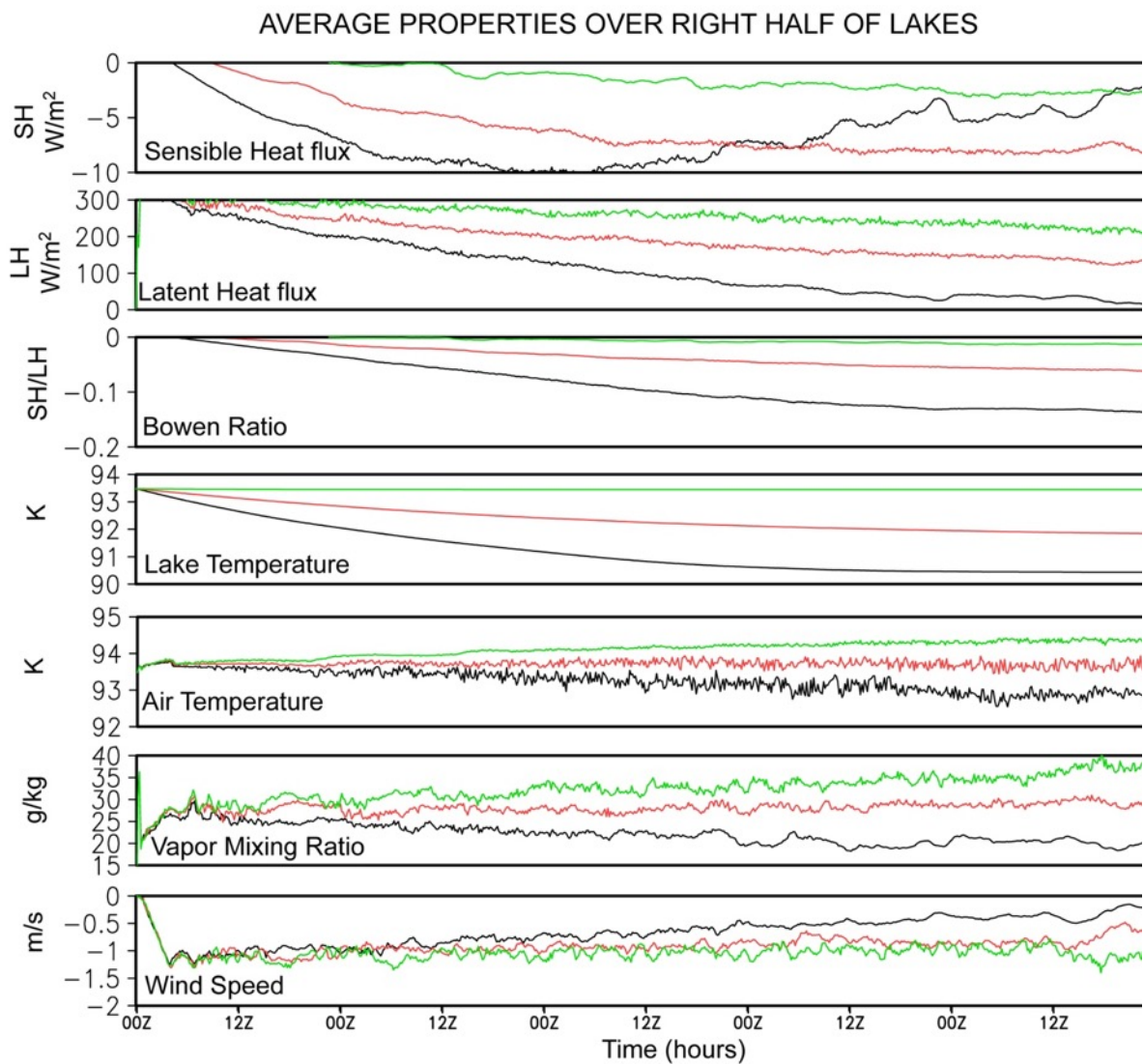


Figure 17. Time series of key physical variables for a 10 m (Sim #23, black), 30 m (Sim #25, red), and 100 m (Sim #24, green) lake mixed layer depth.

In the 30 m mixed layer lake scenario (red curves) there is a clear response in the lake. Still, the overall response is sufficiently muted so that the net cooling of the air is negligible and no sea breeze forms. The magnitude of the Bowen ratio is larger than in the 100 m case, but it is still very small. Near-surface wind speeds are only slightly less than in the 100 m scenario, but do show some deceleration with time. Overall, the rate of change of the fluxes, Bowen ratio, and lake temperature indicate a diminishment of air-sea exchange with time. Although there is no sea breeze to completely counteract the plume circulation, there is enough forcing to slow turbulent flux exchanges and to at least slow the plume circulation. The vapor mixing ratio is lower than in the 100 m case, but still well above the canonical solution.

The 10 m mixed layer scenario (black curves) initially mirrors the deeper mixed layer cases, but exhibits an important change in character compared to the other cases. The sensible heat flux shows an inflection point at ~ 2 tsols. At this point the lake and atmosphere have cooled sufficiently to produce a cool marine layer, and the change in sensible heat flux signals the genesis of a very weak sea breeze circulation that begins to counter the plume circulation. The increased stability associated with the marine layer tends to decrease the turbulent surface fluxes. The wind and vapor field at 5 tsols, averaged over 6 hours, is shown in Fig. 18. The robust and dominant plume circulation is obvious, but a very shallow (<100 m) sea breeze is evident just onshore. The average horizontal wind in Fig. 17 indicates the dominance of the plume circulation at the surface, but there is an onshore flow just inland of the lakeshore. Although the onshore winds are locally confined, they do reach almost 0.5 m/s and produce a region of strong convergence at the sea breeze front (Fig. 18 inset).

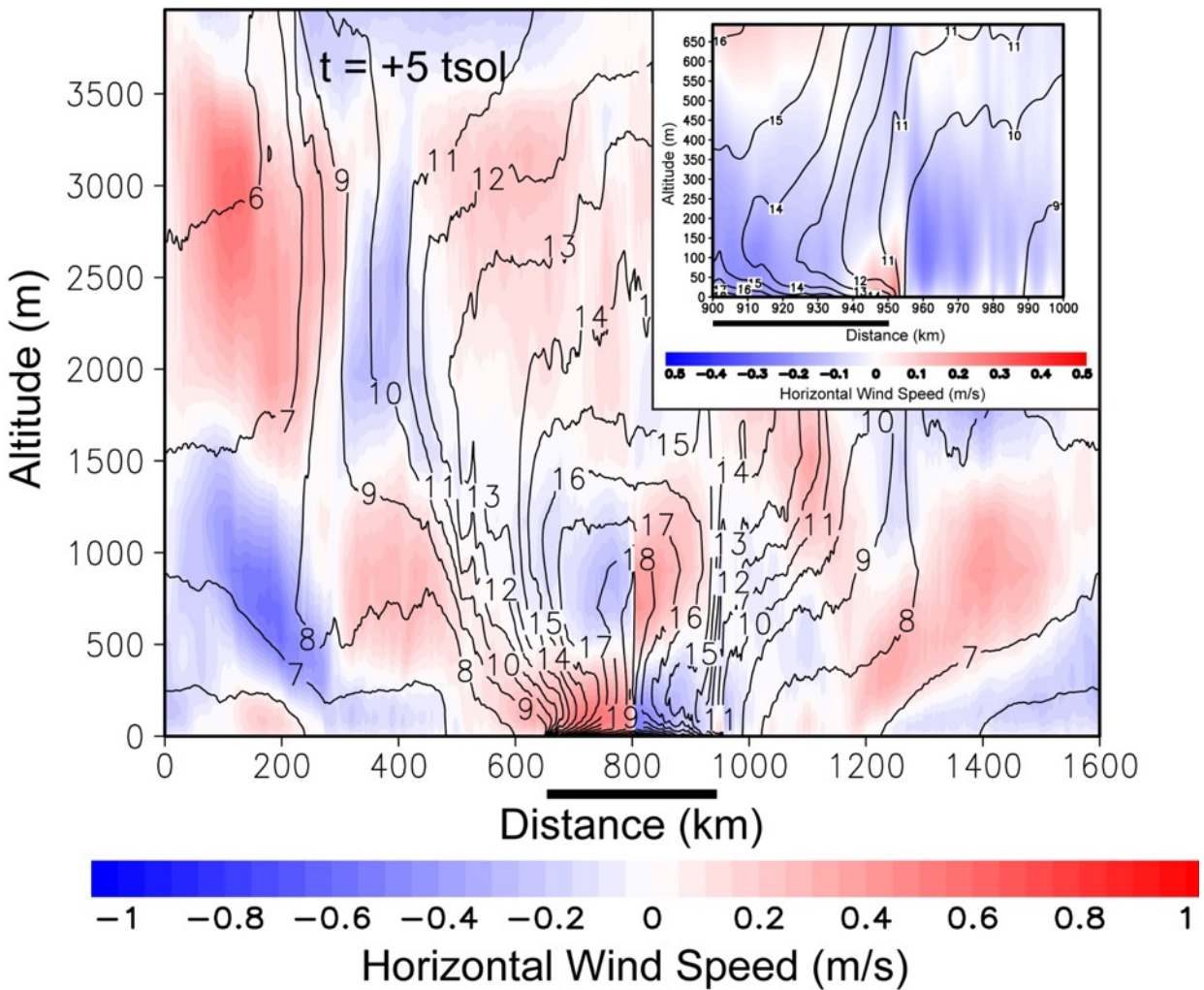


Figure 18. The 6-hour average circulation for the 10 m mixed layer (Sim 23) at 5 tsols. The inset in the upper right focuses on the right side sea breeze. The black bar below the horizontal axis shows the lake domain. Wind speed is shaded. Methane vapor mixing ratio (g/kg) is contoured.

For lakes with deep mixed layers it may be concluded that if the atmosphere and lake are initialized isothermally but out of vapor equilibrium, the circulation will be dominated by a plume circulation. Further, the deeper the mixed layer, the longer it takes to cool the lake, establish a cool marine layer, and establish an opposing sea breeze, if at all. Only very shallow mixed layers (e.g., 1 m) can produce a sea breeze of sufficient strength to substantially alter let alone reverse the plume circulation. It is clear that

the lake temperature has a strong influence on the equilibrium vapor content of the marine layer. A warm lake pumps more water into the air than a cold lake. If actual Titan lakes and atmosphere are in thermal equilibrium but in large vapor disequilibrium, there may be a pronounced plume circulation, and if the mixed layer is sufficiently deep, that circulation may be persistent and at the exclusion of a sea breeze. In the 30 m case, extrapolation of the data beyond the simulation period suggests the establishment of any significant sea breeze could take 10s or 100s of tsols. The lake and atmosphere cooling are asymptotically flattening with time while the sensible heat flux decreases in magnitude. In the 100 m mixed layer depth, a sea breeze would effectively never be established, because the atmosphere never cools and the lake cools imperceptibly. Moistening of the atmosphere would occur aloft, but not substantially over the land surface, except for what might be mixed down to the surface by turbulent motions.

An immediate question follows from these results. What is a typical or representative mixed layer depth? On Earth, water has a maximum density at ~ 4 °C. Cooling of warm water will result in negatively buoyant parcels sinking until they reach their thermal equilibrium level, entraining warm water along the way. Thus, the depth of an ocean or lake mixed layer depends on the thermal, or equivalently, the density profile as a function of depth. If, for example, a water lake has an isothermal profile well above 4 °C, a cooled surface water parcel will sink to the bottom if there is no entrainment.

Pure liquid methane (or ethane) has a similar behavior to warm water. If a large Titan lake like Kraken Mare with a maximum depth of >100 m is assumed to be pure methane, a cooled surface parcel would be expected to sink to the bottom, or at least to a lesser depth determined by the amount of warm liquid methane entrainment. Over time, continually entraining fluid will ultimately mix to the bottom of the lake. Looking back to the 1 m mixed layer depth simulation, the cooling of the mixed layer is significant

(many Kelvins), and if a lake were deeper than the assumed mixed layer, it would be highly likely that the mixed layer depth would grow from the initial 1 m. Thus, the initial shallow mixed layer might be expected to evolve towards the 10 m scenario, and if the process continued, to 30 m, and 100 m. In other words, assuming a reasonably deep lake, the evolution of the lake temperature in the 1 m mixed layer case would be unrealistic, because as the surface cooled that fluid would sink and would be replaced by warmer fluids. In turn, the convective overturn would reduce the sensible heat flux while enhancing the evaporatively-driven plume. Although a shallow mixed layer is most conducive to generating a sea breeze, it is simultaneously a self-limiting if not self-defeating process. A cold lake surface and shallow mixed layer are, for the most part, physically inconsistent. This is not all that different from Earth. Stable stratification of a lake is warm water over cold water (a thermocline) and not the other way around. Consequently, the 1 m mixed layer depth scenario should be very close to upper limit of the ability of the Titan air-sea system to generate a marine layer and sea breeze circulation over a pure methane lake.

The above argument holds for pure methane, but Titan's lakes are likely to have other solutes, especially ethane [Lorenz, 2014]. Depending on composition, it is possible that the lake liquids will exhibit a non-standard behavior similar to water below 4°C. Namely, the fluid may decrease in density as it cools [Tan et al., 2015]. In this case, a shallow mixed layer and cooling lake is physically consistent. The coldest fluids will remain near the top of the lake and even freeze if sufficiently cooled.

4.3. Air-Lake temperature Differential and Initial Relative Humidity

The simulations presented up to this point all suggest that the air-sea system will tend to evolve to a state where the lake is cooler than the air and to an atmosphere that is moist but not saturated. The time

constant of this evolution depends strongly on the mixed layer depth, but it would be reasonable to expect that the actual background conditions have some amount of disequilibrium between the lake and atmosphere. If a simulation is initiated with a lake colder than the atmosphere and with a moister atmosphere, both of which are possibly closer to reality, then the intuitive expectation might be for a diminished buoyancy plume circulation and an enhanced sea breeze circulation. Simulations 31-33, 54, 55, and 59 test the expectations for a cold lake while simulations 34-36 and 60-62 test the expectations under different incarnations of an increasingly moist initial atmosphere. We note that the coldest lake cases are likely below the freezing point, but the point here is to test the response to increasingly large differences between the atmosphere and lake, and the cold lake cases serve that purpose; the very cold lake represents a bounding case. The variable humidity experiments also test by proxy the effect of an impure methane lake. The addition of ethane or other volatile compounds decreases the saturation vapor pressure of methane via the solute effect. Moistening the atmosphere decreases the vapor pressure gradient between the atmosphere and the lake, which is essentially the equivalent of adding contaminants to the lake, as expressed by Eq. (1).

The results of the cold lake experiments are roughly in accordance with intuitive expectations. With an initial cold lake, the diagnosed surface fluxes are smaller than in most previous cases, because the atmosphere quickly cools and stability increases. The saturation vapor pressure over the colder lake is lower, which also lowers the latent heat flux, all other things being equal. There is a moistening of the atmosphere due to evaporation, but it is much smaller than when the lake and atmosphere are initially at the same temperature, while the sensible heat flux is proportionately larger, as indicated by the Bowen Ratio. We find that the colder the lake is, the lower the evaporation and the greater the sensible heat flux.

In all the 100 m mixed layer cases with an initially cold lake, the rate of change of the lake temperature associated with the net turbulent flux is so small that it falls within machine error. Consequently, the lake doesn't change temperature all. This finding initiated simulations with a 1 m mixed layer lake (Simulations 54, 55, and 59) where the rate of change of lake temperature should be roughly 100 times greater. Once again, the implications of the weak forcing on numerics is discussed in Section 9.

While the lake doesn't cool in the deepest mixed layer case, the sensible heat flux is large enough to cool the atmosphere. Thus, there is an energy leak in the system. The atmosphere is responding to surface fluxes while the lake is not. In the short term, this is acceptable. Even if machine precision were not a problem, the actual cooling rate of the lake is so small that it is nearly inconsequential to the physics of the problem. Per Fig. 3, for a flux of a few W/m^2 , a 100 m lake will only cool by ~ 1 K over a 100 tsol period.

In the two coldest, 100 m mixed layer cases, a robust sea breeze develops quickly with very little evidence of a plume circulation. The representative solution is shown for Simulation 31 in Fig. 19. The sea breezes slowly propagate inland. In contrast, the modestly cold lake case (Simulation 33) shows a plume circulation and little to no evidence of a sea breeze (Fig. 19). Thus, for the deep mixed layer case, there is a transition from a plume-dominated circulation to a sea breeze-dominated circulation as the lake cools.

The time series of relevant physical parameters are very similar for the coldest, deep mixed layer cases (Fig. 20). Wind speed is very low, sensible heat fluxes are 5 Wm^{-2} or less, latent heat fluxes are small and stay small compared to previous simulations, and the Bowen Ratio remains almost constant. The coldest lake case (Simulation 31) has the largest magnitude Bowen Ratio, indicating that the sensible heat flux

plays a greater role compared to the other cases, although latent heat fluxes still dominate. On the other hand, Simulation 33 is out of family with the two colder cases. Again, with a lake only 2 K colder than the atmosphere, the solution shows a strong initial plume circulation and little to no sea breeze. This suggests there is a relatively strong bifurcation in the air-sea temperature differential solution space. For a lake more than 2 K colder than the atmosphere, a sea breeze circulation dominates, while for warmer lakes the plume circulation dominates. Commensurate with the plume circulation, the winds for Simulation 33 are much stronger, and even though the air-sea temperature difference is less than the colder cases, the heat flux is actually larger in magnitude. The strength of the wind does matter (Eq. 1). The latent heat flux is larger than the other two cases, as would be expected, and it greatly dominates over the sensible heat flux, as seen in the Bowen Ratio. The air barely cools at all, and actually appears to warm very slightly with time even though there is a cold lake. Dynamics must be countering the atmospheric cooling effect of the sensible heat flux. With a smaller lake (Simulations 28-30) and 100 m mixed layer, the solution (not shown) is similar to 31, 32 and 33, and in many ways almost indistinguishable. Lake size does not play a major role in the overall solution in these scenarios.

COLD AND DEEP LAKES

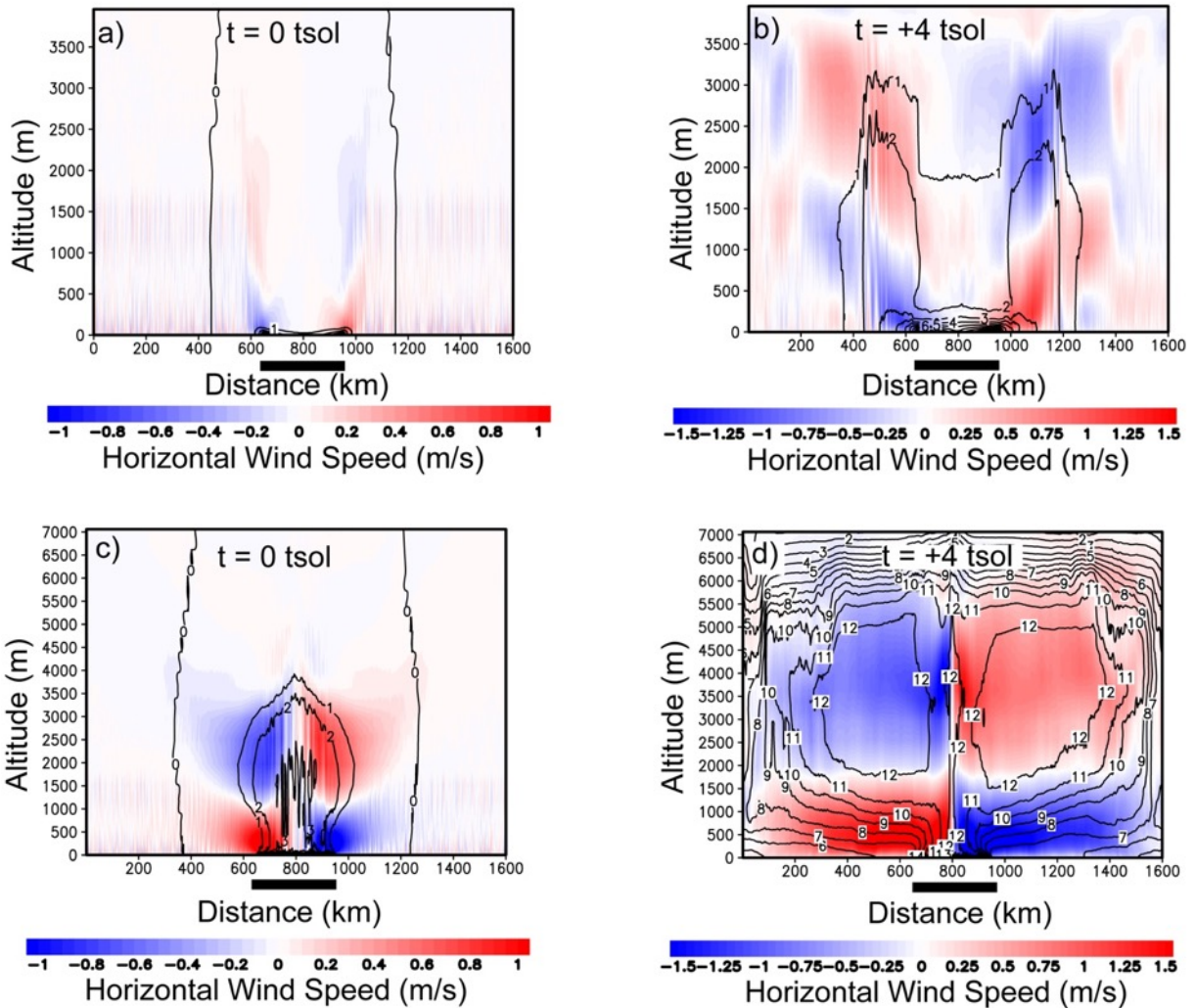


Figure 19. Results from cold, deep mixed layer cases sim 31 (left) and sim 33 (right). The initial circulation (top row) depends strongly on the lake temperature deficit with a sea breeze for the coldest case and a plume circulation for the warmest lake. The solution 4 tsols later reflects the initial circulations. Note the different vertical scales between the two cases. The black bar below the horizontal axis shows the lake domain. Wind speed is shaded. Methane vapor mixing ratio (g/kg) is contoured.

Experiments 54, 55, and 59 are identical to 31, 32, and 33, but with a shallow lake mixed layer. The shallower mixed layer results in a larger lake temperature tendency for a given latent heat flux compared to the 100 m case, which eliminates the machine precision issue. The two coldest 1 m mixed layer cases

are dominated by a sea breeze, as was the case for the deep mixed layer. The modestly cold lake (Simulation 59), however, deviates from its companion deep mixed layer result (Simulation 33). Instead of a dominant plume circulation, a sea breeze circulation is well established and superimposed on a relic plume circulation. This is explained by the cooling of the lake in Simulation 59 (Fig. 21). Thus, when the lake is shallow and is allowed to cool, the transition from a plume solution to a sea breeze solution appears more gradual. Still, a 2 K differential between lake and atmosphere is approximately where the sea breeze influence becomes noticeable. In the coldest case, the sea breeze is clearly dominant and has begun to propagate inland.

In all the shallow, cold lake cases, the average wind over the lake trends very close to calm. Even so, the fluxes are nonzero by the end of 5 tsols and appear reach a quasi-steady state. The lake temperatures are also nearly stabilized. While lake cooling is taking place, the fluxes are small enough that the rate of cooling is almost negligible. From an air-sea exchange point of view, the end results of all the shallow cold cases are nearly indistinguishable with the exception of the lake temperature in the modest cold lake simulation (Simulation 59).

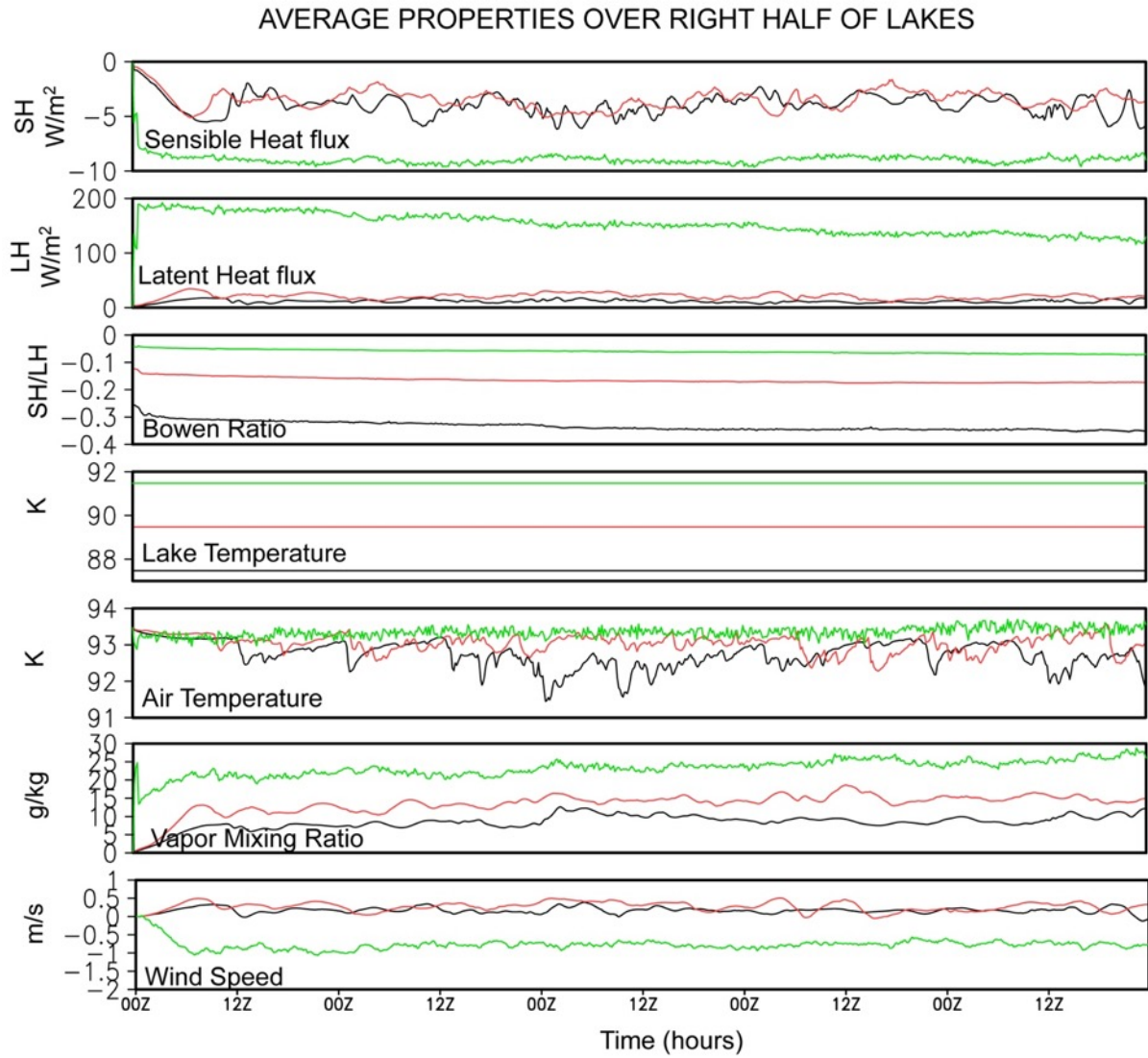


Figure 20. Time series of key physical variables for the cold and deep lake simulations 31, 32, and 33.

COLD AND SHALLOW LAKES

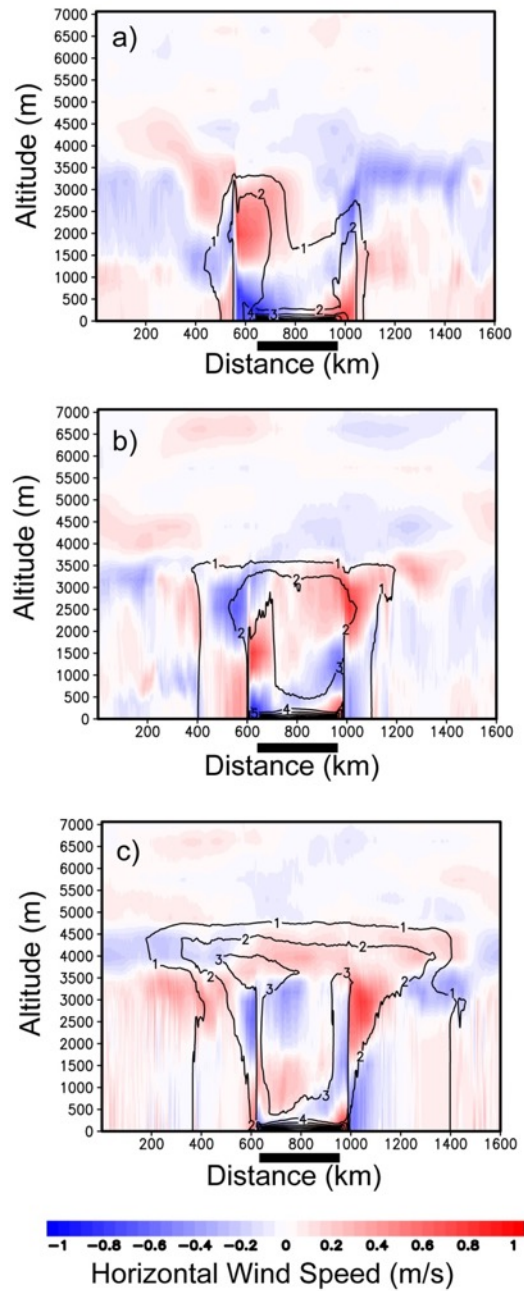


Figure 21. Shallow, cold lake scenarios at tsol 5. Sim 54, 6 K colder (a); Sim 55, 4 K colder (b); Sim 59, 2 K colder (c). The sea breeze becomes more dominant and the plume circulation less dominant as the lake gets colder. The black bar below the horizontal axis shows the lake domain. Wind speed is shaded. Methane vapor mixing ratio (g/kg) is contoured.

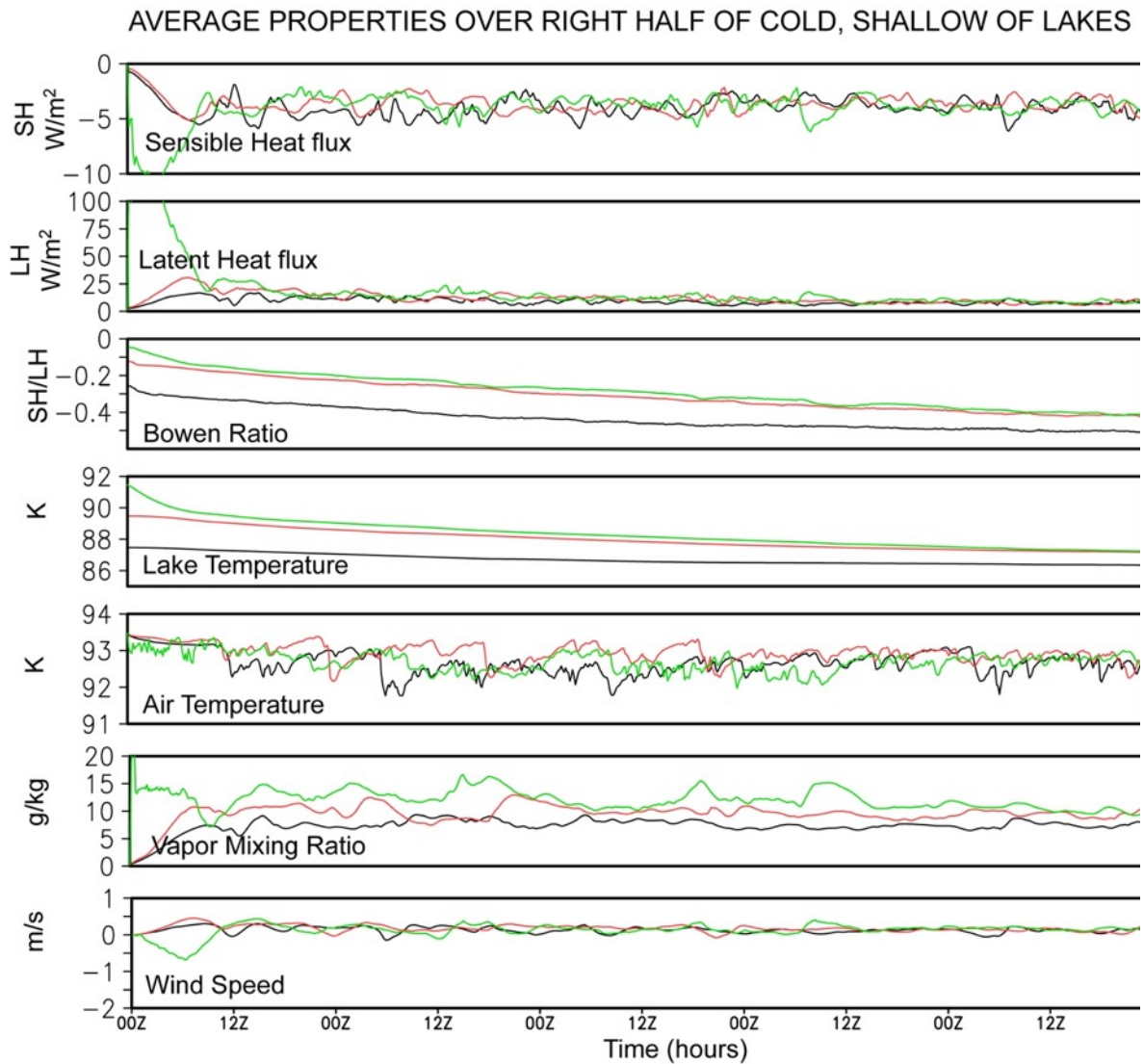


Figure 22. Time series for the cold, shallow lake simulations. Sim 54, 6 K colder (green); Sim 55, 4 K colder (red); Sim 59, 2 K colder (black).

The effect of increasing atmospheric humidity (using the “stable” initial conditions of Simulations 60, 61, and 62) is also roughly in concert with the intuitive expectations. As initial atmospheric humidity is increased, the initial evaporation rate is decreased and the resultant plume circulation is diminished (Fig. 23). However, the reduced evaporation also means the lake cools more slowly and the development of a stable marine boundary layer is slowed. Eventually, as the lake cools, a sea breeze does eventually

emerge. The asymmetry above the shallow sea breeze in the RH=20% case is pronounced (Fig. 23b). If any version of the “unstable” relative humidity cases is used, the solution is dominated by a plume circulation due to the initial atmospheric buoyancy prior to any air-sea interaction. These unstable initial conditions (Simulations 34, 35, and 36) are not presented here, but the data are available in the supplementary material.

The sea breeze is superimposed on the remnant plume circulation. In the two highest humidity cases, the fluxes are effectively zero within two tsols even though Bowen ratio remains solidly negative (Fig. 24). The magnitude of the Bowen Ratio decreases as humidity is increased. This is not intuitively obvious, since the increase in humidity could lead to a compensating reduction in sensible heat flux due to the more slowly cooling lake. By 4 tsols, the Bowen Ratio is nearly constant for all cases, as is the lake temperature. The air temperature also fluctuates around a near constant value. Net energy exchange between the lake and atmosphere amounts to less than a few W/m^2 . This energy flux is inconsequential for further lake temperature changes given the thermal mass of the liquid. The flux does continue to provide moisture to the atmosphere, which is then advected away from the lake by the circulation, and the air is cooled to maintain the marine layer.

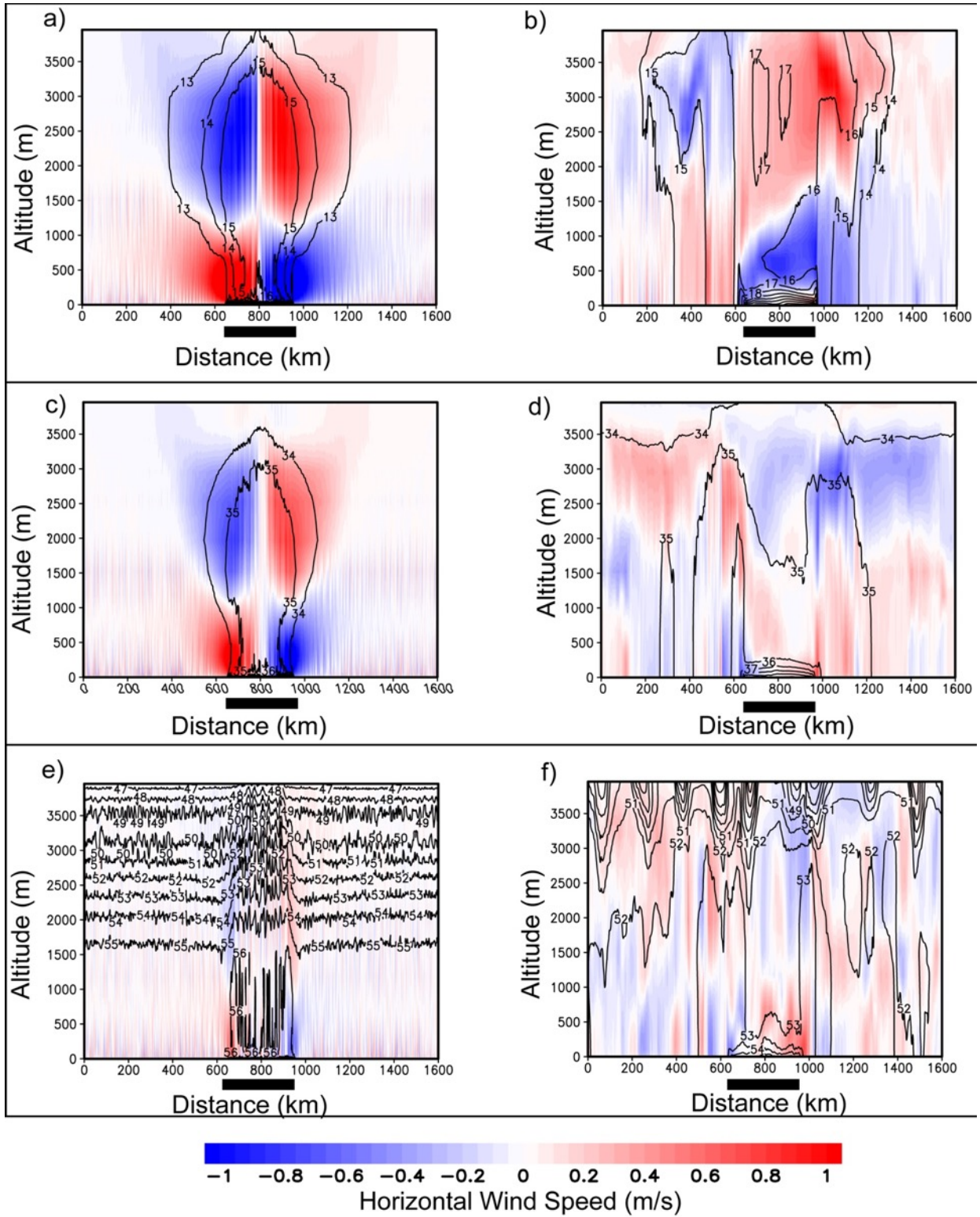


Figure 23. Initial and +4 tsol circulations for the 20% (top), 50% (middle) and 80% (bottom) RH cases (Sims #60-62). Note the asymmetry for the 20% RH simulation at 4 tsols. The black bar below the horizontal axis shows the lake domain. Wind speed is shaded. Methane vapor mixing ratio (g/kg) is contoured.

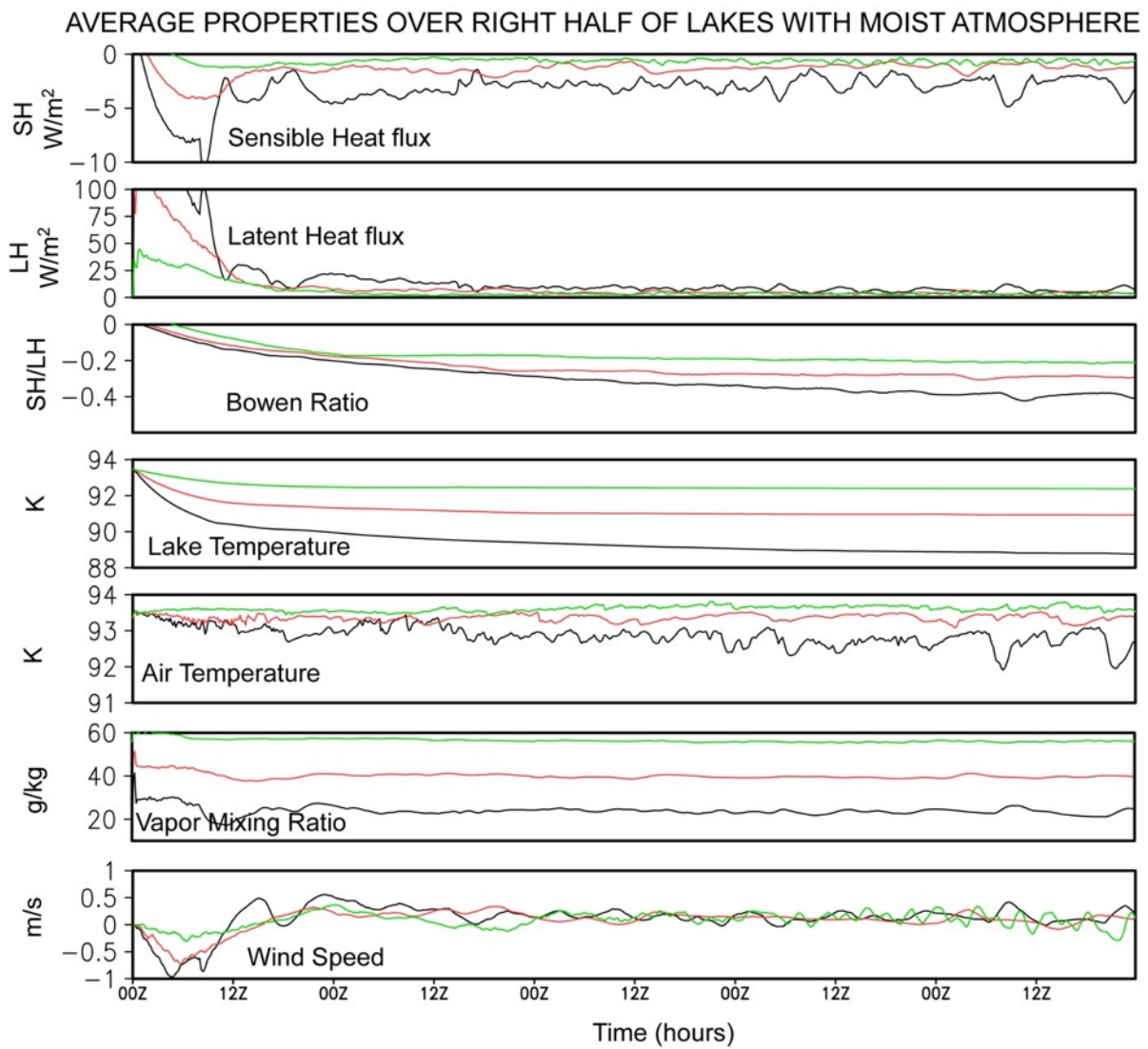


Figure 24. Results for increasing humidity cases 60 (20% white), 61 (50% red), and 62 (80% green).

As previously described, an increase in atmospheric humidity can be viewed as a proxy for a reduction of saturation vapor pressure over the lake associated with a mixture of solutes. There is a reasonable expectation that lakes are not pure methane, but have some non-negligible amount of liquid ethane and perhaps other volatile organics [Lorenz, 2014]. As the fraction of liquid methane is reduced, the methane saturation vapor pressure over the lake will be reduced, and thus the intensity of the initial plume circulation will be reduced due to a reduction in the lake to air vapor gradient. The reduction in the vapor gradient is analogous to increasing the initial atmospheric humidity. Ethane and higher order organics have a higher molecular weight than methane and nitrogen, so the virtual buoyancy contribution of these volatiles, which is not included in these simulations, counters that of methane. The concentration of these heavier gases would almost certainly be insufficient to substantially reduce the methane buoyancy. On the other hand, it is possible to imagine a nearly pure ethane lake with evaporative cooling and negative virtual buoyancy. Under such conditions, only an ethane vapor-rich sea breeze circulation would be possible.

4.4. Effect of Background Wind

With the exception of the convective storm environment [Barth and Rafkin, 2007; Charney et al., 2015; Rafkin and Barth, 2015], Titan is thought to have a sluggish atmosphere with large-scale surface winds of ~ 1 m/s or less [Bird et al., 2005; Tokano et al., 2009]. The mtWRF-simulated near-surface winds in and around the lakes are also generally small (~ 1 m/s or less), but it is not unreasonable to expect that the air-sea interaction circulations could be embedded in a large-scale mean wind environment that is at least of comparable magnitude to the local circulations. On Earth, mean winds distort sea breeze circulations [Leopold, 1949; Blanchard and López, 1985; Finkelle, 1988; Atkins and Wakimoto, 1997; Miller et al., 2003;

Gilliam et al., 2004; Crossman and Horel, 2010]. Sea breeze fronts propagating in the direction of the mean tend to push faster and more deeply inland. In contrast, a sea breeze opposed to the mean wind moves inland more slowly and can even become locked to the coastline or remain entirely offshore. The frontal contrast along the opposing sea breeze tends to be greater and more compact, whereas the sea breeze front moving with the mean wind tends to be more diffuse and more poorly defined.

Many simulations were conducted to explore mean background winds of 1 m/s and 3 m/s with either periodic or open boundary conditions, with different mixed layer depths, and with different initial lake temperatures. Although small by Earth standards, 1 m/s and 3 m/s are a stiff breeze for Titan and are similar in magnitude to the simulated local lake circulations. Importantly, even though the initial background wind is specified as a constant, friction reduces the wind speed near the surface with the greatest decrease over the land where the roughness is higher. Thus, the imposed mean wind condition is really a constant wind “above the deck” with a frictional decrease in wind speed toward the surface.

Periodic boundary conditions (e.g., Simulations 26 and 27) are somewhat problematic in that they allow the circulation to blow downwind and then re-enter the domain on the other side. At 1 m/s, an air parcel will move through the domain in about 1 tsol. Once the simulation time exceeds the Lagrangian advective time scale, the simulations are representative of an infinite chain of lakes rather than an isolated lake. At the same time, it is reasonable to argue that the northern lake district could be roughly characterized as a series of lakes that are potentially downwind of one another. In this case, periodic boundary conditions allow for the simulation of multiple circulations interacting with one another.

Open boundary conditions allow circulations to exit the domain, but at the possible expense of spurious boundary condition effects on the interior solution. Indeed, this was seen in Simulation 65 after about 1.5 tsols. Spurious winds from the boundary push into the domain, produce massive asymmetry, and overwhelm the physical solution. The effect seems to be triggered by the arrival of the plume outflow circulation at the boundary, and the solution degrades quickly thereafter. Prior to 1.5 tsols, the solution appears largely unaffected. Even without spurious boundary noise, once a system exits the domain, there is no longer any numerical information on the structure or evolution of that system. The exiting of the system can be mitigated by increasing the size of the domain, but that solution quickly becomes computationally impractical.

The deep mixed layer simulations with a mean wind have very slowly cooling lakes, as expected based on previous simulations. The latent heat flux is large enough that the lake temperature tendencies are generally above machine precision, unlike the zero-wind, cold lake cases (Simulations 31-33). The results from Simulation 57 are shown in Fig. 26 as a representative example of the deep mixed layer results. The initial plume circulation is tilted downwind (Fig. 26a), but then becomes more erect over time. A moist, but not very cold marine layer forms with the plume circulation. By four tsols, the circulation overwhelms the mean wind (Fig. 26b). The null wind location is shifted downwind, which reflects the influence of the overall mean wind background. The shift is less pronounced with weaker mean winds (not shown). In the absence of a weak to non-existent sea breeze and the perpetual plume forcing associated with a deep mixed layer, the plume circulation dominates over the mean wind. Where the plume inflow is opposed to the mean wind, the sea breeze front is sharp. On the upwind side the low level plume inflow is in the same direction as the mean wind that sea breeze front is more diffuse.

Simulations 65 and 66 have shallow mixed layers (1 m), and were designed to test the effect of the mean wind in cases where a mature, cold marine layer with a well-defined sea breeze should form. Simulation 65 becomes unstable shortly after 1.5 tsols; however, results are shown in Fig. 25, because they are relevant to a discussion of numerical instabilities in a later section.

The 3 m/s mean wind case with a shallow mixed layer remains stable and produces representative results. The initial plume is tilted downwind (Fig. 25e) similar to the deep mixed layer case (Fig. 25a). This makes sense since the shallow mixed layer has not had much time to cool and therefore mimics a situation where the lake temperature remains nearly constant. Over time, the shallow mixed layer lake does cool, which diminishes the forcing for a plume circulation and strengthens the forcing for a sea breeze circulation. By four tsols, the plume circulation is nearly non-existent and the remnants of the initial plume have been largely advected out of the domain. What remains is a very shallow marine layer. The sea breeze front on the upwind side of the lake is sharp and has propagated a few tens of kilometers onshore. If there is any onshore wind, it is very weak. Thus, the marine layer moves onshore even though the winds remain close to calm once the front passes. In contrast, the sea breeze front is more diffuse on the downwind side, and the marine layer has advected farther inland. The behavior of the marine layer and sea breeze are completely consistent with terrestrial analogues.

Simulation 67 was designed to test the effect of an initial cold lake under a mean wind background. With an initial cold lake, the initial plume circulation is strongly suppressed, while the cold marine layer and sea breeze develop quickly. The quasi-steady solution (not shown) very quickly approaches the long term solution for the shallow lake initialized at the same temperature of the air.

The time series of physical parameters for Simulations 56, 57, and 66 are shown in Fig. 26. With the exception of wind speed, results from 56 and 57 are nearly identical. This behavior is primarily because the deep mixed layer lake does not cool substantially even with the very large latent heat flux. Without a cold lake, plume circulations dominate, and these circulations are able to beat back the mean wind (Fig. 25a). The difference in wind speed between Sim 56 and 57 is due to the shift of the plume circulation null point with respect to the lake. The Bowen Ratio is closer to zero than in any simulation. The air and lake temperatures remain almost unchanged so that the sensible heat flux remains very small. In fact, some of the deep mixed layer simulations show a dynamically-driven warming of the air associated with the initial and perpetual plume circulation. In contrast, the mean wind and the plume circulation are able to produce sufficient wind and subgrid mixing so that the latent heat flux is constant at almost 350 W/m^2 .

With a shallow mixed layer and wind (Simulation 66), the lake cools very quickly and the air temperature follows. Wind speed is dramatically reduced due to the very stable marine layer and the destructive interference of the sea breeze with the mean wind. It appears that the initial mean wind accelerates the formation of the cold marine layer and sea breeze compared to the zero wind simulations. In the zero wind cases, the plume circulation must first develop in order to cool the lake. The direct thermal circulation must then work to oppose the plume circulation. An initial mean wind produces the same effect without the creation of a strong, opposing plume circulation.

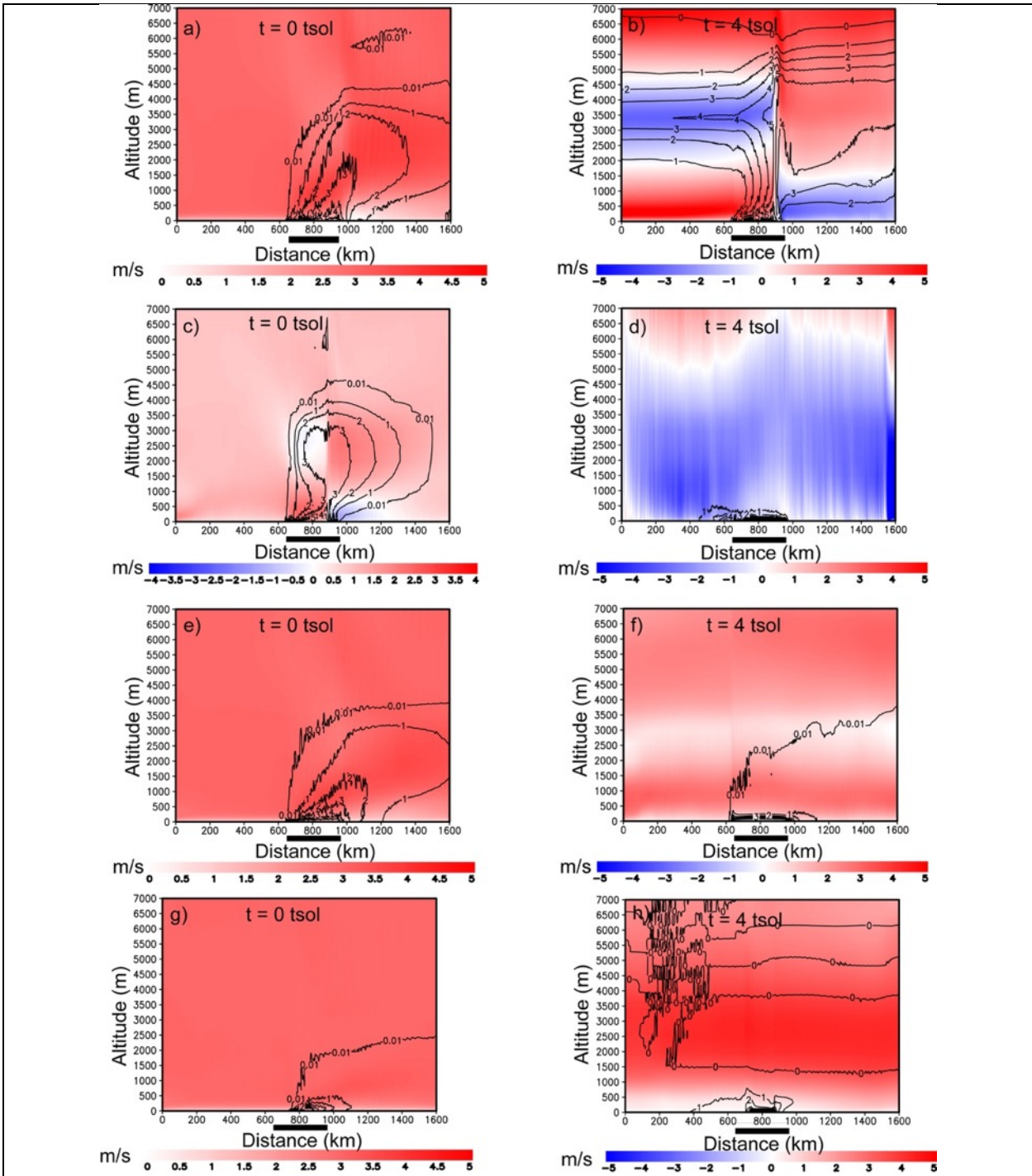


Figure 25. Results from mean wind simulations 56 (top row), 65 (second row), 66 (third row), 67 (last row). For the deep mixed layer cases (Sim 56, top row), a plume circulation dominates. When the wind is reduced to 1 m/s with a shallow mixed layer (Sim 65, second row), a plume circulation dominates initially, but then the simulation becomes unstable. When the wind is increased to 3 m/s with the shallow mixed layer (Sim 66, third row), an initial plume develops followed by a transition to a marine layer and sea breeze. If a cold, shallow lake is considered (Sim 67, last row), a cold marine layer and sea breeze develop with little to no evidence of a plume circulation. The black bar below the horizontal axis shows the lake domain. Wind speed is shaded. Methane vapor mixing ratio (g/kg) is contoured.

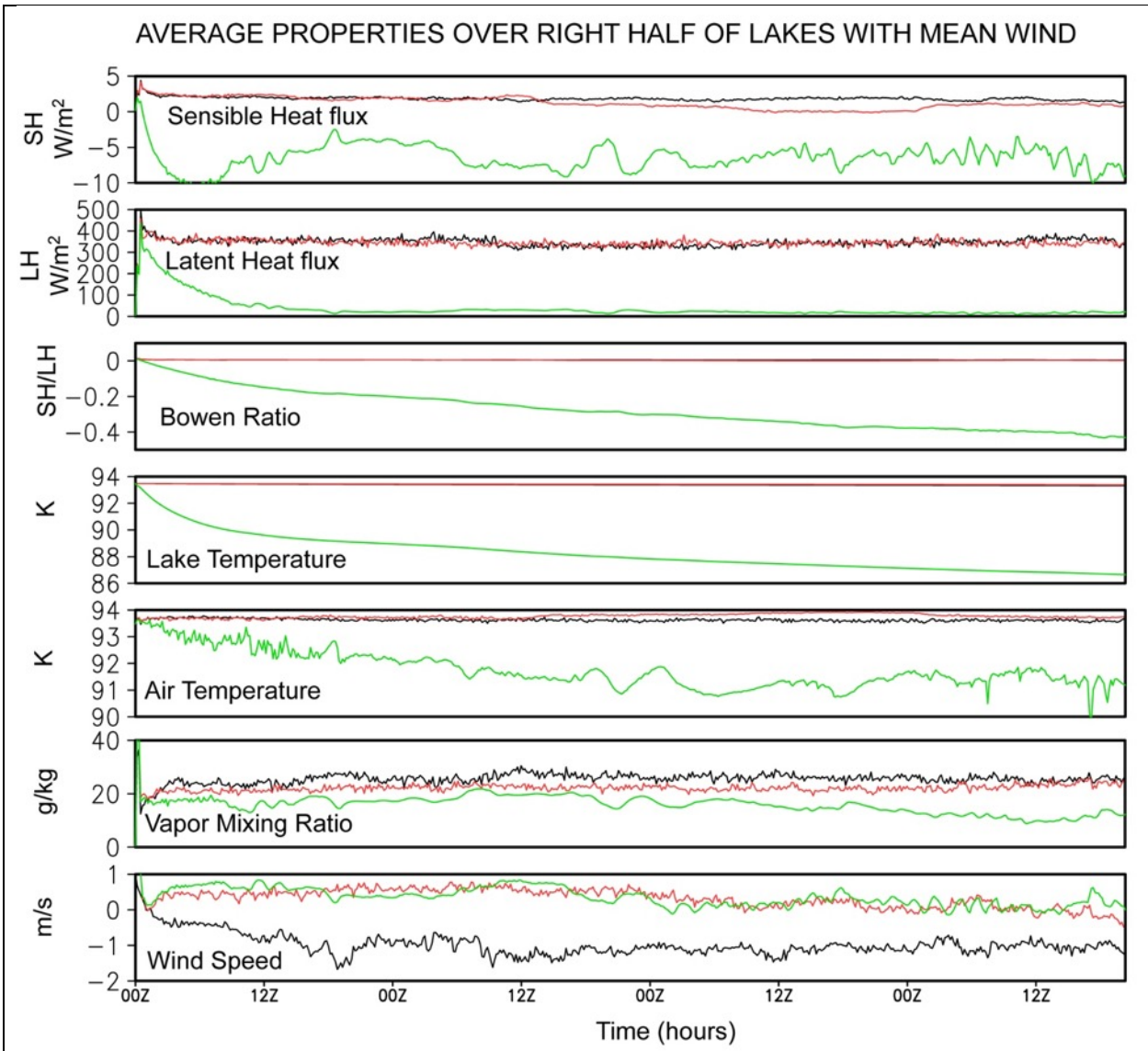


Figure 26. Time series of relevant physical parameters for Simulations 56 (black), 57 (red), and 66 (green). With the exception of wind speed, results from 56 and 57 are nearly identical, primarily because the deep mixed layer lake does not cool substantially. The wind speed difference is explained by the shift of the plume circulation with different wind speeds. The Bowen ratio in these cases is as close to zero as seen in almost any simulation due to the very large latent heat flux. With a shallow mixed layer and wind (Simulation 66, green), the lake cools very quickly and the air temperature follows. Wind speed is dramatically reduced due to the very stable marine layer and the destructive interference of the sea breeze with the mean wind.

4.5. Effect of Radiative Heating and Cooling

At the onset of this investigation, the assumption was that the magnitude of the surface fluxes would be much greater than the radiative forcing. Equivalently, it was assumed that the radiative time constant was much longer than the time constant of changes associated with the air-sea interaction. This assumption appears reasonable for some of the scenarios modeled here, but there are numerous cases where the fluxes, and especially the sensible heat flux, is the same order of magnitude or less than a reasonable value for radiative forcing at the surface ($\sim 1 \text{ W/m}^2$) [Tokano, 2005; Lora et al., 2011]. Thus, the impact of radiative forcing should be explored. We note that the biggest impact of radiative forcing is likely to be on the atmosphere, where the sensible heat flux can be small and perhaps comparable to the insolation. In contrast, the cooling of the lake by the latent heat flux tends to be one or two orders of magnitude larger than the insolation, so radiation probably has little effect. Ultimately, the goal is to include a full radiative transfer scheme into mtWRF. In the meantime, the effect of radiation is mimicked with a Newtonian relaxation scheme.

A tendency computed from the difference between the instantaneous temperature, $T(t)$, and the initial temperature, T_o , is applied as follows:

$$\frac{\partial T}{\partial t} = \frac{-(T(t)-T_o)}{\tau}, \quad (2)$$

where τ is specified relaxation time constant. Values ranging from 1 to 96 hours are tested (Table 2). The forcing is applied only to the atmosphere, and not to the lake or land. The 1 hr time constant simulations were found to be numerically unstable, because the atmosphere is forced so strongly back to the initial state that most dominant circulations that develop are due to numerical noise. These circulations amplify

over time and eventually bring the model down. Time constants of 12 hours and longer were all numerically stable.

By forcing the atmospheric profile towards the initial state, the development of a cold marine layer is suppressed. Where the sensible heat flux attempts to cool the air, that cooling is partially offset by the Newtonian forcing. Meanwhile, the plume circulation, which is a function of the saturation vapor pressure at the temperature of the lake, is essentially unaffected or perhaps imperceptibly strengthened. Overall then, radiative forcing generally tends to suppress the sea breeze and enhance the plume circulation.

The greatest effect of the Newtonian forcing is found with the shortest time constant (not including the unstable simulations). Fig. 27 shows the results after 2 tsols for experiments #38 and #45, which have this strong forcing for mixed layer depths of 1 m and 100 m, respectively. These results may be compared directly with Figure 8. The plume circulation dominates and remains dominant for the entire simulation; no obvious sea breeze develops. Nevertheless, the more rapidly cooling lake in #38 does significantly impact the strength of the plume, as marked by the lower wind speeds and substantially less atmospheric vapor content compared with the deep mixed layer case.

The time series of parameters for Simulations 38 and #5 are highly informative (Fig. 28) and may be compared with results from identical simulations in the absence of Newtonian forcing (Fig. 11). The sensible heat flux for the shallow mixed layer is larger in magnitude than most prior simulations. This is because the lake is cooling very rapidly while the atmosphere is continually being forced back to its initial warm state. The latent heat flux falls quickly and dramatically to a value near zero. This is explained by

the cooling lake and the decreasing wind over the lake. The large sensible heat flux and relatively small latent heat flux produce one of the largest magnitude Bowen ratios in all the experiments.

In contrast, the deep mixed layer has a constant lake temperature, which keeps the sensible heat flux near zero. The constant lake temperature drives a large latent heat flux, since the saturation vapor pressure remains high, and the plume circulation maintains a relatively strong wind. The Bowen ratio is near zero. The vapor does reach a near steady mixing ratio, which indicates that the circulation is efficiently exporting the vapor that is rapidly sourced from the lake.

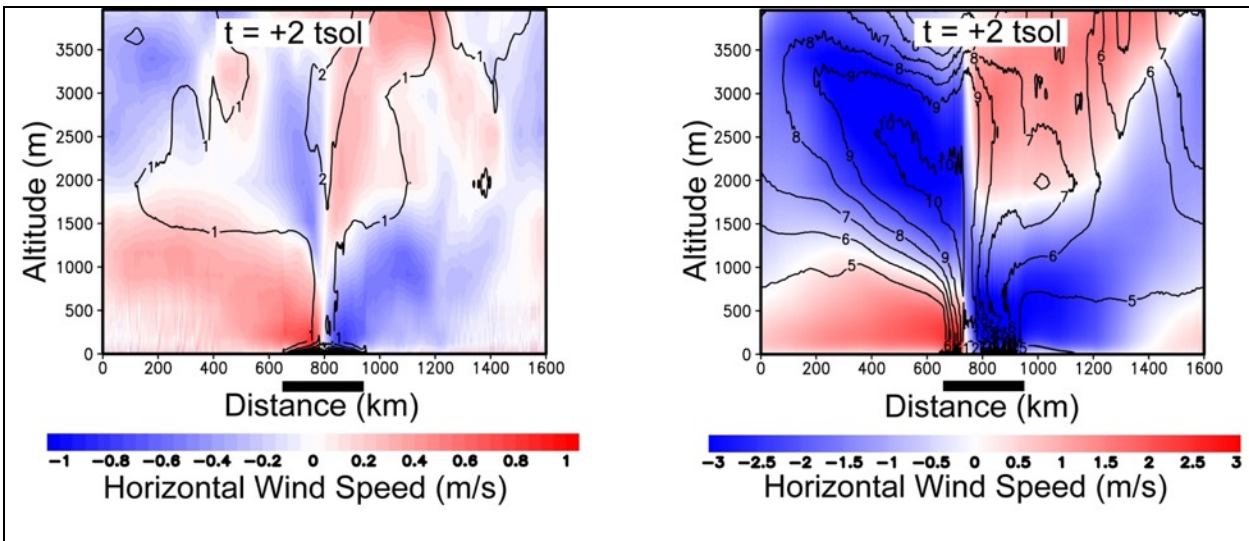


Figure 27. Simulation 38 ($\tau=12$) and 45 ($\tau=12$) with 1 m and 100 m mixed layers for 6 hr average beginning at $t_{sol}=2$. Note the asymmetry appearing in the right panel, and to a lesser degree in the left, as the left boundary values bleed into the right side of the domain due to the imposed periodic boundary condition. The black bar below the horizontal axis shows the lake domain. Wind speed is shaded. Methane vapor mixing ratio (g/kg) is contoured.

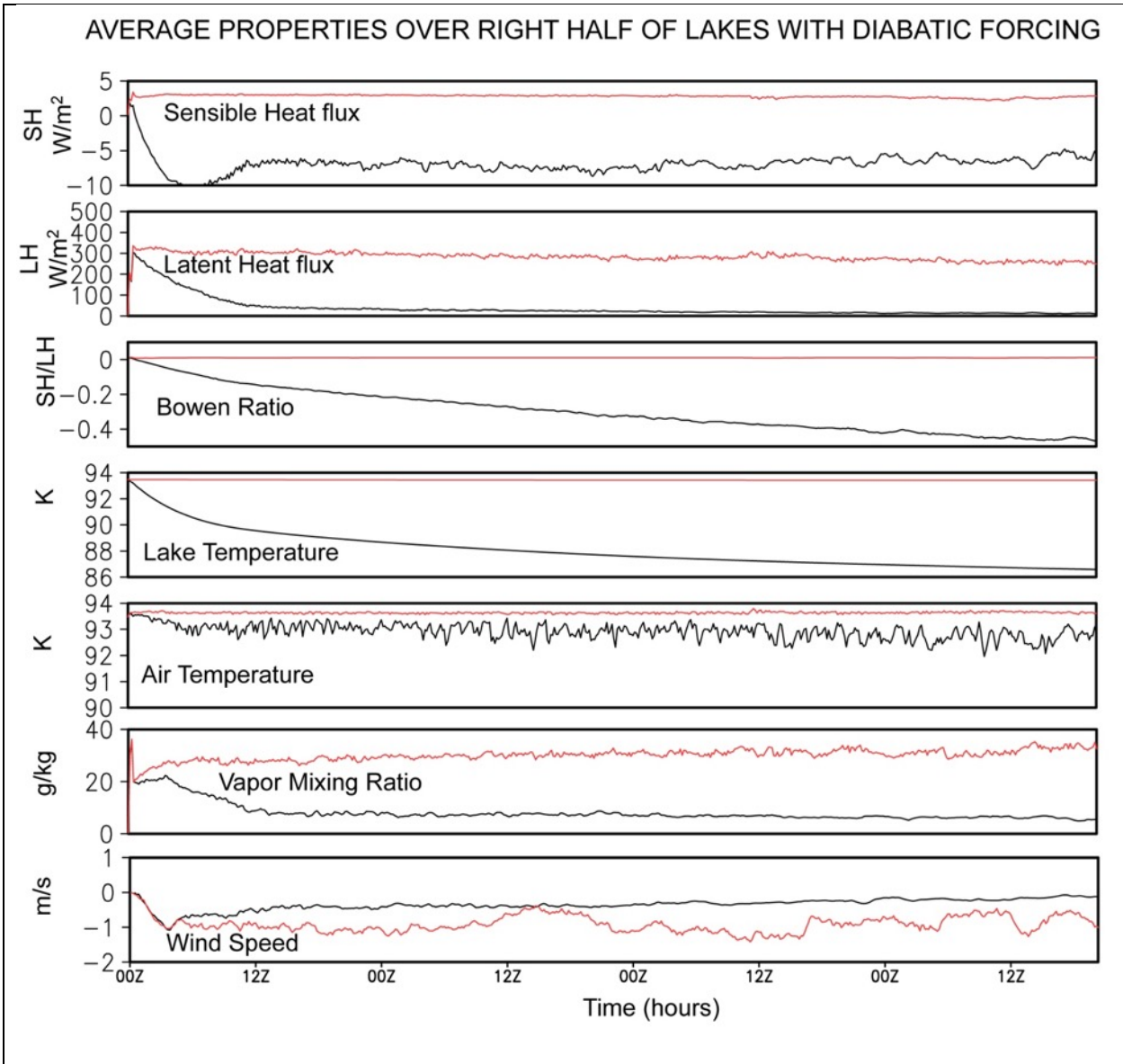


Figure 28. Time series of parameters for Simulation 38 (black: 1 m mixed layer) and 45 (red: 100 m mixed layer). The 100m mixed layer lake does not cool and the diabatic forcing keeps the air temperature very near the initial temperature. As a result, sensible heat flux is near zero while latent heat flux remains large.

Fig. 29 shows the circulations for the 1 m (Simulation 43) and 100 m (Simulation 50) mixed layer depths, but with the longest Newtonian time constant ($\tau=96$ hours). Also shown is the 100 m mixed layer depth without Newtonian relaxation (Sim 24). The expectation is that as the relaxation constant increases, the

solutions should asymptotically approach the non-Newtonian cases, which have an effectively infinite time constant.

There are differences between the unforced and forced experiments with the long, 96 hour time constant. In particular, the plume circulation is shallower with forcing. Yet, the differences are inconsequential in the big picture; there is a strong, persistent plume circulation. The shallower mixed layer experiment has a weaker plume circulation, which is what would be expected since the marine layer is colder and forces a counter-plume direct thermal circulation. A key difference, however, is the lack of any obvious sea breeze. Even the weak Newtonian forcing is able to warm the marine layer sufficiently to prevent a sea breeze from reversing the initial plume circulation.

While the longer time constant simulations do look more like the unforced simulations than the shorter time constant simulations (as expected), there are differences. From this it may be concluded that radiative forcing could very well be important, particularly for the development of a sea breeze. Future work should include radiative forcing of the atmosphere as well as the ground and lake to more accurately estimate and understand the impact of diabatic forcing.

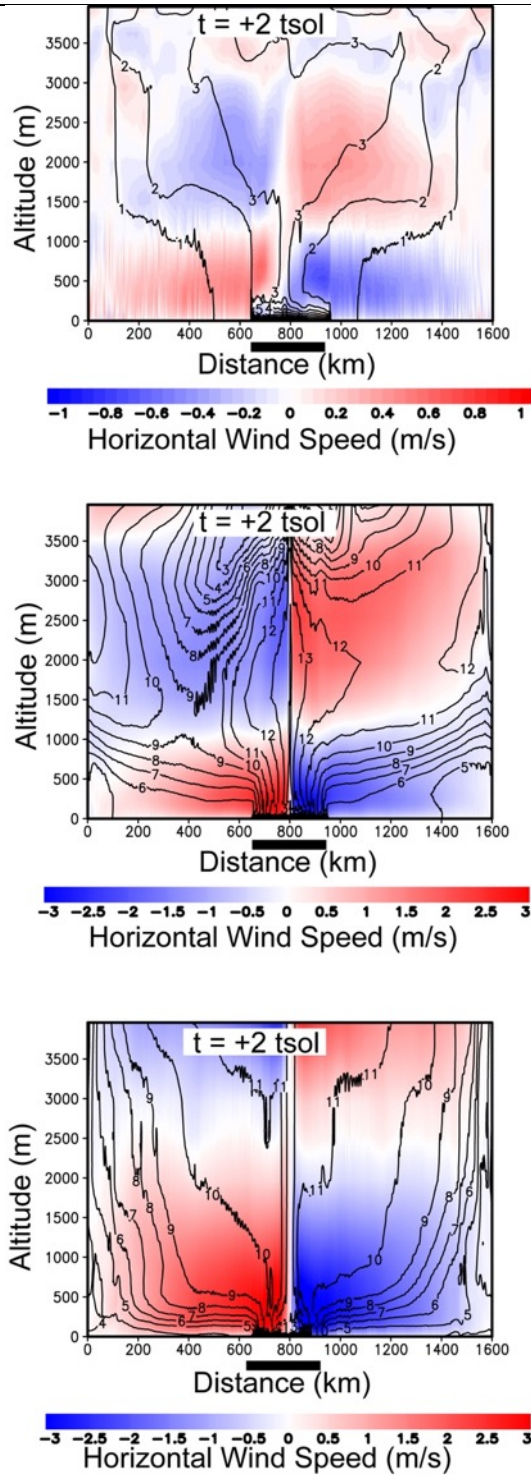


Figure 29. Long Newtonian time constant simulations ($\tau=96$ hours) at $t_{sol}=2$ for mixed layer depths of 1 m (top; sim #43) and 100 m (center; sim #50). The bottom panel shows results for an unforced 100 m mixed layer depth simulation (sim #24). The result for an unforced 1 m mixed layer (sim #4) is shown in Fig. 4. The black bar below the horizontal axis shows the lake domain. Wind speed is shaded. Methane vapor mixing ratio (g/kg) is contoured.

5. Comparison with Analytical Air-Sea Interaction Models

It is instructive to compare the range of results from mtWRF with the analytical model of Mitri et al. (2009), hereafter M09. The mtWRF solutions provide an opportunity to explore both the validity of key assumptions made by M09, as well as the overall analytical solution space. In M09 an atmosphere with unchanging temperature is assumed to blow over a lake that can evaporate and cool via both a latent and sensible heat flux exchange with the atmosphere. A bulk eddy exchange formulation is used (Eq. 1), but with a fixed transfer coefficient that implicitly has no dependence on ambient conditions. Likewise, there is an implicit assumption that no circulation is present other than a mean wind blowing across the lake, and the wind speed is fixed in time. Finally, M09 seeks a steady solution that requires a balance between the sensible and latent heat fluxes. The sensible heat flux will necessarily increase monotonically in time, because the lake is cooling and the atmosphere temperature is static; the air temperature remains unaltered despite the nonzero sensible heat flux. The latent heat flux decreases monotonically in time due to the decrease in saturation vapor pressure associated with the falling lake temperature and the moistening atmosphere. Under the assumptions above, a steady-state solution where the sensible and latent heat fluxes are equal in magnitude but opposite in sign may be found from which an equilibrium lake temperature and lake evaporation rate may be determined. Under some conditions, an equilibrium solution is not physical, because the equilibrium lake temperature falls below the freezing point; the lake will freeze before flux equilibrium is reached.

Few of the M09 assumptions are consistent with the mtWRF solutions. In most simulations with a cooling lake, the temperature of the air blowing over the lake decreases quickly as soon as it encounters the lake. This is consistent with what is generally seen on Earth: Most of the cooling of air blowing over a cold lake

occurs within the first several km [Phillips, 1972]. Consistent with M09, it is true that the simulated lake cools more substantially than the air, especially for shallow mixed layers. Thus, to first order, the assumption by M09 of a static air temperature might be considered reasonable in some scenarios, and the sensible heat flux is often driven more by the drop in the lake temperature than the change in air temperature.

Secondary buoyancy and sea breeze circulations develop in mtWRF, which alters the initial wind or creates a wind if there was none initially present. The bulk exchange coefficient also changes with time due to changes in the bulk Richardson Number (i.e., static stability changes and wind shear changes). The magnitude of the sensible and latent flux never come close to equality in any of the simulations, although it could be argued that over very, very long time scales such a balance might eventually be achieved. Those timescales, however, are so long that they become comparable to or greater than seasonal timescales, and in that case the overall background conditions would change (e.g., seasonal changes in the thermal, moisture and wind state). In all scenarios, the latent heat flux dominates over sensible heat. An equilibrium condition is also unlikely to be achieved in the mtWRF scenarios until the lake temperature is far below freezing even if one could wait it out.

It could be argued that although a flux balance condition is never achieved in mtWRF, there are scenarios where an effectively trivial balance solution is achieved. The trivial case is where the turbulent fluxes become so small that they provide essentially no forcing even if they are unequal. This scenario is achieved when a very stable and moist marine boundary layer develops. A stable marine layer has weak winds, small bulk turbulent transfer coefficients, and reduced air-sea gradients in temperature and moisture. While latent heat flux may dominant as indicated by the Bowen ratio, the actual fluxes are

inconsequentially small and may be considered effectively zero. In this sense, the equilibrium flux solution of M09 becomes effectively valid.

On Earth, an equilibrium between the turbulent fluxes is rarely observed. Bowen ratio measurements over lakes, oceans and wetlands are typically -0.5 to 0 [e.g., Roulet et al., 2986; Den Hartog et al., 1994; Vallet-Coulomb, 2001; Lenters et al., 2005; Elsaywaf et al., 2010] and are never observed to approach -1.0. Only over semi-arid land does the sensible heat flux equal the latent heat flux in magnitude [e.g., Goutorbe et al, 1994]. This reality holds from the tropics to the arctic with exceptions for extreme events where arctic air passes over warm lakes [e.g., Philips, 1972], which is not likely for Titan where the pole to equator temperature gradient is only a few Kelvins and local values are less [Tokano et al., 2005] Thus, the mtWRF simulations are in concert with the overwhelming weight of terrestrial observations.

Both the buoyancy circulation and the sea breeze circulation have the ability to transport moisture vertically and horizontally. The buoyancy circulation in particular has the ability to export heat and moisture aloft, well beyond the horizontal scale of the lake itself. When viewed as thermodynamic system, energy balance potentially requires consideration of a large boundary for the system rather than just between the bounding shoreline. Energy balance need not be achieved over the lake, yet alone in a single atmospheric column over the lake. Latent and sensible heat fluxes over the lake can be balanced by exchanges far away. On Earth, when the net energy flux exceeds that available from radiative forcing and subsurface conduction, it is known as the Oasis effect [e.g., Holmes and Robertson, 1958; Linacre et al., 1970], and is usually associated with dry desert air encountering a lake or irrigated land. In most of the mtWRF cases, the secondary circulations that develop play a large role in the air-sea exchange, and the impact of the buoyancy and sea breeze circulations must be accounted for in addition to whatever

exchanges may be driven by the initial mean wind. The atmosphere immediately above the lake does not continually moisten due to ongoing latent heat flux, although moisture is continually added to the atmosphere system. Instead, the moisture tendency from evaporation is offset by export of that moisture by the circulation.

Despite the substantial differences between the assumptions of M09 and the mtWRF assumptions, it is fair to say that M09 did accurately describe the qualitative nature of the problem. The lake does cool from evaporation (even if it is excruciatingly slow in some cases) and the atmosphere does moisten. Equality of the fluxes might be achieved over a very long time scale, but the state of the lake and atmosphere would be different from what M09 predicted. Accordingly, the rate of evaporation would be different, as would the threshold conditions for when a lake would freeze. The mtWRF solutions indicate, however, that the details of the solution are highly dependent on a large number of parameters and initial conditions. It is very difficult (perhaps not even possible) to reduce the problem to a simple analytical model.

Depending on the initial condition, latent heat fluxes from mtWRF can be effectively zero or up to several hundred W/m^2 . Without further constraints, the mtWRF results provide only upper and lower limits on lake evaporation rates equivalent to this range of latent heat flux. M09 indicate that a flux of $6 \times 10^{-4} \text{ kg m}^{-2} \text{ yr}^{-1}$ over the whole planet is required to balance the photochemical loss of methane. For a flux given in W/m^2 and the latent heat of vaporization, L , in Table 1, evaporation rates in units of $\text{kg m}^{-2} \text{ yr}^{-1}$ are given by:

$$\text{Evaporation (kg m}^{-2} \text{ yr}^{-1}) = 0.17 * \text{Flux (W m}^{-2}\text{)}. \quad \text{Eq (3)}$$

Thus, as noted by M09, even a few W/m^2 and a lake coverage of a few percent is sufficient to balance the photochemical loss rate. For example, a flux of 1 W/m^2 with a global lake coverage of 1% is equivalent to a net global evaporation rate of $1.7 \times 10^{-3} \text{ kg m}^{-2} \text{ yr}^{-1}$, which is an order of magnitude larger than what is required.

The above calculations do not take into account precipitation. For the lower end of the estimated latent heat fluxes from mtWRF, and assuming that much of the vapor is returned somewhere to the surface, the net evaporation (evaporation minus precipitation) could, in fact, be close to the photochemical loss rate. The low end of the evaporation rates in mtWRF would not produce a noticeable change in lake levels. For the larger evaporation rates of several hundred W/m^2 , it would be remarkable if the evaporation and precipitation could balance globally to within the $\sim 10^{-4} \text{ kg m}^{-2} \text{ yr}^{-1}$ needed to match the photochemical loss rate. In the absence of an exact balance, that would mean the atmospheric abundance of methane could fluctuate from Titan year to Titan year with amplitudes well above the average loss. Since the reservoir of methane in the atmosphere is large ($\sim 6000 \text{ kg/m}^2$) compared to the known surface reservoir, however, the atmospheric variation would be fractionally small. From the standpoint of the lakes, pumping as much as $50 \text{ kg m}^{-2} \text{ yr}^{-1}$ of methane over their surface would result in noticeable changes in lake level in the absence of resupply, as noted by M09.

6. Freezing Lakes and Swamps

Since the flux equilibrium condition of M09 is never reached in the simulations, and since a large number of the simulations show appreciable cooling of the lake, the possibility of lakes freezing is reasonable consideration. The exact temperature at which freezing occurs would depend on the composition of the

lakes. Stofan et al. [2007] indicate that the presence of dissolved nitrogen is sufficient to depress the freezing temperature by 3 to 5 K below the nominal equatorial temperature of 93.6 K. Many simulations show it is possible to cool below 5 K in a reasonable time (i.e., fractions of a Titan season). Hoftgartner and Lunine [2013] find similar results depending on the fraction of ethane. Tokano [2009b] suggested that pure and shallow methane lakes could freeze seasonally, while the deeper and less pure lakes were more likely to remain liquid. All of these theoretical conclusions, however, make assumptions, at least implicitly, about the poorly understood density behavior of liquid methane and methane solutions near the triple point.

Based on the mtWRF simulations, the most conducive conditions for freezing are shallow mixed layers, low atmospheric humidity, and a non-zero background wind. Deep mixed layers are not conducive to freezing, and it is reasonable to conclude that lakes with deep mixed layers will not freeze. That is not to say that deep lakes will not freeze; they can, as long as the cooling fluid remains near the surface of the lake (i.e., a shallow mixed layer in a deep lake). Deep lakes are also not deep everywhere. Radar bathymetry [Hayes et al., 2010; Wall et al., 2010; Mastrogiuseppe et al., 2014] indicates the lake bottoms have a relatively gentle slope from the shoreline. The depth of the mixed layer can be no deeper than lake itself at any given point, thus the areas near the shoreline may behave as shallow mixed layers that could be more susceptible to freezing, particularly if horizontal transport (i.e., currents) is minimal. If cold fluids are more dense than warm, the cooling of the shallows would necessarily produce a buoyancy-driven current with a surface return flow of warmer fluid directed toward the shoreline.

Radar backscatter indicates very smooth lake surfaces right up to the shoreline (excluding “magic islands” [Hoftgartner et al., 2016]), which were interpreted to be liquid when dielectric properties and brightness

temperature are considered [Stofan et al., 2007; Wye et al., 2009]. These results would seem to rule out ice covered lakes as a widespread phenomenon. Yet, given the exotic and poorly constrained properties of the lakes, ice cannot be completely ruled out for all lakes at all times; Cassini conducted flybys and not continuous global mapping. The smoothness of the lakes, if liquid, requires low wind speeds. Given Titan's sluggish circulation, low wind conditions are probable, but the mtWRF simulations show that evaporation from a liquid surface does generate local circulations that can be intense by Titan standards. If the largest lakes are indeed liquid then this places constraints on wind speed, which at least reasonably exclude initial conditions that generate the strongest simulated circulations. While the freezing of the large seas and lakes of Titan cannot be completely ruled out, the overwhelming consensus based on solid evidence is that the reservoirs are liquid. What is possibly more likely is the freezing of very small and shallow lakes or ponds, or infrequent events that might temporarily freeze at least part (the shallows) of a large lake.

It remains a curiosity that so few clouds were observed in the northern summer if the lakes are liquid [e.g., Turtle et al., 2018]. While the appearance of clouds nearby lakes is not guaranteed (see Section 8), liquid lakes should be an active source of methane vapor even with relatively low latent heat fluxes. General circulation models predicted deep convective clouds associated with the warm summer boundary layer, but these clouds failed to show themselves during any of the Cassini flybys [Schneider et al., 2012; Lora et al., 2015]. The mtWRF simulations show that the nearby lake environment can be stabilized due to the cold marine layer, but that effect appears to be localized. Perhaps the northern lake district taken as a whole acts to stabilize all of the northern high latitudes against deep convection. Barth and Rafkin [2007] found that moistening a Huygens-like thermal profile results in convective available potential energy (CAPE) that feeds deep convection. If the atmosphere is moistened while also cooling the lower levels, it

is possible to remain convectively stable with no CAPE. The methane that is released in this scenario would then be transported globally, including to the southern high latitudes, where deep convection becomes possible half a Titan year later during southern summer. This is more likely if the southern high latitude surface is relatively dry so that heating results in low level heating, unlike a possibly damp northern high latitude surface.

Damp ground can also cool by evaporation, and unlike a lake it cannot mechanically mix. Instead, the thermal structure is controlled by the turbulent fluxes and conduction/diffusion processes with the subsurface. Although we do not model damp ground in this study, extrapolation of the lake simulations may provide guidance on the behavior. Swamp-like surfaces might behave somewhat like a lake with subsurface energy conduction replacing the mixing process. It is worth considering whether a damp surface could cool to the frost temperature or even produce a frozen crust. Early analysis of Huygens penetrometer data suggested that it landed on a crust, which after heating failed and released methane [Abbott, 2005]. This could be consistent with the melting of an ice crust and the release of methane vapor from the damp ground beneath; however, this preliminary interpretation has generally given way to an explanation of the signal that favors rocks and pebbles in conjunction with the kinetics of landing on a heterogeneous, bumpy surface. A moist or damp surface without a crust is still reasonable at the Huygens landing site [Zarnecki et al., 2005; Atkinson et al., 2010]. If damp ground could freeze due to evaporation, the process may be especially favored in the cold polar night. If this happens near the marine layer environment, hoar frosts and ice-coated ground could be a regular feature in the polar marine microclimate.

7. Winds and Waves

Building on various previous predictions about the existence and dynamics of waves on Titan (e.g., Ghafoor et al. [2000] and Lorenz and Hayes [2012]), Hayes et al. [2013] analytically explored the conditions required to generate and grow capillary-gravity waves in Titan's lakes and seas. They determined the threshold wind speed required for wave generation as a function of lake composition. They quantified these threshold wind speeds using the wind as measured at 10 meters above the surface, which is denoted as U_{10} . The U_{10} diagnostic is used to compare the threshold surface wind stress calculated by Hayes et al. (2013) and the winds predicted by mesoscale models and general circulation models. For a pure methane lake, Hayes et al. [2013] derived a threshold of $U_{10}^{th} = 0.4$ m/s for the onset of wind-driven waves. By inverting equation 2.3 in Hayes et al. [2013], we derive the threshold surface friction velocity, u_*^{th} , to be 0.012 m/s. This surface friction velocity represents the speed of the atmosphere in the constant flux layer above the lake/sea surface. (We encourage future studies to employ u_* or surface stress rather than U_{10} , since the prior are standard outputs for most models and are also standard parameters in micrometeorology).

Our canonical experiment (Simulation 4), discussed previously, provides a good example of how our simulated surface friction velocities compare to the u_*^{th} . Fig. 30 shows the value of the friction velocity for every horizontal grid point over the lake as a function of time for the canonical simulation. Over the first half of a $tsol$, a large fraction of the winds exceed the threshold for the generation of waves on the sea. The initial buoyant methane plume that forms during the early phases of these idealized simulations creates these strong winds. As the mesoscale dynamics evolve from a circulation dominated by a plume land breeze to a circulation dominated by a sea breeze, the magnitude of the largest winds weakens by approximately a factor of four.

Our simulations, however, predict that wind gusts that exceed the threshold friction velocity are infrequent. This can be seen in Fig. 31, which compares the histogram of u_* for tsol 1 versus tsol 5 of the simulation. In the tsol 1 histogram, a large number of the wind gusts exceed the threshold for wave generation. The tsol 1 winds, however, are part of the spin-up (plume phase) of the simulation and likely do not represent physically realistic or likely circulations.

The histogram of u_* for tsol 5 of the simulation is likely more representative. During this stage of the simulation, a sea breeze circulation exists over the lake, with a small, but not insignificant fraction of gusts exceeding the threshold for generating wind-driven waves. On the order of 2000 out of 20,000 wind counts exceed the wave threshold (i.e., 10%) at tsol 5. A reasonable interpretation is that this frequency should be sufficient to produce a wave somewhere, although it may not be sufficient to be observed if it is a very brief disturbance and/or highly confined in area. It's also worth noting that a slight shift of the threshold to higher winds (e.g. from 0.01 to 0.2 m/s) can drastically alter the statistics. The uncertainty in the actual threshold for lakes must be considered as part of the interpretation of the modeled friction velocity distribution.

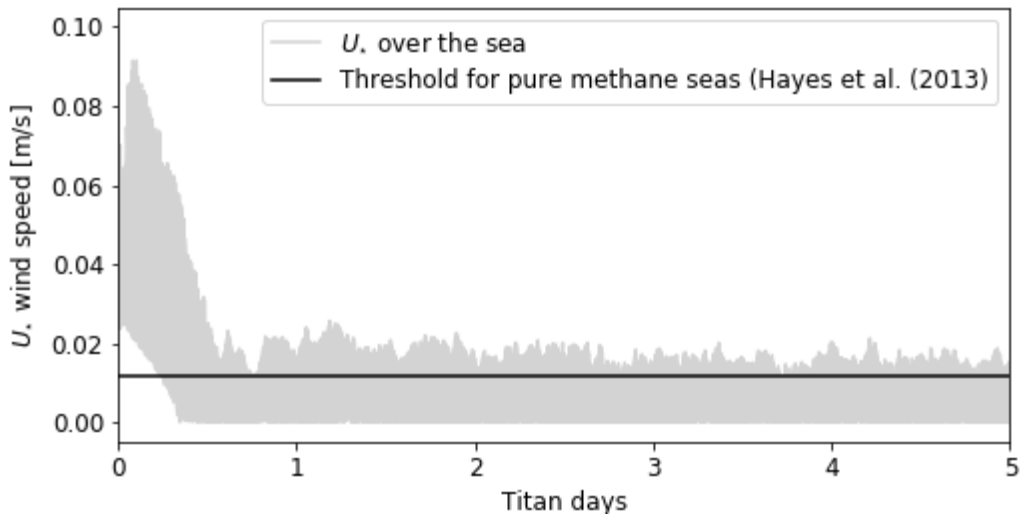


Figure 30. All of the simulated wind speeds over the lake as a function of time for the canonical simulation (Sim 4). A grey line is plotted for each horizontal grid in the lake, 150 lines in total, which results in this collection of overlapping wind evolutions. The black line marks the threshold friction velocity for the generation of waves, based on Hayes et al. [2013].

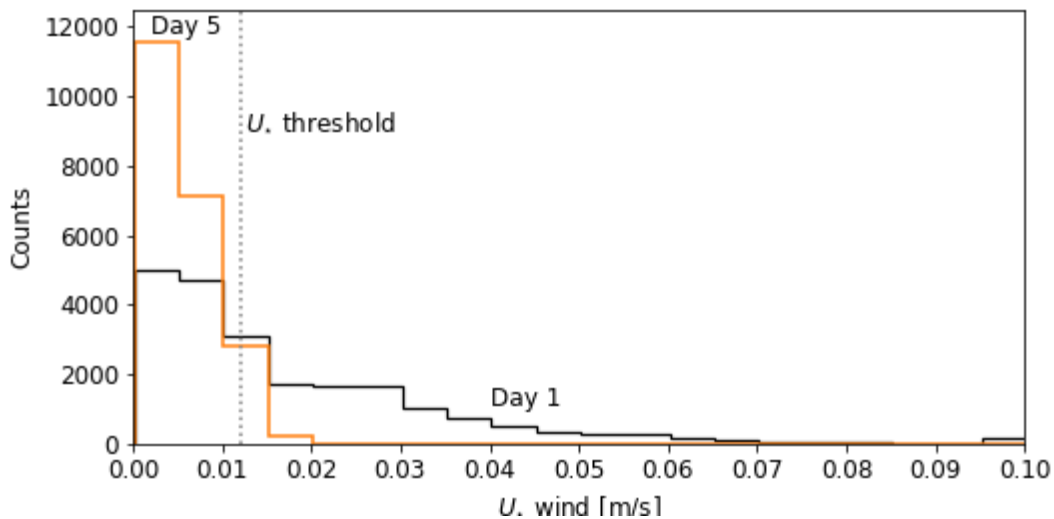


Figure 31. Histograms at two different times in the canonical simulation show how the likelihood of exceeding the wind-drive wave threshold changes with time. The dashed vertical lines indicate the $U_*^{th} = 0.012$ m/s threshold for the generation of wind-driven waves. The black line is the histogram of wind speeds for tsol 1 of the simulation and the grey line is the histogram of wind speeds for tsol 5 of the simulation.

The existence of waves on Titan’s seas and lakes remains unconfirmed. Cassini did infrequently observe surface features of the lakes of Titan that are consistent with wind driven waves [Barnes et al., 2014;

Hofgartner. et al., 2014]. These surface features, however, are also consistent with other possible formation mechanisms, including floating and/or suspended solids and bubbles [Hofgartner. et al., 2014]. Therefore, there is insufficient evidence to definitively claim that the observed surface features are wind-driven waves.

Many simulations show winds that are stronger than those of Simulation 4. All of these are situations where a plume circulation dominates. In those cases, it becomes more likely that waves would appear, while it simultaneously remains true that there is no definitive observational evidence for widespread wave activity. This could mean that the initial conditions and configurations that result in strong and persistent plume circulations are not realistic, and that simulations with at least a sea breeze circulation that damps the plume circulation are more realistic. For those simulations with a sea breeze case, mtWRF suggests that waves driven by the mean wind are occasionally possible, especially given the uncertainty in wind thresholds. Wind gusts might be able to occasionally produce waves, but turbulent gusts decrease in magnitude as the marine layer strengthens in magnitude. The paucity of observational evidence that could be interpreted as wave activity strongly suggests that the conditions over the lakes of Titan are more likely to resemble the subset of mtWRF outcomes with strong and stable marine layers and minimal air-sea interaction. Absence of evidence is not evidence of absence, and the paucity of wave observations cannot definitively constrain the magnitude of air-sea circulations that occur on Titan.

8. Clouds

Microphysics are not active in the simulations, but we can evaluate if and when the model atmosphere approaches or exceeds saturation. None of the simulations initialized with a dry atmosphere come

anywhere close to producing a saturated atmosphere. Even the most extreme evaporation cases are unable to generate an environment conducive to cloud formation. Generally speaking, the circulations export evaporated moisture, and the stronger the evaporation the more rapid the transport of vapor. Almost all of the simulations with an initial relative humidity (RH) of 80% produce a saturated atmosphere, only one of the RH=50% cases does, and none of the RH=20% cases do. These non-zero RH configurations are the focus of this section.

Before proceeding to discuss the most favorable cloud formation cases, it is essential to reestablish the historical and genetic cloud nomenclature used by the terrestrial community, but which has become muddled in the Titan literature. First, fog is a cloud that is contact with the ground (American Meteorological Society, 2018). “Ground fog” would then seem a redundant terminology, but instead refers to a patchy fog with mostly unclouded skies above (American Meteorological Society, 2018). There are other types of fog that can be further identified, based primarily on the formation mechanism (e.g, mixing fog, radiation fog, frontal fog). While fog is a low cloud, low clouds are not necessarily fogs and the two terms should not be used interchangeably. The distinction is important, because the radiative and microphysical forcings in fog are distinctly different from other low clouds [Cotton et al., 2010]. Unfortunately, from a satellite perspective, fog and stratus (a type of low cloud) are often indistinguishable.

Second, “lake effect” clouds are generally not just clouds caused by a lake. Lake effect clouds almost always refer specifically to the clouds generated when cold air blows over a warm lake accompanied by concomitant large turbulent energy fluxes. The lake effect snowstorms in the Great Lakes region are the prime example of lake effect clouds (Holroyd III, 1971; Lavoie, 1972; Hjermfelt, 1990; Niziol et al., 1995).

Large sensible and latent heat fluxes produce shallow but intense convective clouds that can result in copious amounts of precipitation near the shoreline, particularly if the air is forced over rising terrain. The reference to lake effect clouds in the Titan literature (e.g., Brown et al. 2009a), while colloquially accurate, seems unlikely to be referring to the scientific meaning of lake effect clouds generally accepted by the terrestrial meteorological community.

There are sea breeze or lake breeze clouds. These are clouds generated by the upward forcing of moist air, possibly moistened by the lake or sea, along the sea or lake breeze convergence boundaries. If the air is conditionally unstable, convective clouds may develop along the sea breeze, but not necessarily so. A prime example of these types of clouds is found along the Florida peninsula (Pielke, 1974; Blanchard and López, 1985; Kingsmill, 1995). It is likely that these are the types of clouds that have been improperly identified as lake effect clouds in the Titan literature. We encourage future papers to more strictly follow terrestrial nomenclature and genetic descriptions of clouds to avoid further confusion.

Scenarios that start with a humid atmosphere are one place to look for the possibility of cloud formation. We explicitly exclude in our analysis the upper domain of the model where the atmosphere may be initialized to saturation (Fig. 5); those regions would be conducive to cloud formation, but that situation is not due to air-sea interaction and is irrelevant to cloud formation mechanisms associated with the lake. In nearly all the 80% humidity cases, saturation conditions are reached in the outflow of the initial plume circulation, and the conditions persist for the duration of the simulation even if the plume circulation dies away. For example, in Simulation 36, extensive supersaturation ($RH > 120\%$) is produced at altitudes between 3.5 km and 5 km in the outflow of the initial plume circulation over the entire lake. Saturation is just barely reached in a 1 km deep layer centered at 4 km altitude for Simulations 52, 53, 63, and 64.

Interestingly, none of the RH=80% simulations produce supersaturation anywhere other than in the outflow region of the initial plume circulation. In particular, the atmospheric relative humidity in the marine layer is usually *lower* than the initial relative humidity, typically ranging from 50% to 75%. The initial plume circulation vertically transports the initial very moist atmosphere, and the combination of vapor from evaporation and the developing net atmospheric circulation is unable to return the atmosphere to the initial state. In terms of total methane vapor, the atmosphere is continually gaining methane mass, but that vapor is unable to condense anywhere near the lake due to the horizontal export of that vapor.

The observational lack of extensive cloudiness extending over lakes argues for the absence of a plume circulation when the background relative humidity is high. Further, as previously noted, if the background relative humidity were at 80%, deep convection would be expected for a Huygens-like temperature profile. The only way to prevent such convection would be to stabilize the lower atmosphere through cooling. This cooling can be achieved by the air-sea interaction, but the model simulations indicate that this cooling also comes with a net drying with respect to relative humidity. Of course, if the lakes are frozen, that could also explain the general lack of observed clouds, but that situation has mostly been ruled out, as previously discussed.

The inability of the RH=80% simulations to produce saturation in the marine layer after the initial plume phase also argues that marine layer clouds should be rare. Thus, the model simulations are consistent with observations of almost universally cloud-free lakes. Lakes provide a source of vapor, but the ensuing

dynamics associated with the air-sea interaction keep the atmosphere from saturating and producing clouds. The single instance of a cloud found near a lake (Brown et al., 2009a) could be an exception to this rule, or the appearance of the cloud by the lake could be coincidental and completely unrelated to air-sea interaction whatsoever.

The baseline lower relative humidity cases (Simulations 34 and 35) produce an elevated layer of enhanced relative humidity in the outflow region of the initial plume circulation, but remain well below saturation. The 20% case has RH \sim 40% in the plume outflow and in the marine layer, and the 50% case has a plume outflow that peaks at RH \sim 65% and a marine layer that settles to RH \sim 50% after a near-surface peak of \sim 70% during the initial plume phase.

A cold, deep lake experiment with RH=80% (Simulation 52) was conducted to see if a more rapidly developing sea breeze circulation might allow the near-surface atmosphere to cool and moisten more than the baseline simulation. It did not. The plume circulation was suppressed, as expected, but the near-surface relative humidity drops to under 70%. A mean wind (1 m/s), shallow mixed layer case with RH=80% was then performed (Simulation 53) to investigate whether that combination of parameters might enhance the evaporation and cool the near-surface air to saturation. It did not. No configurations were found that could produce a saturated marine layer, and only the RH=80% simulations produced an initial saturated layer in the plume outflow.

Based on the non-zero relative humidity simulations, we conclude that the neglect of condensation processes in the mtWRF simulations is reasonable. Except for the initial plume circulation and in the upper

model domain where relative humidity is initialized to 100%, no clouds would be expected to form. Activating a microphysical scheme would do nothing except increase the integration time.

9. Importance of Model Numerics

Titan is a weakly forced system. The magnitude of the tendencies in the model prognostic variables when compared to machine precision and numerical error (e.g., errors in advection operators) can be orders of magnitude smaller for Titan than for planets like Earth or Mars. For example, the diurnal range in temperature for Earth can be 10 K or more, while Mars can approach 100 K. On Titan, 1 K or less may be typical. Yet, the machine precision and the accuracy of numerical operators do not change. Consequently, the magnitude of the errors for Titan can be a significant fraction of the magnitude of the forcing and prognostic variables.

Errors of 0.01 K may not matter much for Mars, but on Titan they can. Indeed, we showed in the case of an initially cold lake for which the lake cooling tendency was too small to produce a change in the lake temperature (Simulations 31, 32, and 33). By going directly into the code, we were able to determine that the lake temperature tendency was non-zero, but small. When multiplied by the time step and then added to the lake temperature from the previous time step, floating point arithmetic resulted in no net change in the lake temperature. This numerical error is an energy leak in the system—latent heat is being removed from the lake and deposited into the atmosphere, but the lake energy is not changing. One solution is to accumulate the lake temperature tendencies over a long enough time scale so that the value eventually becomes large enough to be represented by the floating precision (i.e., a split-time scheme).

Going to double precision instead of the standard single four byte precision can help to reduce the issue, but it does not eliminate the general concern.

The most pronounced and initially obvious numerical issues were associated with the dynamical fields and not with the lake thermodynamics. In the purely symmetric scenarios (those without mean wind), the left side of the domain should be a mirror image of the right. In no simulation is this condition precisely true, and in a few cases is it strongly violated. Good examples of asymmetries were noted in Fig. 14d and Fig. 23b. Many of the asymmetries appear to be a direct result of how periodic boundary conditions are implemented. The rightmost boundary is arbitrarily assigned to the value on the leftmost side. This does satisfy the periodic boundary condition, but is indeed arbitrary. The leftmost boundary could just as easily been assigned the value of the rightmost boundary, in which case the asymmetry would be reversed. The appearance of any asymmetry is still due to numerical noise, since a perfect model would produce equal values at both boundaries, in which case an arbitrary mapping is inconsequential. But there are no perfect models, and the arbitrariness is not inconsequential. For example, if the outflow of a plume circulation reaches the left boundary a little before the right boundary, the solution in the left half of the domain will bleed more and more into the right domain and produce an asymmetry. Given enough time, the entire solution may become nonphysical. This puts an inherent time limit on the total integration time. We have examined all the simulations to ensure that the results presented here are at integration times that show reasonably symmetry (unless otherwise noted).

Numerical instabilities were also found for the 1 m/s background wind case with open boundary conditions (Simulation 65; Fig. 25d). In this case, the solution was expected to be asymmetric, but the appearance of domain-wide momentum directed completely opposite to the initial mean wind cannot be

physically correct. Once again, the boundary condition appears to play role, because the momentum reversal appeared shortly after the plume outflow reached the domain boundary and the instability amplified quickly. Interestingly, the stronger background wind case of 3 m/s did not exhibit this behavior. Apparently, the stronger wind was sufficiently far from zero so that boundary condition inaccuracies were unable to flip the sign of the wind field. It is also interesting to note that Simulation 56 with a 1 m/s background wind and open boundary conditions did not exhibit instability. Apparently, the persistent strong plume forcing associated with the deep mixed layer was sufficient to overwhelm numerical instabilities.

The issues with numerics lead to the very serious question of whether these simulations, and really simulations of any weakly forced planetary system, can be trusted at all. Embedded within this issue is a lesson about blindly taking perfectly adequate and proven Earth models and applying them to alien worlds that occupy an atmospheric parameter space far outside terrestrial norms. This paper would have likely have been completed more than two years ago had we started with a WRF code base rather than our existing TRAMS model [Barth and Rafkin, 2007]. We found numerical errors and conservation issues in TRAMS that were too large for the air-sea interaction problem and spent considerable time trying to understand and (unsuccessfully) correct the errors. Often the TRAMS errors were manifested in a very rapid growth of strong, unidirectional (asymmetric) winds alternating in height. Like mtWRF, these nonphysical modes could be further amplified by the numerical boundary conditions (e.g., zero gradient or constant gradient lateral boundaries). TRAMS remains a perfectly adequate for deep convective cloud simulations, because those forcings are enormous—comparable to Earth—and dominate by orders of magnitude over the background numerical noise.

After more than a year of attempting to unsuccessfully reduce TRAMS numerical artifacts to an acceptable level, we decided to try WRF, which was a considerably more modern and hopefully more quiet numerical core. This turned out to be the case, and after considerable more effort of testing and documenting the growth and behavior of asymmetries in the solution, we became increasingly confident in the majority of the model solutions. Nearly all the simulations, if run long enough, eventually become substantially asymmetric and non-physical. For all the simulations from which we've derived conclusions, the asymmetric component (i.e., nonphysical solution) is small. Nevertheless, there are some mtWRF configurations that have large inherent instability, as we've noted.

It may very well be that running TRAMS or mtWRF as traditional mesoscale models with imposed GCM boundary conditions will help solve the problem. The imposition of physical boundary conditions should keep the model from running toward nonphysical solutions. We expect to implement the 3-D, GCM-forced simulations soon and we will test this hypothesis.

The ultimate solution is to work with model core developers early in the design stage to ensure that the model numerics better deal with weakly forced conditions, including the instances that might be encountered on Earth. This problem is not just a Titan air-sea problem. Similar problems can plague Venus and Titan GCMs where the forcing on the angular momentum budget can be very small—perhaps comparable to numerical error [e.g., Read and Lebonnois, 2018]. Anytime a process is regularly producing small tendencies compared to the prognostic variable, or where the final forcing is the residual of large terms, there is potential for problems.

10. Summary and Conclusions

The terrestrial WRF model was modified to study air-sea interaction on Titan under a variety of idealized scenarios in two dimensions. The effect of lake size, lake mixed-layer depth, lake-atmosphere temperature differences, atmospheric humidity, mean background wind, and diabatic forcing were all investigated. The general, quasi-steady solution is a non-linear superposition of a plume circulation driven by the buoyancy of evaporated methane and a sea (or lake) breeze circulation driven by the thermal contrast between the cold marine layer over the lake and the warmer inland air. The specific solution depends on the configuration and ranges from a persistent and strong plume circulation with little to no sea breeze, or a rapidly developing sea breeze and highly suppressed plume circulation.

Solutions favoring a plume circulation are those where the lake temperature cools slowly or not at all. Deep mixed layers are most associated with the persistent plumes. Simulations dominated by plumes tend to have the strongest winds. The general lack of wave activity on Titan as inferred by radar strongly suggests that strong plume circulations are unlikely. Strong plume circulations also produced supersaturated outflow layers in the RH=80% simulations. No such widespread clouds are observed. The most rapid lake cooling is associated with initial plume circulations. In many cases, the lakes cool to temperatures that are close to or possibly below the uncertain freezing temperature. Frozen lakes have not been observed. All of the model results taken together with observational constraints strongly suggest that widespread, strong plume circulations are not present on Titan. This then implies that there must be some semblance of sea breeze circulations to counter the plume circulation tendencies, and this in turn implies the presence of a cold marine layer that is needed to drive that sea breeze circulation.

Conditions favoring a damped plume circulation or an outright sea breeze are cold lakes and shallow mixed layers. Initial background wind, relative humidity and lake size have a minor impact on this general finding. If the lake remains near the temperature of the air, a plume circulation will dominate. It was found that a differential of ~ 2 K was the transition from a plume-dominant circulation to a sea breeze-dominant circulation. If plumes are not present on Titan, it can be inferred that the lakes are at least ~ 2 K colder than the air.

Sensible and latent heat fluxes vary in magnitude from near zero to 50 W/m^2 and 400 W/m^2 , respectively, while their ratio (the Bowen ratio) remains remarkably stable. The largest fluxes are generally associated with a plume circulation since the wind speeds are strongest in those cases. Once a marine layer develops, the increased static stability and lower wind speeds are less favorable for vigorous turbulent exchange. If we restrict the analysis to simulations without a strong plume circulation, without excessively cold lakes, and without wind speeds sufficient to trigger waves, the highest magnitude fluxes may be considered unrealistic under current observational constraints.

The result from Simulation 61 is an example of a solution consistent with observational constraints. The atmosphere is initialized with a modest relative humidity. Although the lake starts at the same temperature as the air, the lake cools quickly to the approximate 2 K threshold needed for the suppression of the plume circulation. Wind speed drops dramatically, and sensible and latent heat fluxes are -2 W/m^2 and $\sim 6 \text{ W/m}^2$, respectively. This would lead to global evaporation rates that are small, but still sufficient to balance photochemical loss rates. That same latent heat flux, however, would produce only a 0.2 cm drop in lake level per year assuming no other sources or sinks.

Unfortunately, Cassini measurements alone are unlikely to provide strong constraints on the magnitude of the fluxes. Lake levels changes, if observed, are not only due to evaporation, but precipitation and possible resupply from surface and subsurface flows. An observed decrease in lake level could be due to evaporation, or it could be due to some other process entirely. Further, even if evaporation is enormous, the lake levels could be maintained by recharge. Finally, if the latent heat fluxes are small, as in Simulation 61, then lake level changes are not good indicators unless measurement accuracy is better than ~ 1 cm/year. Additional analysis of radar brightness temperatures would be extremely helpful. Jennings et al. [2011] suggested that lake temperatures should be colder in the spring and summer due to differences in thermal mass between the land and the seas, and there was some indication of this in their analysis of radar-derived surface temperatures.

If the smaller magnitude fluxes are realistic, then radiative processes should be considered. We attempted a preliminary investigation of diabatic forcing using Newtonian relaxation of the atmosphere, which was shown to have an effect even for long (96 hour) time constants. More detailed simulations with a radiative scheme for the atmosphere and surface is an area for future investigation.

Background wind shifts and distorts the plume and sea breeze circulations in ways that are expected based on terrestrial analogs. Sea breeze fronts that oppose that mean wind tend to be sharp and strong while those moving in the direction of the mean wind are more diffuse. A 3 m/s wind is sufficient to keep the impact of air-sea interactions restricted to the downwind direction. With a 1 m/s wind, the plume circulation and the sea breeze can be of sufficient strength to propagate their effects upwind. In the cases

where a cold and stable marine layer develops, the underlying lake is effectively shielded from the influence of the background wind.

The lake dimensions did not strongly impact the overall solution. The dimensions and to a lesser degree the strength of the plume and sea breeze circulations scaled with the lake. There is certainly to be some size limit below which the scaling fails. For example, puddles may produce an evaporative plume but are unlikely to force much of a sea breeze. We did not investigate the limiting size, but based on Earth it is likely to be $O(1 \text{ km})$, since this is the fetch over which air typically adjusts to the underlying lake condition [e.g., Phillips, 1972].

No simulation was found to achieve the flux balance assumed in M09, although the basic behavior of the lake temperature and fluxes were properly identified in that earlier study. In our results, the air does cool, and the development of an atmospheric circulation impacts the initial wind. Changes in atmospheric stability also play an important role in determining the fluxes. Unlike M09, this study provides little constraint on the actual methane source rate from lakes unless the low flux simulations are assumed to be the most representative of reality.

The 2 km resolution mtWRF simulations may be of use in parameterizing air-sea interaction in general circulation models (GCMs). Titan GCMs can use similar bulk transfer turbulent closures [e.g., Lora and Ádámkóvics, 2017], but the resolution of the global models may be insufficient to fully capture the dynamics of sea breezes or plume circulations. Further, it is not clear that the virtual buoyancy effect is considered, which is important.

If the plume circulations with high initial atmospheric relative humidity are excluded, none of the 67 simulations were able to produce an environment conducive to cloud formation. This is consistent with the very infrequent cloud observations from Casinni [e.g., Turtle et al., 2018]. The observed cloud asserted to be associated with a lake [Brown et al., 2009a] is inconsistent with any of the model configurations that were investigated. The observed cloud is almost certainly not a lake effect cloud, as commonly referred to in the terrestrial literature, but a causal formation mechanism tied directly to air-sea interaction cannot be ruled out based on the simulations presented here. There may be some reasonable range of air and lake configurations that could favor cloud formation. Conversely, the appearance of a cloud near a lake could be entirely coincidental.

Air-sea interaction on Titan depends on a great number of factors, and the physics is complex and nonlinear. As complex as it is in this study, radiative effects and three dimensional circulations driven by irregular coastlines and topography have not been considered. Future work is needed to explore how the shape of coastlines and surrounding topography can influence the atmospheric circulation. The simulations have also shown that lake circulations, particularly the effective lake mixing depth, are extremely important. Ideally, future work would involve coupling a dynamic lake model to the atmospheric model. The uncertainty in lake composition and the physical behavior of liquid and ice remains problematic, but parameteric sweeps could be done with the lake model in a manner similar to what has been done here.

Numerical stability and model precision were found to be important, particularly in the most weakly forced cases. A couple of simulations became numerically unstable and produced non-physical wind regimes, while a few retained some semblance of reality but had troubling asymmetries. Numerical boundary conditions played a large role in the instabilities. The boundary condition issues may be resolved by imposing realistic properties derived from a GCM. Initial attempts of the simulations using TRAMS were unsuccessful due to numerical issues, and this motivated the use of mtWRF, which turned out to have lower magnitude nonphysical computational modes. Application of well-tested and proven terrestrial models to extraterrestrial conditions can be problematic, and care needs to be taken to ensure solutions are physically consistent while nonphysical signals are acceptably small.

As is always the case, more and higher fidelity observations would be beneficial. A mission like the Titan Mare Explore (TiME) previously proposed to the NASA Discovery Program would be the most direct way to obtain the measurements and observational constraints needed to quantify air-sea interaction on Titan [Stofan et al., 2013]. The Dragonfly mission currently under consideration for the NASA New Frontiers exploration program is destined for the tropical dunes, but the meteorological measurements would still be useful in providing constraints, especially if there is moist ground exchanging methane with the atmosphere. Direct measurement of wind, temperature, and moisture profiles coupled to surface temperature and surface properties can provide strong constraints on turbulent fluxes, and these can be extrapolated to conditions over liquid reservoirs.

Acknowledgements

This work was primarily supported through the NASA Planetary Atmosphere Program with important contributions from Southwest Research Institute and the substantial investment of the authors' personal time.